Eva Lackner, Dipl.-Ing.

Optimization of CMOS integrated tin oxide gas sensors using metallic and bimetallic nanoparticles

Dissertation

zur Erlangung des akademischen Grades

Doktorin der technischen Wissenschaften

eingereicht an der

Technischen Universität Graz

Betreuer

Assoc.Prof. Dipl.-Ing. Dr.techn. Roland Fischer

Institut für Anorganische Chemie

und

Univ.Doz. Mag. Dr. Anton Köck

Materials Center Leoben Forschung GmbH

Graz, Juni 2017

EIDESSTATTLICHE ERKLÄRUNG

Ich erkläre an Eides statt, dass ich die vorliegende Arbeit selbstständig verfasst, andere als die angegebenen Quellen/Hilfsmittel nicht benutzt, und die den benutzten Quellen wörtlich und inhaltlich entnommenen Stellen als solche kenntlich gemacht habe. Das in TUGRAZonline hochgeladene Textdokument ist mit der vorliegenden Dissertation identisch.

_____   _____

Datum   Unterschrift

Abstract

The combination of gas sensing materials with CMOS technology is key to realize smart gas sensor devices for mobile applications. Gas sensors on the market today are rather bulky devices with high power consumption. The integration of gas sensors on CMOS based microhotplates enables the fabrication of miniaturized sensor devices with low power consumption. Highly sensitive and selective gas sensing materials are of significant importance for the application of smart gas sensor devices in consumer electronics. In this thesis, SnO_2 thin film gas sensors are integrated on CMOS microhotplates and functionalized with metallic and bimetallic nanoparticles. The CMOS-compatible deposition of 50 nm thin SnO_2 films is achieved by a spray pyrolysis process. The morphology, crystallinity, and roughness of the sensing material is characterized. Different deposition techniques for functionalization of the CMOS integrated gas sensors with nanoparticles are investigated. The functionalized gas sensors are operated at elevated temperatures up to 400 °C and the sensor performance to the exposure of CO and H_2 in the ppm-level range in dry and humid atmosphere is evaluated. The impact of metallic and bimetallic nanoparticles on the gas sensitivity and selectivity, as well as response and recovery time of CMOS integrated SnO_2 thin film gas sensors is determined.

Acknowledgements

Content

7

I. Introduction and Motivation

Historically, the need for gas sensors appeared for the first time in the mining industry. Detecting the highly explosive gas methane and monitoring oxygen levels in coal mines was and still is important for the worksite safety of miners. In the last few decades, due to the industrialization and fast development of new technologies, various other applications for gas sensors have emerged in numerous industries, in the health sector and in outdoor environmental monitoring [1]. Over the years, a vast variety of gas sensors based on different working principles has been developed for monitoring and controlling the emission of hazardous and flammable gases. One of the most promising sensor technologies is based on conductometric gas sensors using metal oxide semiconductors [2].

In 1962, Seiyama *et al.* reported on the first practical use of a conductometric gas sensor using zinc oxide (ZnO) thin films at elevated temperatures for the detection of inflammable gases in air [3]. In the same year, Taguchi applied for a patent using a sintered porous tin oxide (SnO_2) block for detecting gas leakages in domestic homes. After extensive research and development, Taguchi - together with his research colleagues - commercialized the first gas sensor based on SnO_2 in 1968 [4]. Since then, researchers all over the world have studied the properties and sensing performances of different metal oxides, but so far SnO_2 is the most studied and used metal oxide for gas sensing [5]. Conductometric gas sensors have many advantages compared to other sensor technologies, including low cost due to easy and flexible production, fast response and high sensitivity to a large number of gases [6]. The sensitivity to various gases is, at the same time, also the biggest disadvantage of metal oxides because it leads to a low selectivity of the gas sensors. Temperature modulation, gas-filtering layers, detection algorithms, or catalytically active additives are some of the many methods for improving selectivity [7]–[9].

Apart from industrial and environmental applications, cheap and reliable gas sensing systems need to be developed for controlling and monitoring indoor air quality (IAQ). Air pollutants, such as volatile organic compounds (VOCs), or particle matter (PM), are generated in the household by emission from furniture, building materials, or using coal

and wood for heating and cooking. People, who nowadays spend up to 90 % of their time inside buildings, are affected by the household-generated pollutants, which can cause health problems and can even lead to death [10], [11]. At the moment, the applications of gas sensors are limited to industrial processing or laboratories because gas sensor systems are still bulky and expensive devices. For the application of gas sensor systems in everyday life, the cost has to be reduced extensively. This can only be achieved by combining the sensing element with low-cost manufacturing technologies (e.g. CMOS technology). The combination of nanostructured sensing materials with CMOS technology leads not only to cost reduction but also to lower power consumption and miniaturized devices. A new market in portable electronics (e.g. smart phones, wrist watches, laptop computers, etc.) could be accessed by CMOS integration of gas sensors [12].

In 2016, a market study on multi-gas and particle sensing was performed by IHS Markit [13] within the framework of the project "MSP – Multi Sensor Platform for Smart Building Management", coordinated by Materials Center Leoben Forschung GmbH. The market study showed that in the next couple of years, new application fields for multi-gas sensors and particle sensors will emerge. Especially, the integration of gas and particle sensors in air purifiers will be a consumer mass-market application. Another new type of device will be smart lighting fixtures including different sensors for fire prevention, human presence detection, and control of heating, ventilation, and air conditioning (HVAC).

The aim of this thesis is the functionalization of CMOS integrable SnO_2 gas sensors with metallic and bimetallic nanoparticles for enhanced gas sensitivity and optimized selectivity. SnO_2 thin films are deposited on microchips by a CMOS compatible deposition technique. By the heterogeneous integration of the sensing layer on microchips, which include electronics and microhotplates as heating elements, a "smart" gas sensor system is developed. Microhotplates, which are thermally isolated from the rest of the chip to reduce heat dissipation, enable precise temperature control and low power consumption for operating temperatures of up to 400 °C. Functionalization

with nanoparticles is a powerful strategy to enhance the gas sensitivity and improve the selectivity of metal oxide gas sensors. Within this thesis, the impact of different metallic and bimetallic nanoparticles on the sensitivity as well as the selectivity of SnO_2 thin film gas sensors is investigated. This work has been performed within the projects "Multi Sensor Platform for Smart Building Management" (MSP), funded by the European Commission, and "Industrielle Realisierung innovativer CMOS basierter Nanosensoren" (RealNano), funded by the Austrian Research Promotion Agency. The goal of the MSP project is the 3D integration of sophisticated sensor devices on CMOS electronic platform chips by employing Through-Silicon-Via (TSV) technology. RealNano aims to develop an innovative process chain and new production machines for full wafer scale industrial fabrication of CMOS based nanosensors.

This thesis is organized as follows:

I – Introduction and Motivation

II – Theoretical Part   The fundamentals and gas sensing characteristics of metal oxide semiconductor gas sensors are defined. Deposition techniques of metal oxides and methods to improve the gas sensitivity and selectivity of metal oxide gas sensors are summarized.

III – Experimental   In this part, the procedures for fabricating CMOS integrated tin oxide gas sensors are presented. The spray pyrolysis process for depositing tin oxide thin films on different substrates is explained in detail. The fabrication of silicon based and CMOS based tin oxide gas sensors is summarized. Different deposition techniques of nanoparticles for functionalizing the metal oxide gas sensors are presented and the gas sensing characterizations of bare and functionalized tin oxide thin film gas sensors are summarized and discussed.

IV – Summary and outlook   The last part summarizes the results of this thesis and gives an outlook on future activities in this field.

II. Theoretical part

1 Metal oxide semiconductor gas sensors

Monitoring and controlling air quality is an important issue for today's society. Nowadays, gas sensors are not only needed in industry for process control and work safety, but have become pervasive in our live. Outdoor environmental monitoring, medical diagnostics, or indoor air quality control in building technologies are some of the many application fields of gas detection. Over the years, various types of gas sensors, based on different detection principles, have been developed. Chemical gas sensors based on metal oxide semiconductors are one of the most promising sensor types and subject of this work. In this chapter, the definition of chemical sensors and their classification, as well as sensing materials for conductometric gas sensors and their sensing characteristics with focus on tin oxide will be discussed.

1.1 Definition and classification

In general, chemical gas sensors consist of two main parts, a receptor and a transducer. A material or a materials system is acting as a receptor by changing its own properties (e.g. work function, electrode potential, mass or dielectric constant) or by emitting light or heat when interacting with a target gas. The transducer is a device, which measures the change in property of the receptor and transforms it into an electrical signal [14]. Semiconductors can be divided into two groups: oxide and non-oxide semiconductors. Non-oxide semiconductors are protected by an insulating layer. They cannot be used as receptors but they can be used as transducers (e.g. MIS FETs). At elevated temperatures and in harsh environments, oxide semiconductors are chemically and physically stable and can therefore function as receptors and transducers [15]. Apart from semiconductor gas sensors, a variety of other gas sensors with different detection mechanisms have been developed so far. Table 1.1 summarizes some of those gas sensor types and their working principle. Field effect transistors can be used as gas sensors by attaching gas sensing elements onto the insulated gate. Due to the interaction with gas molecules, the electrical activity at the interface of the gate and the sensing element changes and the change in the

Table 1.1: Types of gas sensors and their detection principle, adapted from [15].

Device type	Detection principle
Conductometric gas sensors	Electrical conductivity of the semiconductor changes due to the interaction with gaseous analytes.
Field effect gas sensors (diodes, transistors, capacitors)	Interaction of the gas with the gas-sensitive gate leads to a voltage shift of the FET.
Piezoelectric gas sensors (Quartz crystal microbalances (QMB), surface acoustic wave (SAW), microcantilevers)	Acoustic wave with resonant frequency is created by an applied AC voltage across piezoelectric material. Resonant frequency is altered when the mass of the gas sensitive membrane changes on interaction with a test gas.
Optical gas sensors (fiber optic or thin film)	Optical properties (e. g. surface plasmon resonance, absorbance, fluorescence, refractive index) change.
Catalytic gas sensors (pellistors)	Heat generation due to oxidation of target gas (e.g. H_2, CO, CH_4) on the surface of catalytic material.
Electrochemical gas sensors (potentiometric or amperometric)	Oxidation or reduction of a target gas at an electrode changes the electromotive force or electrical current in a solid state electrochemical cell.

gate voltage can be used to determine the species concentration. Depending on the sensing material immobilized on the gate insulator, FET-based sensors can be used for various applications, including hydrogen sensing, measuring ion concentrations in solutions or pH sensing [16]. The surface acoustic wave (SAW) device and the quartz crystal microbalance (QCM) are the two types of piezoelectric sensors used for gas sensing. The adsorption of gas on the coating of the piezoelectric sensor changes its mass and therfore alters the frequency of the wave, which is generated by applying an ac signal to the piezoelectric material. Both types of piezoelectric sensors work on the same principle, the difference is the path and depth of the propagating wave. In the SAW device, the wave travels along the sensor surface and the wave of the QCM travels through the bulk of the sensor [17]. Gas sensing by optical methods is based on absorption and emission spectrometry. Optical gas sensors show higher sensitivity, selectivity, stability and longer lifetimes than non-optical systems. Nevertheless, gas sensors based on optical principles are limited in their applications due to expensive and bulky components, such as laser diodes as light sources, and infrared detectors [18]. Catalytic sensors detect combustible gases by resistively measuring the heat generated by oxidation of the gas analyte on the catalyst layer surface. Catalytic sensors are able to accurately measure and determine gas concentrations but they suffer from high power consumption and catalyst poisoning [19]. Potentiometric and amperometric devices are the two most common types of electrochemical sensors. The detection principle of these devices is based on the oxidation or reduction of solid, liquid or gaseous analytes at the working electrode. The electrochemical reactions lead to the generation of a current (measured in amperometric devices) or a potential (measured in potentiometric devices) at the working electrode [20].

Conductometric gas sensors, using semiconducting metal oxides as gas sensitive material, are one of the most studied sensor types. The detection principle of this device is based on the reaction of a gaseous analyte with the metal oxide surface, which leads to a change in the electrical resistance of the semiconductor. Conductometric gas sensors are attractive for many applications due to their various advantages compared to other sensor types, including low cost and flexible production, broad range of detectable gases, low

power consumption and suitability for miniaturization [21], [22]. This thesis focuses on conductometric gas sensors using tin oxide (SnO$_2$) thin films as the gas sensitive layer.

1.2   Gas sensing materials

Semiconducting metal oxides are used as gas sensitive material in conductometric gas sensors. According to the Band theory of solids, there are three main material classes: insulators, semiconductors, and conductors (shown in Figure 1.1). The difference between these three classes can be explained by the electron occupation of the available energy levels (or bands).

In insulating materials, the valence and the conduction band are divided by a large gap. A huge amount of energy would be needed for the electrons to bridge the gap, therefore no electronic conduction occurs. In conducting materials, the valence and the conduction band overlap, allowing the electrons to move freely. The band gap of semiconductors is small enough that with sufficient energy input some electrons can move from the valence band into the conduction band. The energy input must be higher than the Fermi level (E_F, highest occupied state at absolute zero). At T = 0, semiconductors are insulators, but above the Fermi level, electronic conduction can occur [23].
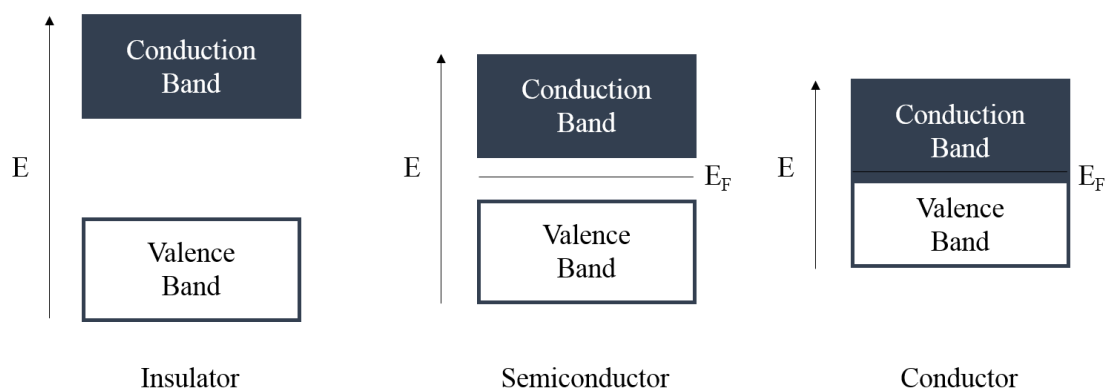
Figure 1.1: Band diagrams of an insulator, semiconductor, and conductor.

Metal oxide semiconductors can be classified into two groups: n-type and p-type materials. The classification is based on the type of dominating charge carriers (electrons or holes), determined by oxygen nonstoichiometry. In n-type metal oxide semiconductors the electronic conduction is based on oxygen vacancies, which act as electron donors. An excess of oxygen atoms, acting as electron acceptors, is responsible for the electronic conduction in p-type metal oxide semiconductors [24]. A large variety of metal oxides are suitable for the detection of reducing and oxidizing gases. Table 1.2 categorizes some of the metal oxides according to their type of conductivity.

The following key properties should be considered when selecting metal oxides for gas sensing applications [25]:

- adsorption ability
- electronic, electro-physical and chemical properties
- thermodynamic stability
- catalytic activity
- crystallographic structure
- reliability
- interface state
- compatibility with materials and technologies for gas sensor fabrication

SnO_2 is the most investigated and used metal oxide for gas sensing applications. Tin shows a dual valency, with oxidation states of +4 and +2, with stannic oxide (SnO_2) and stannous oxide (SnO) being the two main oxides of tin.

Table 1.2: Classification of metal oxides according to their type of conductivity [25].

n-type	p-type	n- and p-type
SnO_2, TiO_2, ZnO, WO_3, ZrO_2, Al_2O_3, MgO, CaO, Nb_2O_5, MoO_3, Ga_2O_3, Ta_2O_5, In_2O_3	NiO, Co_3O_4, Ag_2O, CeO_2, Bi_2O_3, Y_2O_3, Mn_2O_3, TeO_2, La_2O_3, PdO, Sb_2O_3	CuO, Fe_2O_3, Cr_2O_3, HfO_2

Stannic oxide is well characterized and technologically significant. SnO_2 crystallizes in a rutile structure, the tetragonal unit cell contains two tin atoms and four oxygen atoms. Figure 1.2 illustrates the SnO_2 unit cell, green spheres represent tin atoms and red spheres represent oxygen atoms.

Tin atoms that are not on the surface are sixfold coordinated to threefold coordinated oxygen atoms. The lattice constants are $a = b = 0.474$ nm and $c = 0.319$ nm. Tin oxide is a wide band-gap semiconductor ($E_G = 3.6$ eV), and in its stoichiometric form, it is an insulator at room temperature. In reality, metal oxides show a non-stoichiometry due to defects and impurities in the crystal lattice. In the case of SnO_2, oxygen deficiencies as intrinsic defects are responsible for the high conductivity of the material [26].

1.3   Gas sensing characteristics

The detection principle of metal oxide gas sensors is based on electrical conductivity changes of the material. The conductivity of the sensing layer is altered by surface interactions of the metal oxide with the surrounding gases. The exact gas sensing mechanisms are so far not fully understood and are still controversial but the following mechanism theory is the most accepted model for n-type metal oxide semiconductors. An electron-depleted region near the metal oxide surface is formed by the chemisorption of oxygen, which traps conduction electrons of the metal oxide surface.
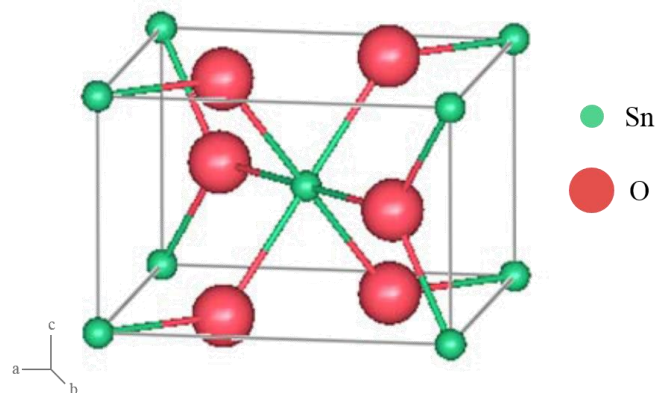
Figure 1.2: Unit cell of SnO_2 [27].

The formation of this electron-depleted region, also called the space-charge layer, leads to an increased surface resistance [28]. The charge transfer results in an upward bending of the energy band with respect to the Fermi level, creating a potential barrier at the metal oxide surface. Figure 1.3 illustrates the band bending after oxygen ionosorption on the surface of an n-type semiconductor. The type and concentration of adsorbed oxygen species determines the height (eV$_{Surface}$) and the depth (Λ_{air}) of the band bending. In Figure 1.3, E$_v$, E$_F$, and E$_C$ denote the energy of the valence band, the Fermi level, and the conduction band, respectively. e$^-$ represents the conducting electrons and the donor sites are represented by +.

Furthermore, the Debye length L_D − a characteristic length for semiconductors − also influences the depth of the band bending

$$L_D = \sqrt{\frac{\varepsilon_0 \varepsilon k_B T}{e^2 n_d}} \tag{1}$$

where ε_0 is the permittivity of free space, ε the dielectric constant, k_B the Boltzmann's constant, T the operating temperature, e the electron charge, and n_d the carrier concentration [29].
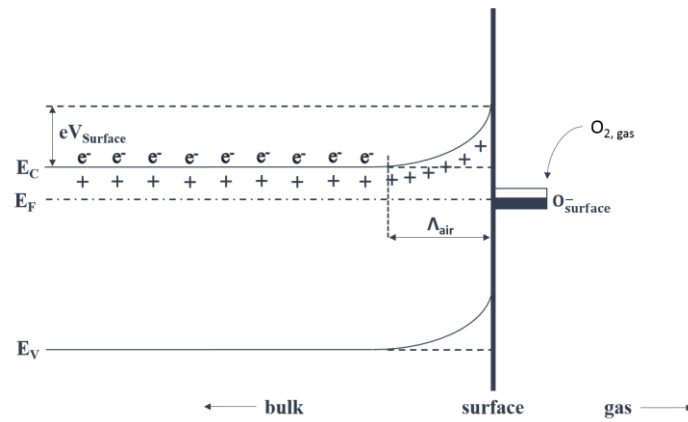
Figure 1.3: Band bending of n-type semiconductor after chemisorption of oxygen [29].

The oxygen species adsorbed on the surface depends on the temperature. Molecular oxygen adsorbs on the metal oxide at low temperatures (below 200 °C). At temperatures above 200 °C, oxygen dissociates to atomic oxygen. The oxygen species can be single or double charged. It is assumed that physisorbed oxygen (uncharged oxygen species) is not part of the gas sensing mechanism [30]. Table 1.3 summarizes the possible surface interactions with oxygen.

Table 1.3: Interaction of oxygen with metal oxide surface [30].

Interaction type	Mechanism
Physisorption	$O_2\,(gas) \leftrightarrow O_2\,(ads)$
Ionosorption	$O_2\,(ads) + e^-\,(CB) \leftrightarrow O_2^-\,(ads)$
Ionosorption	$O_2^-\,(ads) + e^-\,(CB) \leftrightarrow O_2^{2-}\,(ads) \leftrightarrow 2O^-\,(ads)$
Ionosorption	$O^-\,(ads) + e^-\,(CB) \leftrightarrow O^{2-}\,(ads)$
Diffusion	$O^{2-}\,(ads) \leftrightarrow O^{2-}\,(1st\ bulk\ layer)$

Reducing gases, such as CO, interact with the chemisorbed oxygen species:

$$CO + O^-\,(ads) \rightarrow CO_2 + e^- \qquad\qquad (2)$$

or

$$2\,CO + O_2^-\,(ads) \rightarrow 2\,CO_2 + e^- \qquad\qquad (3)$$

Thereby, trapped electrons are transferred back to the conduction band of the metal oxide, which reduces the resistance of the material [31]. Oxidizing gases, such as NO_2, extract more electrons from the surface, resulting in an increase of the resistance:

$$NO_2\ (ads) + e^- \rightarrow NO_2^-\ (ads) \tag{4}$$

In p-type metal oxides, the majority of charge carriers are holes (electron acceptors) and a hole-accumulation layer near the grain surface with low resistance is formed by the chemisorption of oxygen [24]. P-type materials show an opposite behavior to gas exposure than n-type materials. The response of n- and p-type metal oxides to reducing and oxidizing gases is summarized in Table 1.4 [32].

In the case of polycrystalline metal oxide sensing layers, the electronic conduction occurs along the grain-to-grain contacts. The potential barrier (representing the Schottky barrier) at the adjacent grains determines the conductance of the material G and can be expressed as [29]:

$$G \approx \exp\left(\frac{-eV_{Surface}}{k_B T}\right) \tag{5}$$

Figure 1.4 illustrates the formation of the space charge layer on SnO_2 grains and the impact it has on the height of the potential barrier if exposed to a reducing gas. Even low gas concentrations decrease the potential barrier at the grain surface significantly by removing ionosorbed oxygen species from the surface. As already mentioned, the sensing mechanisms of metal oxides are based on surface reactions and therefore it can be expected that the gas sensing properties of the material are improved by the increase of the surface area. By reducing the crystallite size of the sensing layer, the surface-to-bulk ratio is increased. The crystallite size also influences the potential barrier at the space-charge layer [30], [33]. The ratio of the crystallite size (D) to the thickness of the space-charge layer (Λ) determines the magnitude of the potential barrier to the electronic conduction.

Table 1.4: Resistance change of n- and p-type metal oxides to the exposure of reducing and oxidizing gases.

Classification	Reducing gases	Oxidizing gases
n-type	Resistance decrease	Resistance increase
p-type	Resistance increase	Resistance decrease

Crystallites are connected *via* necks and form larger particles. The larger particles are interconnected with neighboring particles via grain boundary contacts. A schematic model of the effect of crystallite size on the electronic conduction is illustrated in Figure 1.5. For larger grains (D >> 2 Λ), conduction electrons have to overcome the potential barrier at the grain boundary contacts, the conductivity of the sensing layer is dominated by the bulk conductivity and the sensitivity of the material is nearly independent of the crystallite size. The space-charge layer penetrates deeper into the crystallites with decreasing crystallite size. When the crystallite size approaches the thickness of the space-charge layer (D ≥ 2 Λ), the sensitivity is influenced by the grain boundary contacts as well as the crystallite size, because conduction channels are formed at the necks within the particles by the space-charge layer.
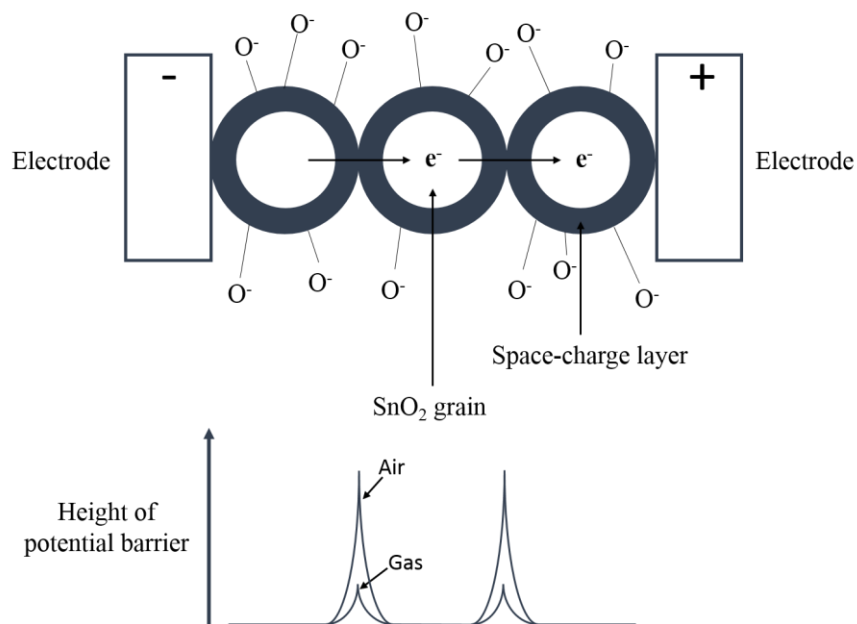

Figure 1.4: Formation of space-charge layer on SnO_2 grains by chemisorption of oxygen; adapted from [34].

The grains are fully penetrated by the space-charge layer, when the crystallite size is smaller than two times the space-charge layer (D < 2 Λ) [35]. The so-called "flat-band condition" ($eV_{Surface} \leq k_B T$) is reached by depleting the crystallite of its mobile charge carriers, the energy difference between the bulk and the surface vanishes and the conductance G is proportional to the difference of the Fermi level (E_F) and the conduction band (E_C) [29]:

$$G \approx \exp\left(\frac{-(E_C - E_F)}{k_B T}\right) \qquad (6)$$

Yamazoe *et al.* investigated the grain size effects on the sensing properties of SnO_2-based gas sensors in the early 1990s and showed that the sensitivity to gases, in this case carbon monoxide, hydrogen and isobutane, increased with decreasing crystallite size [36], [37].

A very important factor, in particular for gas sensor applications in real life conditions, is humidity. A dependency of the resistance to humidity is reported on temperatures of up to 600° C [38], [39]. Exposure of metal oxides to water vapor leads to an increased conductance. Depending on the operating temperature of the sensor, water can be physisorbed or dissociated on the metal oxide surface. Physisorption of molecular water is observed at temperatures up to 200 °C, but the influence of physisorbed water on the resistance is negligible. The surface of SnO_2 - in different atmospheres and at temperatures ranging from room temperature up to 500 °C - have been investigated by infrared (IR) techniques [40], [41] and the temperature programmed desorption (TPD) technique [42], [43]. Hydroxyl groups bound to tin atoms were observed.
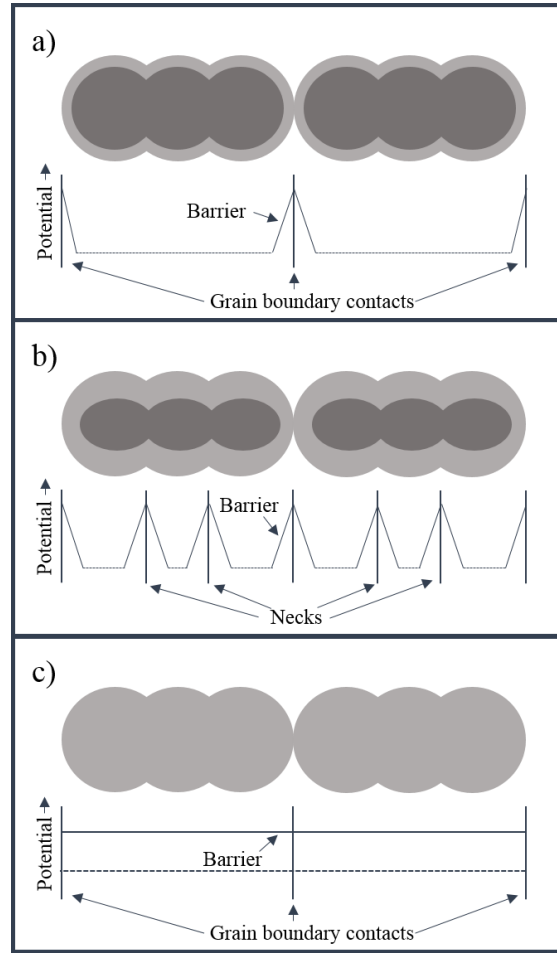
Figure 1.5: Schematic models for grain size effects; adapted from [35]. a) D >> 2 Λ (grain boundary-control), b) D ≥ 2 Λ (neck-control) and c) D < 2 Λ (grain-control), where D = crystallite size and Λ = space-charge layer thickness.

The electron pair of the hydroxyl group is shared with the tin atom and the neutral hydrogen atom can react with lattice oxygen or with chemisorbed oxygen on the surface. The following two mechanisms are proposed in literature [44]:

$$H_2O_{gas} \; + Sn_{lat} \; + \; O_{lat} \; \leftrightarrow (Sn_{lat}^+OH^-) + \; (OH)_{lat}^+ \; + \; e^- \qquad (7)$$

and

$$H_2O_{gas} \; + 2\,Sn_{lat} \; + \; O_{lat} \; \leftrightarrow 2\,(Sn_{lat}^+OH^-) + \; + 2\,e^- \qquad (8)$$
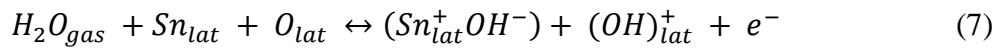
where H_2O_{gas} is water vapor, Sn_{lat} a tin atom in the lattice, O_{lat} an oxygen atom in the lattice and V_O^{++} an oxygen vacancy in the lattice. In Equation 7, the "rooted" hydroxyl group $((OH)_{lat}^+;$ hydrogen bound to lattice oxygen) can be ionised due to the lower electron affinity compared to O_{lat} and acts as an electron donor. The second mechanism (Equation 8) proposes the reaction of hydrogen atoms with the lattice oxygen, and subsequently, the formed OH group binds to the Sn atom, resulting in isolated hydroxyl groups $(Sn_{lat}^+ OH^-)$ and an oxygen vacancy, which generates electrons upon ionization.

The influence of water vapor on the conductivity as an indirect effect is proposed by Morrison [45] and Henrich and Cox [46]. After dissociation of the water molecule, the hydrogen atom or the OH group could interact with an acid or basic group, which are also acceptor sites on the surface, changing their electron affinity after the interaction. Water could also co-adsorb onto an adsorbed species or could displace chemisorbed oxygen.

Water vapor has a considerable effect on the sensing properties of metal oxides, it can reduce the sensitivity to reducing gases and cannot be neglected for the operation of the sensors in real-life conditions.

2 Technology

This chapter is divided into three sections. In the first section, different deposition techniques for metal oxides will be outlined. In the second section, functionalization techniques for optimizing the sensing properties, especially enhancing the selectivity, will be described. The importance of CMOS integration for producing smart gas sensor devices will be discussed in the last section.

2.1 Deposition techniques

In this section, the most common deposition methods for metal oxides, with focus on SnO_2, will be discussed. Depending on the deposition technique, the thickness and the porosity of the metal oxide layer can be tuned. Popular thick-film methods include screen-printing and drop-coating, which result in porous structured films. Thin and compact layers can be achieved by chemical vapor deposition, evaporation or sputtering [47]. Spray pyrolysis - the deposition method of choice in this work - will be described in detail.

2.1.1 Sol-gel based methods

The first step in sol-gel based deposition methods is the synthesis of a coating solution, the sol. A sol is a dispersion of colloidal particles in a liquid or dissolved polymerizable metalorganic precursors. The second step is the deposition of the sol on a substrate. Various techniques - including spin-coating, spray-coating, drop-coating and dip-coating – have been developed for depositing the sol and forming a continuous liquid layer. Hydrolysis reaction of the metalorganic precursors, most commonly metal alkoxides, with water, followed by condensation, forms a gel, which can be described as a solid network in a liquid phase. Thermal treatment of the gel leads to the evaporation of the solvent and pyrolysis of organic residues resulting in an amorphous or crystalline metal oxide layer [48].

Spin-coating:

The coating solution is dispensed on the center of a flat substrate and the solution is spread uniformly over the whole substrate by rotating the substrate at high speed due to centrifugal forces. The spin-coating process comprises of four stages: deposition, spin-up, spin-off and evaporation [49]. Figure 2.1 illustrates the different stages in the spin-coating process. The biggest advantage of spin-coating is the fabrication of thin films in the nanometer range with a uniform thickness, but the substrates which can be used are limited in size and to planar structures [50]. The fabrication of SnO_2 micro gas sensors by using spin-coating as deposition technique is reported in [51], [52].

Drop-coating:

A micropipette or microinjector is used to deposit the colloidal solution, sol or paste onto the substrate surface [47]. By combining the micropipette / microinjector with a micromanipulator and an optical microscope, a fast and accurate deposition of the sensing material onto already packaged and bonded microstructures is feasible with drop-coating [53], [54].
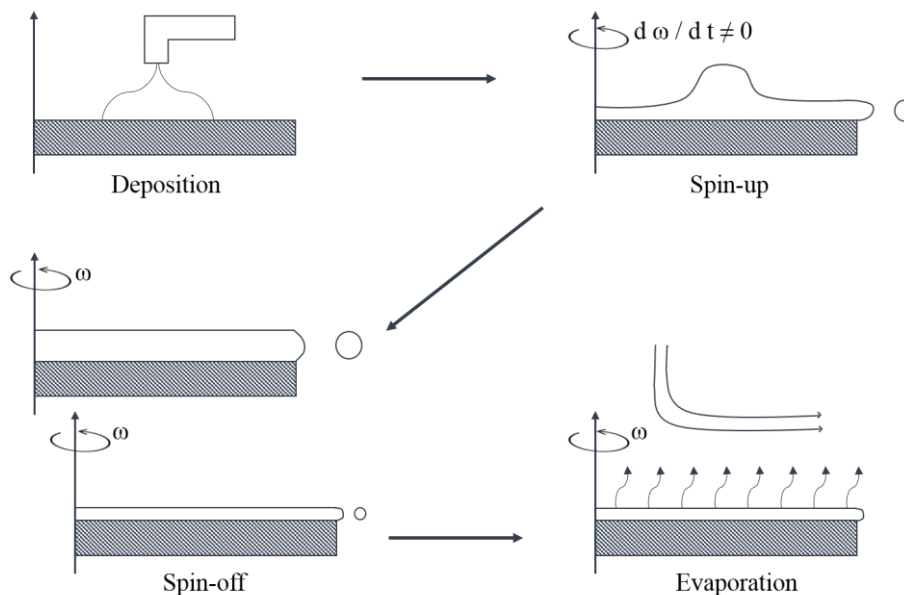

Figure 2.1: Four stages of spin-coating process; adapted from [48].

Spray-coating:

A spray gun is used to deposit a sol evenly on the entire substrate surface. The benefit of spray-coating is that complex structures and large areas can be coated. The wetting of the substrate surface, as well as the size droplet distribution, have to be controlled, otherwise the layers are inhomogeneous and exhibit high surface roughness [47]. Jiménez *et al.* present a computer-controlled spray-coating process for mass production of SnO_2 gas sensors [55].

Dip-coating:

The simplest way to deposit a sol on a substrate, in batch or continuous mode, is dip-coating. The substrate is immersed in a bath of the sol. By withdrawing from the bath, a thin layer adheres to the substrate surface and the solvent evaporates, forming a gel film. Substrates of different shapes, with complex structures, as well as areas in the square meter range can be coated with this method [50]. The critical step in dip-coating is the drying process, where rapid solvent evaporation can lead to the formation of cracks in the film [56].

Screen-printing:

Screen-printing is one of the most popular and established technologies for thick-film deposition. The cheap and simple method is suitable for mass production. A paste is prepared by mixing a pre-processed metal oxide powder with an appropriate amount of organic carrier to achieve the desired viscosity and consistency. The prepared paste is squeezed through a screen with a patterned back-side (stencil). A rubber squeegee is used to push the paste through the screen and transfer the pattern onto the substrate, illustrated in Figure 2.2. The organic carrier is removed by an annealing procedure and a mechanically stable thick-film with good adhesion to the substrate is produced [56]. The resolution of screen-printing used to be poor, but, in the last couple of years, the development of new kinds of stencils combined with computer-aided alignement improved the resolution significantly and made the method suitable for microfabrication of sensors [57].
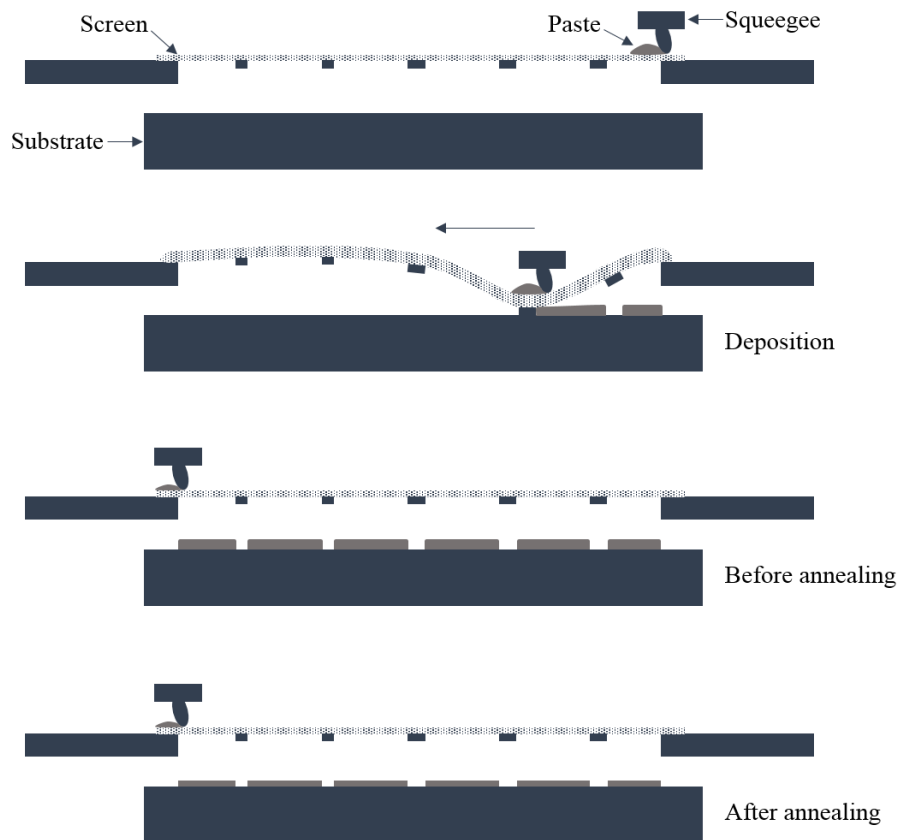
Figure 2.2: Schematic illustration of screen-printing technique for thick film deposition [58].

By using binders, the rheological properties of the paste can be adjusted and the adhesion of the thick-film to the substrate can be improved. These binders, mainly electrical insulators such as glass frits, can strongly influence the conductivity of the thick-film. Riviere *et al.* developed a sol-gel precursor without any permanent binders and the adhesion of the thick-film is achieved by the SnO_2 grain formation during the annealing procedure [59].

2.1.2 Physical vapor deposition

In physical vapor deposition (PVD), atoms or molecules from a solid or liquid source are transported in the gas phase to the substrate, where condensation occurs. PVD can be used for the deposition of films with thicknesses ranging from a few nanometers up to a few micrometers. The two most common PVD processes are evaporation and

sputtering [60]. A wide selection of precursor materials or targets are available for PVD and the fabrication of multi-layers is facilitated by incorporating various precursor materials into the system. The disadvantage of PVD is that the process has to be performed under vacuum, which is time consuming and makes the use of expensive equipment indispensable. Due to high production costs, PVD is not suitable for wide-scale commercial applications [14].

Evaporation:
A source material is evaporated by resistive or inductive heating or by irradiation in a high vacuum. The vapor diffuses to the substrate, which is placed close above the source material, and crystallizes on the substrate surface. The deposition of multi-component materials by evaporation is difficult, due to the dependency of the vapor composition on the vapor pressures of the individual materials [56]. SnO_2 thin films can be deposited by evaporation of SnO_2 powder using an electron-beam, or by evaporation of metallic tin, followed by an annealing step in air at 600-700 °C for several hours to oxidize the metallic film [61], [62].

Sputtering:
Sputtering is the method of choice among PVD processes and is used for depositing high-quality thin films. A glow discharge plasma generates ionized gas atoms (e.g. Ar), which are accelerated towards a target (cathode) by applying a negative bias (DC voltage) to the cathode. Atoms are ejected by the ion bombardment from the target, which condense on a substrate as a thin film. Additionally, secondary electrons are also generated by the impact of ions on the target surface, which are important for maintaining the plasma. In magnetron sputtering, magnets are used to trap secondary electrons in the vicinity of the target. A magnetic field - configured parallel to the target surface − increases the probability of a collision between electrons and atoms, leading to a higher ionization efficiency of gas atoms and a dense plasma. The increased ion bombardment of the target surface leads to higher deposition rates at the substrate and the higher ionization efficiency allows a reduction of the operating pressure as well as the operating voltages for maintaining the glow discharge [63], [64]. A schematic of the magnetron sputtering setup is shown in Figure 2.3. The deposition of thin films from insulating targets is
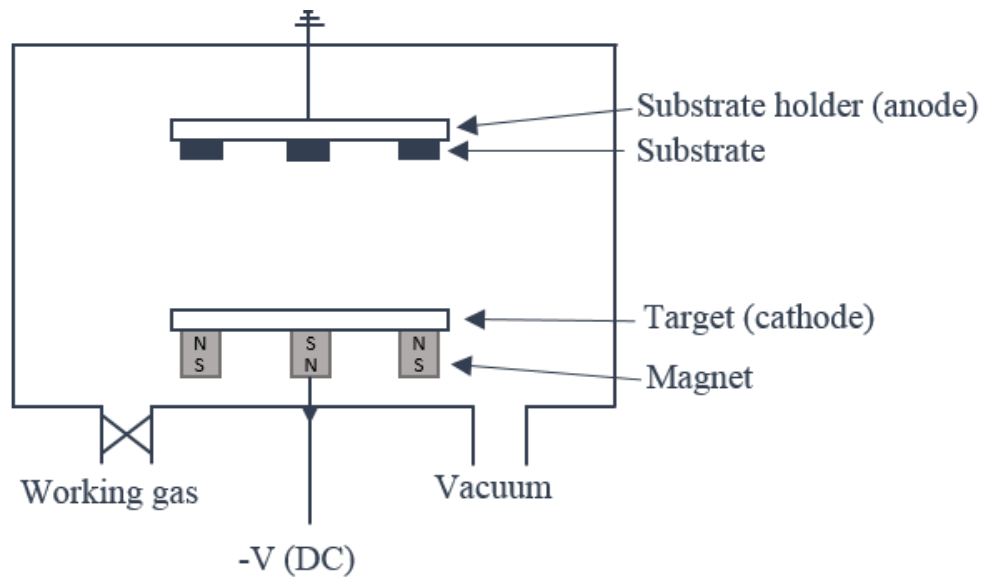
Figure 2.3: Magnetron sputtering setup; adapted from [65].

possible with radio frequency (RF) sputtering. Instead of a DC voltage setup, an alternating voltage in the RF-range (usually 13.56 MHz) is applied to the target [65]. SnO_2 gas sensors on integrated devices have been fabricated by DC magnetron sputtering deposition of metallic tin followed by thermal oxidation of the metal [66].

2.1.3 Chemical vapor deposition

Chemical vapor deposition (CVD), like PVD, is classified as a vapor-transfer process, which means that atoms, or molecules, or both are the deposited species. In CVD, chemical reactions of precursor compounds take place in the gaseous phase near or on a substrate at elevated temperatures, followed by the deposition of a solid material on the substrate surface. CVD is a complex synthesis process, which combines various scientific and engineering disciplines including thermodynamics, kinetics, chemistry, plasma physics, and fluid dynamics [67]. In Figure 2.4, the basic steps in a typical CVD process are schematically illustrated. Volatile precursors are introduced into a reaction chamber by a carrier gas stream at room temperature.
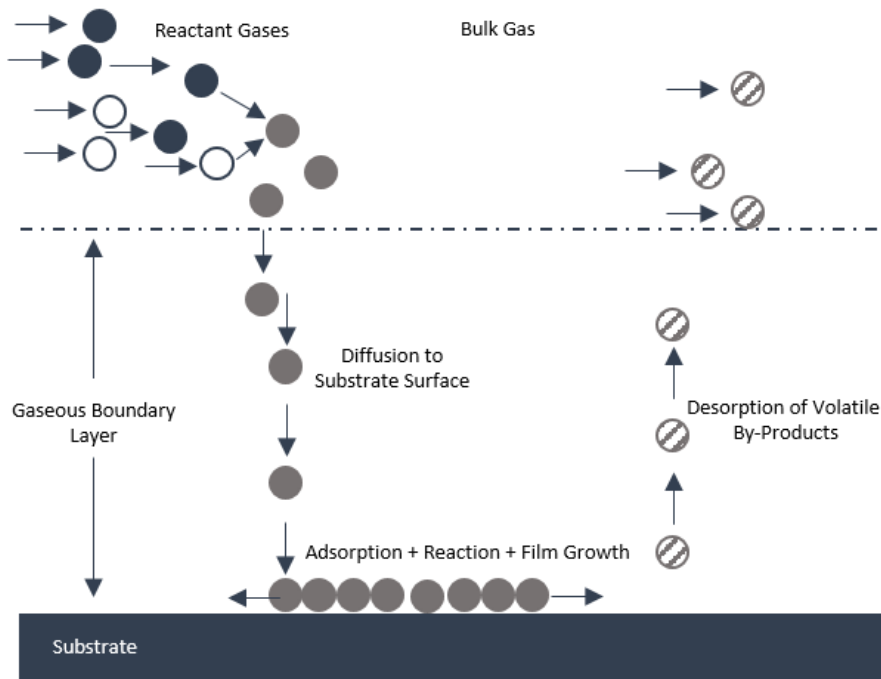
Figure 2.4: Basic steps in CVD process; adapted from [68].

The precursors react and/or decompose on the heated substrate and deposition of the desired material occurs on the substrate surface [56].

The advantages of CVD are:

- In CVD, there is no shadow effect as opposed to PVD. Complex shapes, holes, and deep recesses can be coated uniformly and with relative ease.
- Ultra-high vacuum conditions are generally not required and process variations can be achieved by adapting the CVD setup.
- Compared to PVD, CVD processes have a high deposition rate, which allows an economical competitive fabrication of thick films or coatings.

CVD mostly requires high temperatures (600 °C and higher), which limits the choice of substrates considerably. This is one of the biggest disadvantages, but has been offset by the development of plasma-CVD and metallo-organic CVD (MOCVD). The need for volatile chemical precursors is another disadvantage because the compounds are often hazardous or even extremely toxic and the by-products, created by the chemical reactions,

which are toxic and corrosive as well, require cost-intensive neutralization. Various CVD processes have been developed in the last two decades and new applications are constantly emerging, with the semiconductor industry being by far the most important field of CVD [67]. SnO_2 layers have been deposited by MOCVD in [69] and [70] using tetramethyltin ($Sn(CH_3)_4$) and dibutyltin diacetate (($C_4H_9)_2Sn(OCOCH_3)_2$) as precursor materials, respectively.

2.1.4   Spray pyrolysis

Spray pyrolysis is a solution-based thin film deposition method. The pioneering work for this method was done by Chamberlin and Skarman for the fabrication cadmium sulfide (CdS) films for solar cell applications in 1966 [71]. The application fields for spray pyrolysis are wide spread, ranging from biomedicine to semiconductors and ceramics. In the spray pyrolysis process, a material film is deposited by spraying a precursor solution in fine droplets by an atomizing nozzle (atomizer) onto a heated substrate. Based on the source of energy for the atomization of the solution, spray pyrolysis can be classified as [72]:

- Pressurized spray pyrolysis (gas energy)
- Ultrasonic spray pyrolysis (vibrational energy)
- Electrostatic spray pyrolysis (electrical energy)

A typical pneumatic spray pyrolysis setup includes an atomizing nozzle, a precursor solution reservoir, a substrate heater, a temperature control unit, gas supply with pressure regulation, and an exhaust system for gaseous by-products (shown in Figure 2.5).
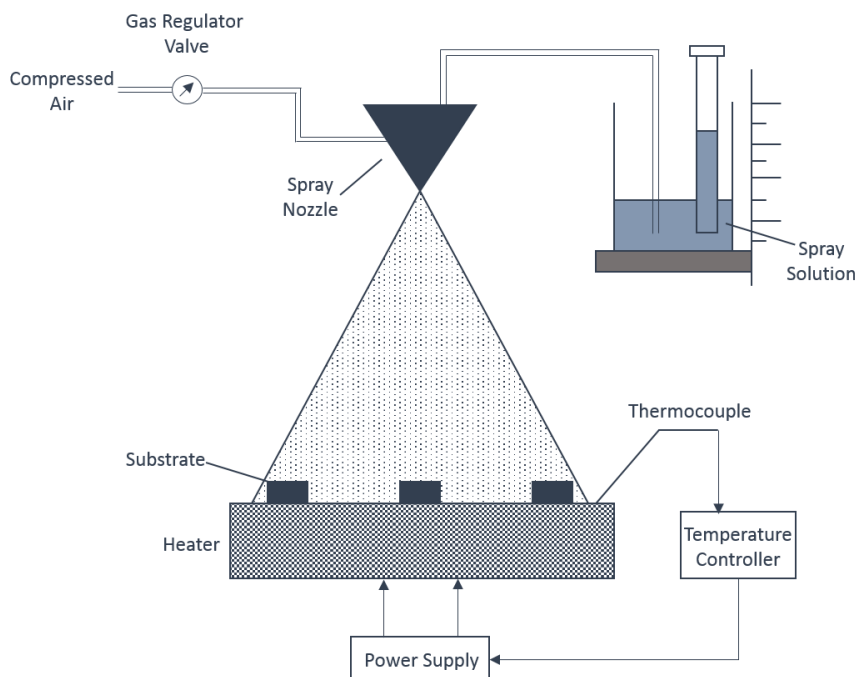
Figure 2.5: Pneumatic spray pyrolysis setup; adapted from [73].

In spray pyrolysis, droplet drying and decomposition of the precursor material are the two main stages in the deposition process. The material and the solvent, which are being used for the spray solution, determine the thermal energy required for the precursor decomposition. Temperature, droplet size, and the distance to the substrate influence the deposition mode of the solution. In Figure 2.6, the four reaction sequences, which can occur during the spray pyrolysis process, are schematically illustrated. At low deposition temperatures, droplets evaporate after reaching the substrate and pyrolysis of the dry precipitate occurs on the substrate surface (sequence A in Figure 2.6). At higher temperatures, droplets evaporate and the dry precipitates pyrolyze after hitting the substrate surface (sequence B in Figure 2.6). Spray pyrolysis can be understood as chemical vapor deposition; when the droplets evaporate, the precursor decomposes by pyrolysis in the vapor phase near or on the substrate surface (sequence C in Figure 2.6). At a too high deposition temperature, the precursor material decomposes and forms solid particles before reaching the substrate (sequence D in Figure 2.6). For the deposition of metal oxides, inorganic salts, mostly nitrates and chlorides, are used as precursor
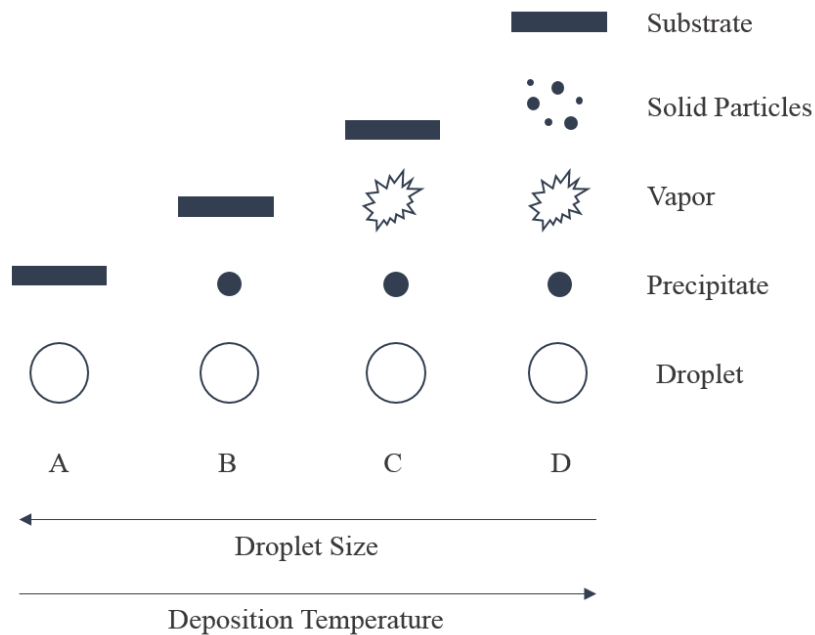
Figure 2.6: Reaction sequences possible during spray pyrolysis depending on deposition temperature and droplet size; adapted from [74].

materials. The solvents typically used for spray pyrolysis are e.g. methanol, ethanol, isopropanol, 2-methoxyethanol, or water [75].

Spray pyrolysis for thin film deposition has numerous advantages compared to other deposition methods (CVD, PVD, spin-coating etc.) [73], [76], [77]:

- Spray pyrolysis requires no vacuum, the equipment is simple, and the precursor materials are cheap, which makes spray pyrolysis an inexpensive deposition method and suitable for industrial scale-up.
- By changing the spray parameters, a high flexibility in deposition rate and film thickness can be achieved.
- Doping of thin films is easily done by adding the desired amount of dopant in some form to the spray solution.
- Thin films can be fabricated on various substrates due to moderate deposition temperatures (100 – 500 °C). There is virtually no limitation regarding substrate material, surface profile or dimension.

- Fabrication of multi-layered films is possible by changing the solution composition during the spray process.

Spray pyrolysis has also some disadvantages. One problem is the quite poor film thickness uniformity over large substrate areas. This problem can be solved by rotating the substrate or moving the atomizing nozzle during deposition. Another problem is the possible cooling of the substrate during spray pyrolysis at high deposition rates, which can lead to low or non-reproducible film parameters. Thus, special attention should be paid to the temperature control and readjustment during the spraying process. For the deposition of thin films on small area substrates, the waste of precursor solution has to be considered. Due to deflection or reflection of droplets from the substrate, a large amount of spray solution is not deposited on the substrate surface and therefore lost [75].

In this work, spray pyrolysis is the method of choice for the deposition of SnO_2 thin films because it is a simple, cheap and fast deposition method, which does not require vacuum conditions at any step of the process, and, most importantly, the moderate temperatures enable the application of CMOS microchips as substrates and the integration of SnO_2 thin films on CMOS microhotplates for the fabrication of smart gas sensors. For the specific CMOS chips employed within this thesis, the maximum allowed temperature is 400 °C.

2.2 Selectivity of metal oxide gas sensors

Resistive gas sensors based on metal oxides, including SnO_2, WO_3, TiO_2, and ZnO, are well-known for their low fabrication cost, long-time stability, and especially, their high sensitivity to a broad range of gases. However, the application of this type of sensors in biomedicine, industry and environmental monitoring is limited by the low selectivity of metal oxide gas sensors. In the last couple of years, numerous strategies for improving the selectivity of metal oxide gas sensors have been developed [7], [78], [79]. In this chapter, the most promising methods are discussed.

2.2.1 Catalysts and promoters

The detection mechanism of metal oxide gas sensors is based on surface reactions which change the conductivity of the sensing material and this change depends strongly on different surface sites for the gas interactions. By using noble metals (e.g. Au, Pd, Pt, or Ag) in the nanosize range, modification of the metal oxide surface is achieved. By this surface modification, the gas response maximum can be shifted towards lower operating temperatures and the sensitivity to a certain gas can be increased or decreased depending on the noble metal nanoparticles. In this way, improved selectivity of metal oxide gas sensors can be achieved [80], [81].

In literature, two possible mechanisms are proposed to account for the effects the catalysts and promoters have on the surface reactions. Both mechanisms are shown in Figure 2.7. The first mechanism, known as chemical sensitization, is characterized by the so-called spillover effect. First, the adsorption of the gas molecule on the nanoparticle surface leads to its activation or dissociation. Then the activated gas molecule migrates (spillover) to the metal oxide surface where it reacts with the adsorbed oxygen, leading to a change in the surface conductivity of the metal oxide. The second mechanism, the electronic sensitization, is based on the direct exchange of electrons between the oxidized nanoparticle and the metal oxide. The reaction of the gas molecule with the nanoparticle surface changes the oxidation state of the nanoparticle and alters the surface conductivity of the metal oxide [82].
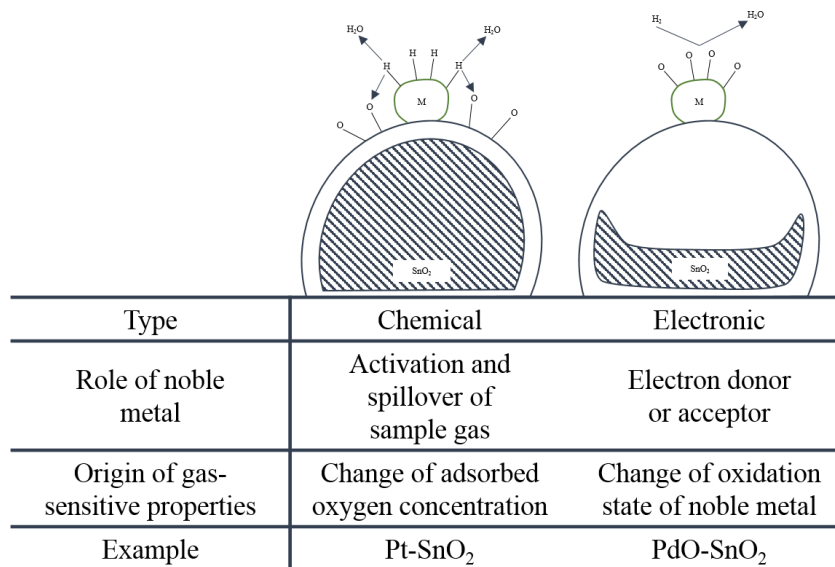
Type	Chemical	Electronic
Role of noble metal	Activation and spillover of sample gas	Electron donor or acceptor
Origin of gas-sensitive properties	Change of adsorbed oxygen concentration	Change of oxidation state of noble metal
Example	Pt-SnO$_2$	PdO-SnO$_2$

Figure 2.7: Chemical and electronic sensitization by noble metals [83].

2.2.2 Filters

Another effective way to improve the sensor selectivity is the use of filters, which can be integrated into the measuring setup or directly on the sensing layer. Depending on the materials which are being used, active and passive filters can be distinguished. For active filters, catalytic films of noble metals (e.g. Pd, Pt) and metal oxides (e.g. Fe$_2$O$_3$, CuO) are fabricated directly on the gas sensing layer for the decomposition of gases [84]. The deposition of a thick porous Pt film on top of a thick Pd-doped SnO$_2$ film showed a reduced cross-sensitivity to ethanol during methane (CH$_4$) detection [85]. The combination of a thick Pd-SnO$_2$ film with a thin sensing layer of Pt-SnO$_2$ allowed the detection of CO and CH$_4$ by reducing the sensitivity to ethanol [86]. Thick metal films directly deposited on the metal oxide layer may shunt the sensing material. An insulating separation layer between the sensing material and the filter extinguishes the influence on the metal oxide resistivity [87].

For passive filters, membranes, porous layers or powders are used for the physical adsorption of gas molecules. Zeolites are often used for passive filters. The pore diameter is in the range of 0.2 to 1 nm and long gas molecules can be stored in the pores [84].

Al_2O_3, SiO_2 and Teflon are other materials used as passive filters, which are used for the adsorption of water vapor or alcohols in CH_4 detection [88], [89]. In commercially available gas sensor devices, activated charcoal is used as a filter inside the sensor cap to eliminate the interference of alcohols and hydrocarbons for CO sensing [90], [91].

2.2.3 Temperature modulation

The sensing properties of semiconductor gas sensors strongly depend on the operating temperature. Selective detection of gases can be achieved if the temperature dependent sensitivity of a gas sensors differs for distinct gases. Temperature modulation is a simple method for improving the selectivity of semiconductor gas sensors, with the reduction of the power consumption being another benefit of the dynamic measurement method [92].

Heilig *et al.* used a 50 mHz sinusoidal modulation of the heater voltage in the temperature range between 200 °C and 420 °C to selectively detect CO and NO_2 with a single SnO_2-based thick film sensor [93].

The influence of temperature modulation with different heating waveforms (e.g. rectangular, triangular, pulse, sinusoidal, saw-tooth) and frequencies on the sensing behavior of a single SnO_2 sensor to ethanol, acetone, butanone, methanol, and formaldehyde was investigated by Huang *et al.* [94].

Temperature modulation in the millisecond range can be achieved by using micro-hotplates. The short temperature pulses enabled the generation of gas specific response patterns/signatures for water vapor, methanol, ethanol, acetone, and formaldehyde. By combining the response signatures with pattern recognition technology, specification of the detected gas with semiconductor gas sensors can be achieved [95].

2.2.4 Electronic nose

An intelligent array of chemical sensors, well known as an electronic nose, is a powerful strategy to discriminate components in a mixture of volatile organic compounds [96]. The first concept for an electronic nose was proposed by Persaud and Dodd in 1982 [97]. In literature, an electronic nose is defined as "an instrument, which comprises an array of

electronic chemical sensors with partial specificity and an appropriate patter-recognition system, capable of recognizing simple, or complex odors" [98].

Electronic noses are sensing systems, which are comprised of three main parts [99]:

- a sampling system for sample conditioning and filtration
- an array of chemical gas sensors, which generate numerous electrical signals due to the different interactions with the sample
- a pattern-classification system for interpretation of the electrical signals using some kind of algorithm

For the fabrication of the sensor array, various gas sensor technologies are available, but currently, only four of the multiple technologies are used for electronic noses. Those four gas sensor types are semiconducting metal oxides, metal oxide semiconductor field effect transistors, conducting organic polymers, and piezoelectric crystals [99].

A variety of pattern recognition approaches using different signal processing techniques, such as fuzzy c-means algorithm (FCMA) [100], artificial neural network (ANN) [101]–[103], self-organizing maps (SOM) and minimum spanning tree (MST) [104], cluster analysis (CA) and cluster validity (CLV) [105], and many more have been developed over the years.

2.3   CMOS integration of metal-oxide-based gas sensors

Since Taguchi commercialized the first metal-oxide-based gas sensor in the early 1970s, many efforts have been made to improve the sensor performance to reduce the fabrication costs and power consumption, and to miniaturize the common gas sensors, which are quite bulky devices. Today, there are several companies – such as Paragon [106], Microchemical Systems [107], City Technology [108], and Figaro [109] – that sell metal-oxide-based gas sensor devices, which almost exclusively are composed of a discrete sensing element and a separate unit for the electronic circuitry [47], [110]. However, combining both components – sensing element and microelectronic circuit – on a single chip, enables the fabrication of low-cost and low-power smart gas sensors. The combination of metal-oxide-based gas sensors with microelectronics would open up high volume markets and solid-state gas sensors could be applied in cars, watches and smart phones [14], [34], [111]. Metal-oxide-based sensors require elevated temperatures for gas detection and standard CMOS technology can be utilized to fabricate a heating platform for the sensing layer, the so called microhotplate. A microhotplate consists of a heating element, thermocouples for temperature regulation, and contact electrodes for the sensing layer. Additionally, a heat spreader can be implemented to ensure uniform heat distribution over the entire surface. Due to the good thermal conductivity of silicon, the microhotplate needs to be thermally isolated from the rest of the chip in a post-CMOS micromachining process (e.g. XeF_2 silicon etching). CMOS microhotplates enable high operating temperatures at comparably low power consumption (< 100 mW), as well as a pulsed temperature mode due to small thermal time constants (in the millisecond range) for enhanced sensor sensitivity and selectivity [112]–[116].

There are two possible approaches for combining gas sensors with electronic circuits: the monolithically integrated system and the hybrid system. In a monolithically integrated system, the sensing layer is combined with the CMOS circuitry on the same chip (single-chip approach). This approach offers advantages such as:

- Cost-effective in high volume production, which makes it commercially attractive.
- Reliable and reproducible performance with reduced noise based on system-on-chip signal processing.
- Small packaging efforts.
- Fabrication of a small footprint sensor array with multiple microhotplates on one single chip.

However, the monolithic system also has some disadvantages. One major disadvantage is the limited number of CMOS-compatible fabrication techniques available for the metal oxide deposition. Temperatures higher than 400 °C in the CMOS post-processing steps for the sensor fabrication have to be avoided. Another disadvantage is the discarding of the complete microsystem due to a defective sensor, although the electronic circuitry may be working properly, lowering the yield and increasing the cost. Hybrid systems use separate chips for the gas sensor and the electronic circuits (multi-chip approach). With this approach the degrees of freedom are higher with regard to deposition techniques and materials for sensor fabrication and optimization. Also, a malfunctioning gas sensor does not lead to the rejection of the whole microsystem, resulting in an enhanced manufacturing yield. The disadvantages of the hybrid approach include an expensive and more complex packaging process, as well as a much higher possibility of parasitic capacitances or resistances due to the required interconnections between the chips, which can result in signal noise and degradation [12], [117]–[120].

This work was performed within the EU-project "MSP - Multi Sensor Platform for Smart Building Management" and the nationally funded project "RealNano − Industrielle Realisierung innovativer CMOS basierter Nanosensoren". The central objective of the MSP project is the 3D-integration of various sensors (gas sensors, particle sensors, IR sensors, UV-A/ UV-B sensors, etc.) with CMOS technology for cost-efficient mass production of miniaturized smart systems for indoor and outdoor environmental monitoring. Through-silicon-via (TSV) technology is employed for the 3D-integration of various sensors on one CMOS platform chip. The goal of RealNano is the industrial

fabrication of CMOS based nanosensors on a full wafer scale by developing an innovative process chain and new production equipment.

In this work, SnO_2 thin film gas sensors were fabricated on CMOS microhotplates by a CMOS-compatible post-processing spray pyrolysis method and subsequent photolithography and etching process steps. The gas sensors can be 3D-integrated on CMOS platform chips for the realization of miniaturized smart systems on a wafer scale. Different deposition techniques for metallic and bimetallic nanoparticles were investigated for the functionalization of the CMOS integrated SnO_2 thin film gas sensors and the influence of these nanoparticles on the sensor performance was evaluated.

III. Experimental

3 SnO$_2$ thin film fabrication by spray pyrolysis

In this work, spray pyrolysis was used to fabricate SnO$_2$ thin films on silicon substrates and CMOS microhotplates. The spray pyrolysis process has been adapted for the integration of SnO$_2$ thin films on CMOS microhotplates in a previous doctoral thesis [121], the deposition temperature has been reduced to be CMOS-compatible and the droplet size has been adjusted to guarantee the CVD-like deposition by spray pyrolysis (see Figure 2.6, sequence C). In this chapter, the spray pyrolysis setup is explained in detail. The results of various characterizations of the deposited SnO$_2$ thin films are presented and discussed.

3.1 Spray pyrolysis setup

For the deposition of SnO$_2$ thin films, a 0.28 molar solution of tin tetrachloride pentahydrate (SnCl$_4$ · 5H$_2$O) in ethyl acetate was prepared. The spray pyrolysis setup is shown in Figure 3.1. An air atomizing nozzle (QuickMist QMJ-SUQF130, Spraying Systems Co. [122]), depicted in Figure 3.2, was used to spray the solution as a fine mist onto the substrates. N$_2$ was used as the carrier gas for the pressure-fed setup and a sheet-type spray pattern was achieved by the employment of a flat spray air cap. The air atomizing nozzle was constructed of PVDF for chemical resistance. A high-temperature titanium hotplate (PZ28-3T, Harry Gestigkeit GmbH [123]), equipped with a program controller (PR5 3T, Harry Gestigkeit GmbH) for fast and accurate temperature regulation, was used to heat the substrates to 400 °C. The deposition rate as well as the droplet size of the mist could be adjusted by applying a certain pressure on the liquid and air inlet, separately. The spray nozzle was equipped with an air pressure switch, which allowed a fast start and stop of the spraying process and therefore, a precise setting of the spray time was achieved. The parameters for the spray pyrolysis process are summarized in Table 3.1.
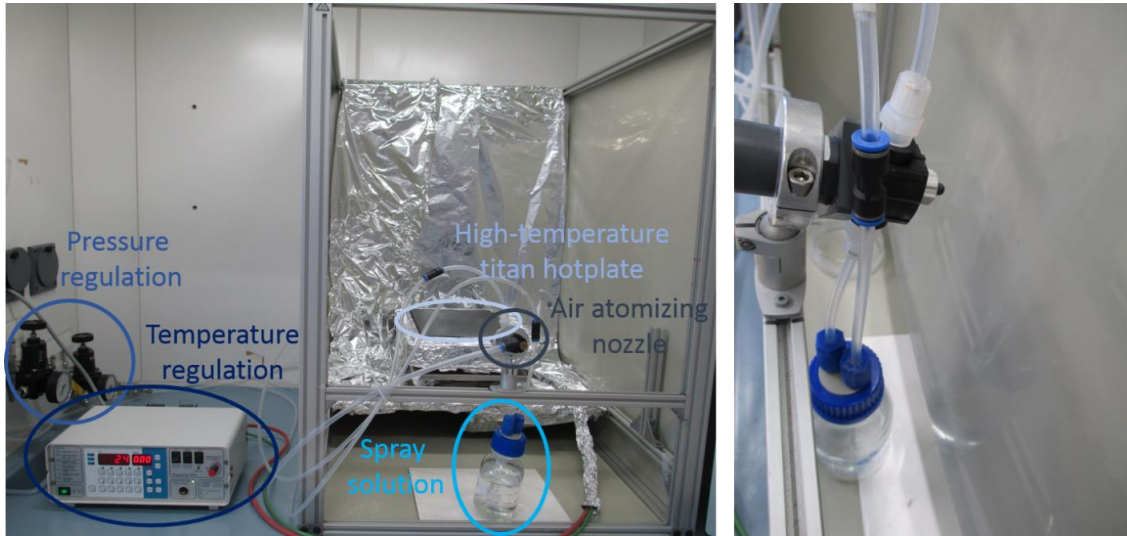
Figure 3.1: Spray pyrolysis setup on the left and close-up of the air atomizing nozzle on the right.

With the spray pyrolysis process parameters in Table 3.1 a deposition rate of 175 nm/min was achieved and the target thickness of 50 nm was deposited after a spraying time of 18 s. On a 40 mm x 40 mm surface, the thickness deviation was ± 2 nm.
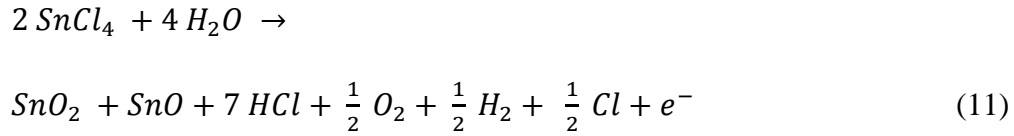
At 400 °C, the tin precursor reacts with the surrounding humidity and high quality SnO_2 thin films are formed by following chemical reaction:

$$SnCl_4 + 2\,H_2O \rightarrow SnO_2 + 4\,HCl \tag{9}$$

According to [124], other side reactions occur during SnO_2 formation. If SnO_2 was the only product of the reaction with water vapor, stoichiometric SnO_2, which is not conductive, would be deposited and could not be used for gas sensing. Incomplete reactions lead to the formation of oxygen vacancies according to

$$2\,SnCl_4 + 4\,H_2O \rightarrow SnO_2 + SnO + 8\,HCl + \frac{1}{2}\,O_2 + 2\,e^- \tag{10}$$
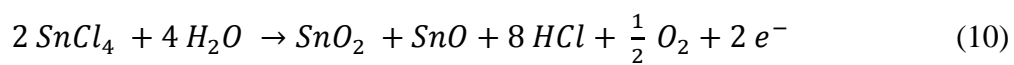
or lead to the formation of residual chloride ions as impurities during the film deposition:

$$2\, SnCl_4 \;+ 4\, H_2O \;\rightarrow$$

$$SnO_2 \;+ SnO + 7\, HCl + \tfrac{1}{2}\, O_2 + \tfrac{1}{2}\, H_2 + \tfrac{1}{2}\, Cl + e^- \tag{11}$$

The oxygen vacancies and chloride ion impurities act as electron donors and make the material electrically conductive.

Other possible reactions, which lead to the formation of SnO_2 films, are [125]:

$$SnCl_4 \;+ O_2 \;\rightarrow SnO_2 \;+ 2\, Cl \tag{12}$$

$$SnCl_4 \;+ 8\, O_2 \;\rightarrow SnO_2 \;+ 6\, H_2O + 4\, CO_2 \tag{13}$$
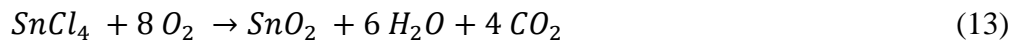
For the fabrication of SnO_2 gas sensors, SnO_2 thin films with a thickness of ~ 50 nm were deposited on 20 mm x 20 mm silicon substrates and CMOS microchips provided by ams AG. A combination of a white light reflectometer (F40-NSR, Filmetrics) and a light microscope (Axio scope.A1, Zeiss) was used to measure the thickness of the deposited SnO_2 layer on native SiO_2/Si substrates. After the deposition, the SnO_2 thin films were amorphous and for the long term stability as well as the sensitivity of the metal oxide thin film an annealing step of 45 minutes at 400 °C was necessary to achieve a stable crystalline structure. Figure 3.3 shows the spray pyrolysis setup during deposition.

Table 3.1: Parameters for spray pyrolysis process.

Parameters	
Temperature of Titan Hotplate	400 °C
Pressure on Liquid	0.35 bar
Pressure of Carrier Gas	1.8 bar
Pressure on Air Pressure Switch	2.5 bar
Horizontal Distance between Sample and Nozzle	29 cm
Vertical Distance between Sample and Nozzle	4.5 cm
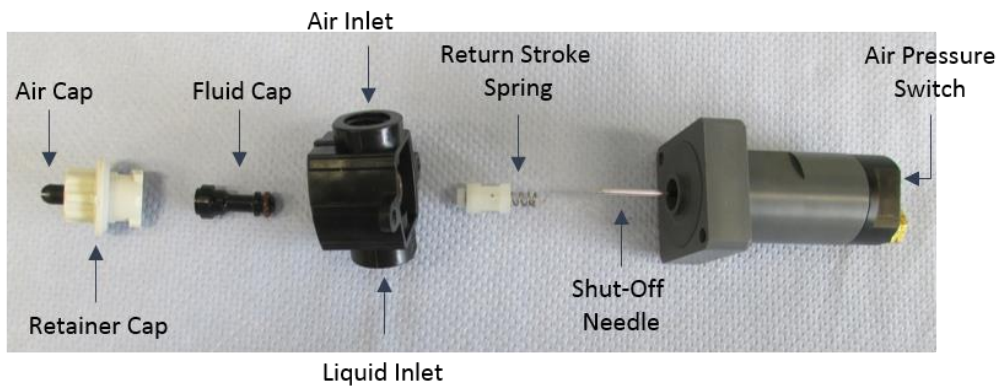
Figure 3.2: Separate parts of air atomizing nozzle used in the spray pyrolysis setup.
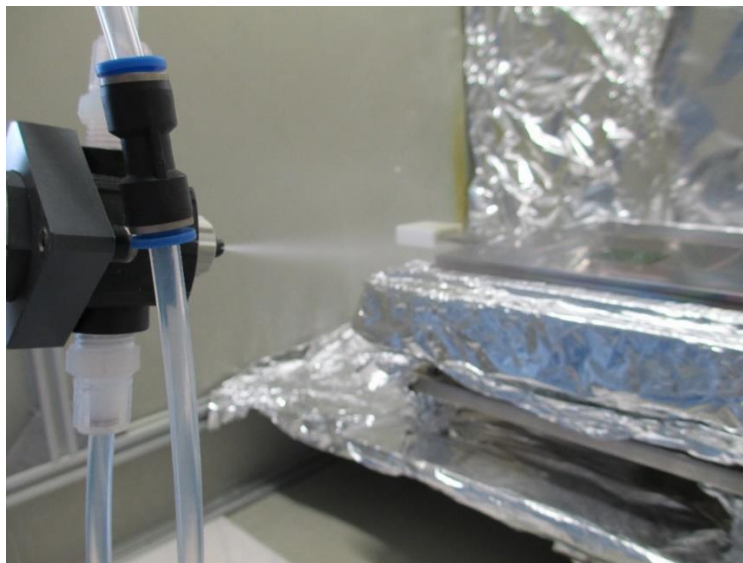
Figure 3.3: Spray pyrolysis setup during deposition of SnO_2 thin films on a 2 x 2 array of silicon substrates.

3.2　Characterization of SnO$_2$ thin film

After the deposition of SnO$_2$ thin films on silicon substrates and CMOS microhotplates, the thin films were characterized by transmission electron microscopy (TEM), and atomic force microscopy (AFM) to determine the morphology of the layer, as well as the roughness of the deposited SnO$_2$ thin film.

3.2.1　Transmission Electron microscopy

The morphology of the SnO$_2$ thin film deposited by spray pyrolysis and annealed at 400 °C for 45 minutes was investigated by TEM. The characterizations were performed at the Austrian Center for Electron Microscopy and Nanoanalysis (FELMI-ZFE [126]). For the characterization, TEM lamellas of the SnO$_2$ thin film were prepared by using a focused ion beam (FIB) lift-out technique (FIB/SEM dual beam microscope; FEI NOVA200). The TEM characterization was performed on an FEI Tecnai F20 with an operation voltage of 200 kV. Figure 3.4 shows the TEM image of the SnO$_2$ thin film deposited on a silicon substrate. The morphology of the SnO$_2$ thin film was also characterized on a CMOS microhotplate (MPW3 microchip) to guarantee the same deposition process on the different substrate, the results of the TEM characterization are shown in Figure 3.5.

A compact crystalline layer is formed by the spray pyrolysis process on both substrates, shown in the high resolution images (Figure 3.4 a and Figure 3.5 a). The layers are polycrystalline with grains showing different orientations and an average grain size of 10 nm. In the Fast Fourier Transform (FFT) images, the reflexes form an arrangement of multiple concentric rings, which confirm the polycrystallinity of the layers and indicate differently oriented grains (Figure 3.4 b and Figure 3.5 b).

a)

SnO₂ layer

20 nm
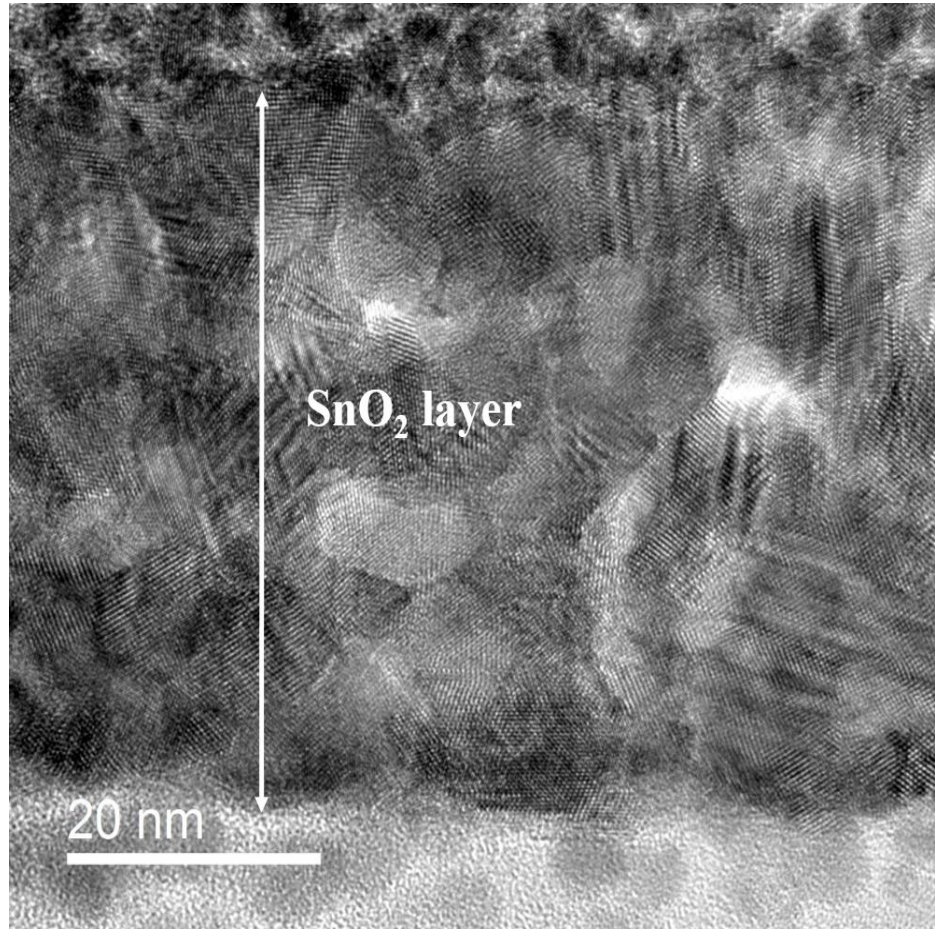
b)
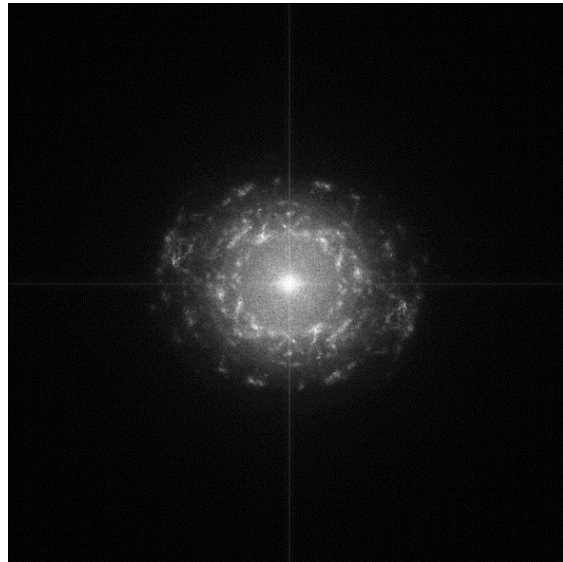
Figure 3.4: Morphology characterization of the SnO$_2$ thin film deposited on a silicon substrate by spray pyrolysis at 400 °C; a) high resolution image, b) Fast Fourier Transform (FFT) image.
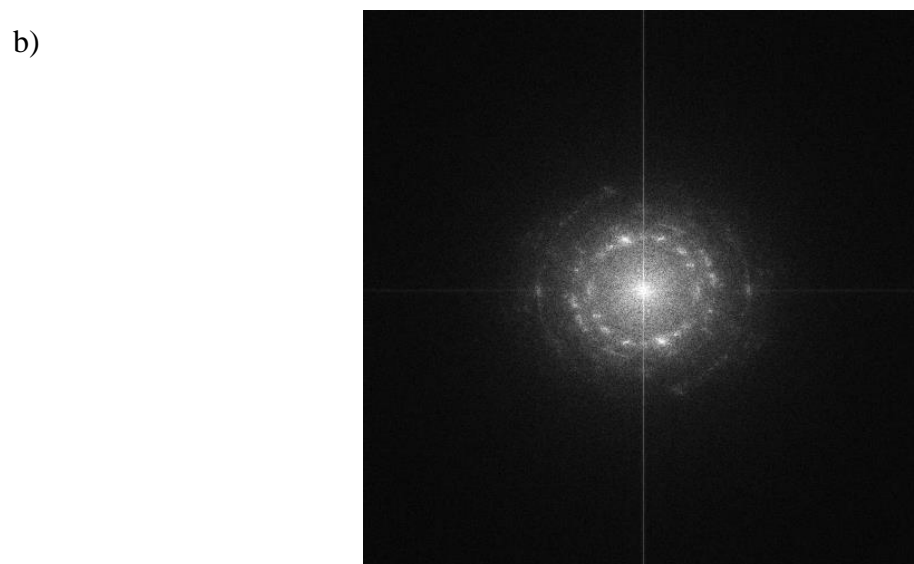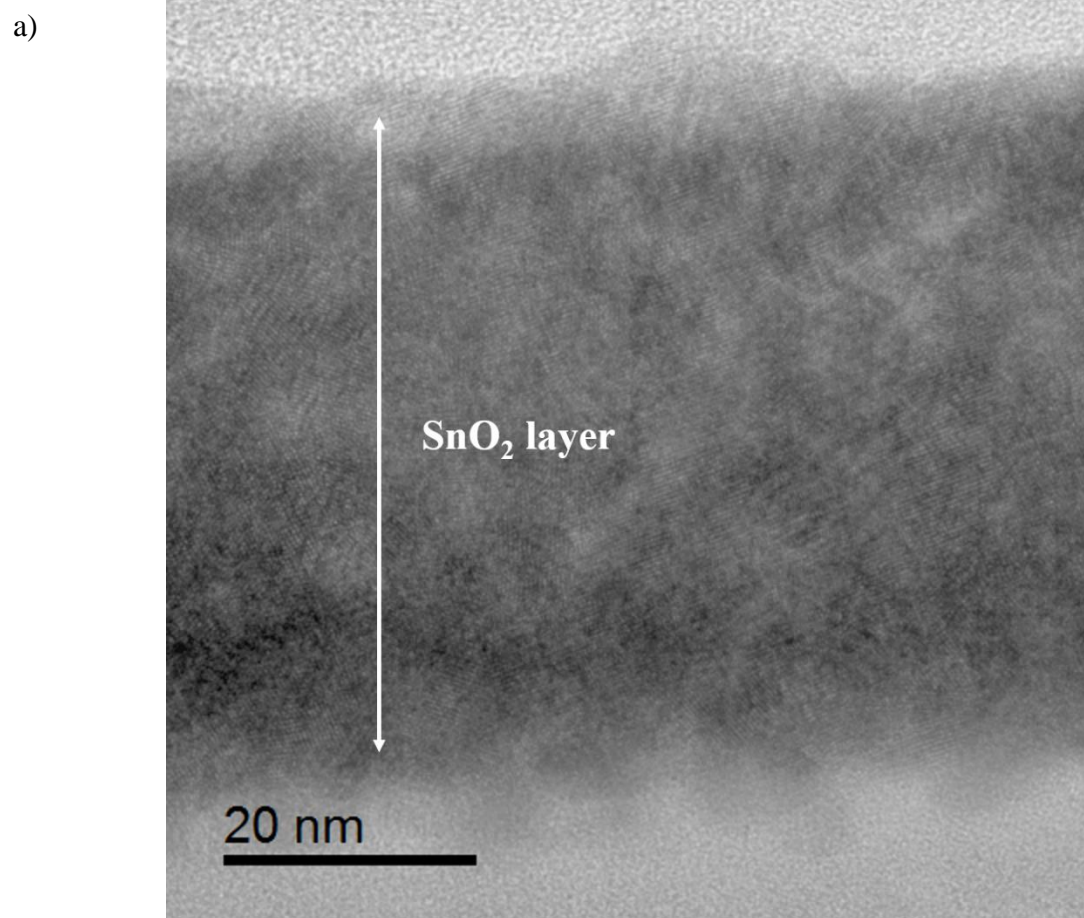
a)

SnO$_2$ layer

20 nm

b)

Figure 3.5: Morphology characterization of the SnO$_2$ thin film deposited on a CMOS microhotplate by spray pyrolysis at 400 °C; a) high resolution image, b) Fast Fourier Transform (FFT) image.

3.2.2 AFM

The surface morphology of the SnO_2 thin film, prepared by spray pyrolysis on a silicon substrate at 400 °C, was examined in detail by AFM (BRR 2770, DME), operated in tapping mode. Measurements of topography were carried out at ambient temperature using a Si cantilever (Arrow-NCR) at a resonance frequency of 245 kHz and a tip curvature radius of $<$ 10 nm. For the precise calculation of the roughness, the measurements were performed at different positions on the sample with a resolution of 256 x 256 pixels. The 2D image recorded at 1.0 μm $\times$1.0 μm in tapping mode is depicted in Figure 3.6.

The AFM images showed that a granular continuous layer over the entire sample surface was prepared. Root mean square (RMS) roughness of the film was obtained from the AFM data, performed at different positions of the sample. With the spray pyrolysis setup, smooth SnO_2 thin films with a mean value of the RMS in the range of 1 nm were deposited on silicon substrates (RMS value of ˜ 0.2 nm).

Additionally, the surface morphology of the SnO_2 thin film deposited on a CMOS microhotplate was also examined by AFM. For measuring the topography of the SnO_2 thin film on a CMOS microhotplate, the same parameters were used as for the SnO_2 thin film deposited on a silicon substrate. The 2D image recorded at 2.0 μm $\times$ 2.0 μm in tapping mode is depicted in Figure 3.7. The same granular continuous layer was deposited on the CMOS microhotplate as on the silicon substrate (see Figure 3.6).
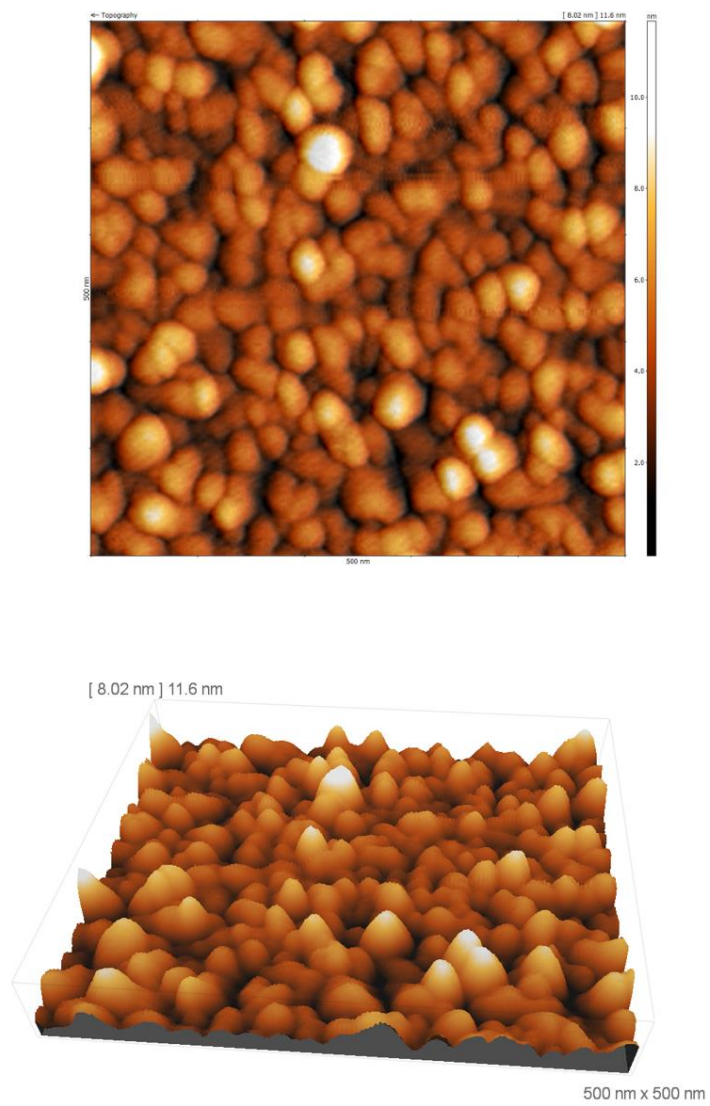
Figure 3.6: AFM image of SnO$_2$ layer on silicon substrate deposited by spray pyrolysis at 400 °C. Top: 2D topography; bottom: 3D topography.
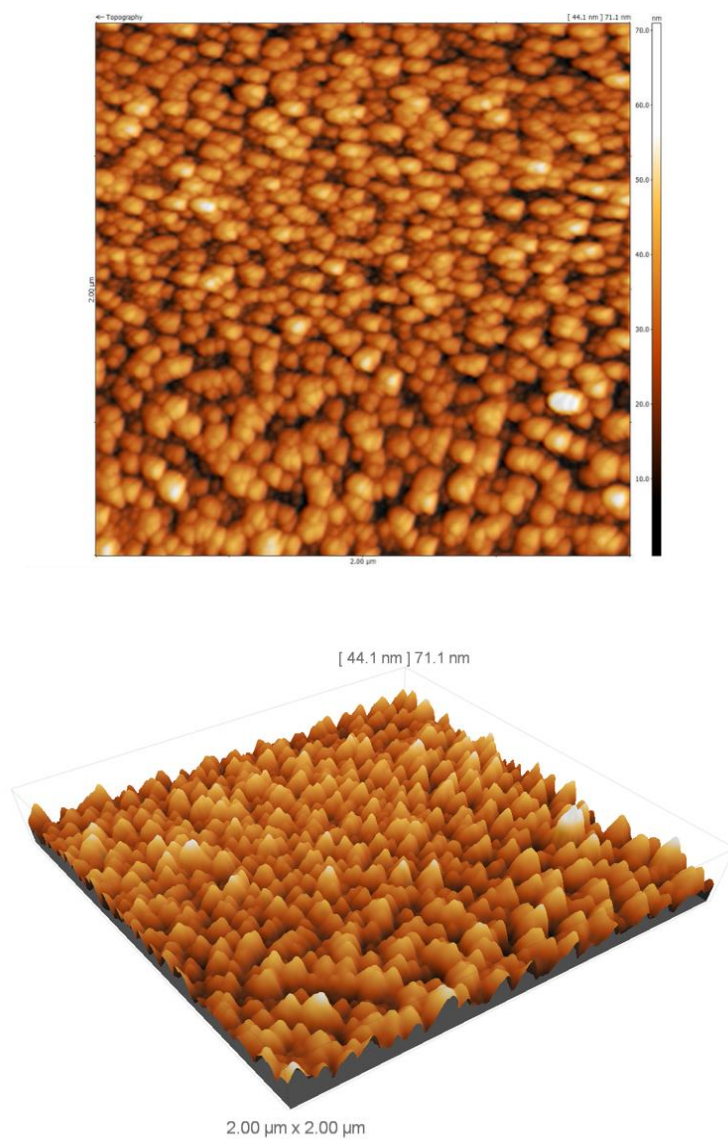
Figure 3.7: AFM image of SnO$_2$ layer on CMOS microhotplate deposited by spray pyrolysis at 400 °C. Top: 2D topography; bottom: 3D topography.

For determining the RMS roughness, AFM images were taken at different positions of the sample. With the use of spray pyrolysis, SnO_2 thin films with a mean value of the RMS in the range of 8 nm were deposited on CMOS microhotplates. The higher RMS values of the thin film on the CMOS microhotplate can be explained by the higher roughness of the substrate, which was characterized by AFM as well (see Figure 3.8). The topography measurements of the bare CMOS microhotplate showed that the mean RMS value was in the range of 8 nm. Through the employment of spray pyrolysis deposition, the SnO_2 thin film followed the shape and roughness of the substrate.
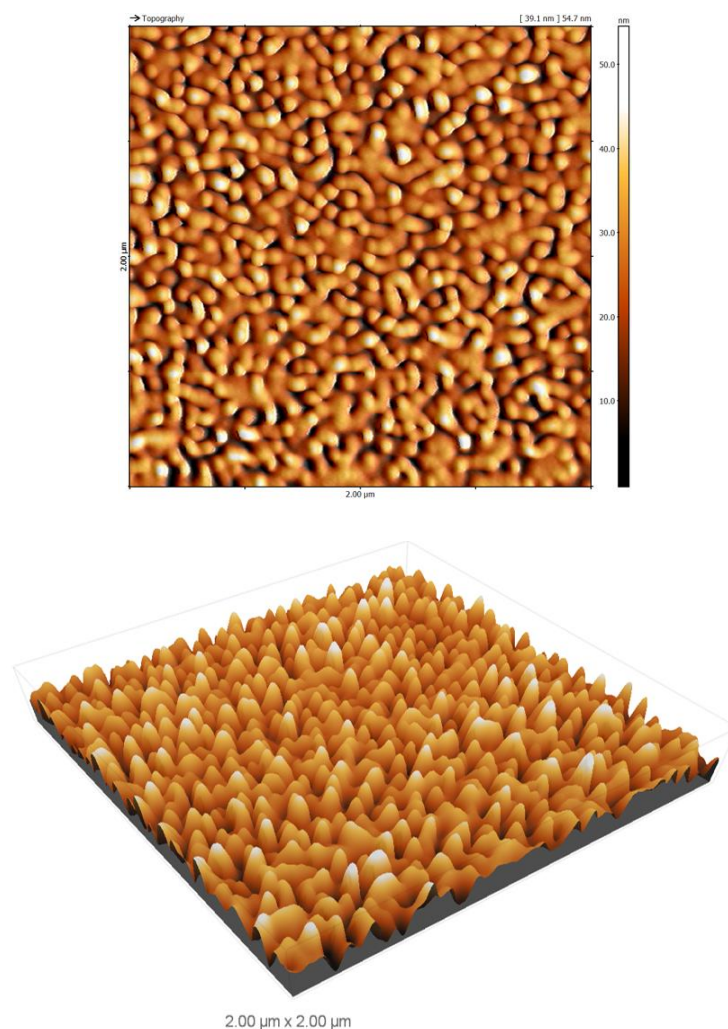
Figure 3.8: AFM image of bare CMOS microhotplate. Top: 2D topography; bottom: 3D topography.

4 Silicon based and CMOS based SnO$_2$ thin film gas sensors

4.1 Silicon based SnO$_2$ thin film gas sensors

For a fast and low-cost investigation of different deposition techniques for nanoparticle solutions and characterization of the influence of different metallic and bimetallic nanoparticles on the sensor performance, SnO$_2$ thin film gas sensors were fabricated on silicon substrates with an insulation layer of 300 nm thermal SiO$_2$ on top.

After deposition of the SnO$_2$ thin film by spray pyrolysis (see Chapter 3.1), the next step in the gas sensor fabrication was patterning the SnO$_2$ layer on the silicon substrate by optical lithography. A positive photoresist (AZ MIR 701, MicroChemicals GmbH) was used for the photolithography process. The pattern that was transferred to the photoresist from a photomask by UV irradiation consisted of an array of rectangles with dimensions of 64 µm x 30 µm (in green, Figure 4.1). A mask aligner (EVG 620, EVGroup) was used for the UV irradiation and for the alignment of the photomask and the substrate. After irradiating and developing (AZ 726MIF, MicroChemicals GmbH) the photoresist, dry physical etching with Ar ions (IonSys 500, Roth und Rau AG) was employed to remove the SnO$_2$ thin film from the areas that were not protected by photoresist. After etching, removal of the photoresist from the remaining SnO$_2$ structures was achieved by O$_2$ plasma treatment. For measuring the resistance of the SnO$_2$ thin film, electrodes in a four-point configuration (in blue, Figure 4.1) were fabricated by another photolithography step followed by the metal evaporation and lift-off. For electrode structuring, a special positive resist was used, which was capable of image reversal to achieve a negative pattern of the mask and is intended for lift-off techniques. Titanium (5 nm) was first deposited as an adhesion layer and gold (200 nm) was used as electrode material. A Univex evaporator (model 450, Leybold AG) was used for the metal deposition. Acetone was used as solvent for the lift-off process. The parameters for the photolithography processes are summarized in Table 4.1 and Table 4.2.

Table 4.1: Photolithography process parameters for SnO_2 pattering.

Spin-coating	
Photo resist	AZ MIR 701
Spin speed [rpm]	4000
Spin duration [s]	35
Baking temperature [°C]	100
Baking duration [s]	60
UV illumination	
Contact mode	Hard contact
Exposure dose [mJ/cm^2]	70
Development	
Developer	AZ 726MIF
Duration [s]	35
Stopper	H_2O

Table 4.2: Photolithography process parameters for electrode fabrication.

Spin-coating	
Photo resist	AZ 5214 E
Spin speed [rpm]	4000
Spin duration [s]	35
Baking temperature [°C]	100
Baking duration [s]	60
UV illumination	
Contact mode	Hard contact
Exposure dose [mJ/cm^2]	80
Post-baking temperature [°C]	100
Post-baking duration [s]	60
Flood exposure [mJ/cm^2]	250
Development	
Developer	AZ 726MIF
Duration [s]	60
Stopper	H_2O
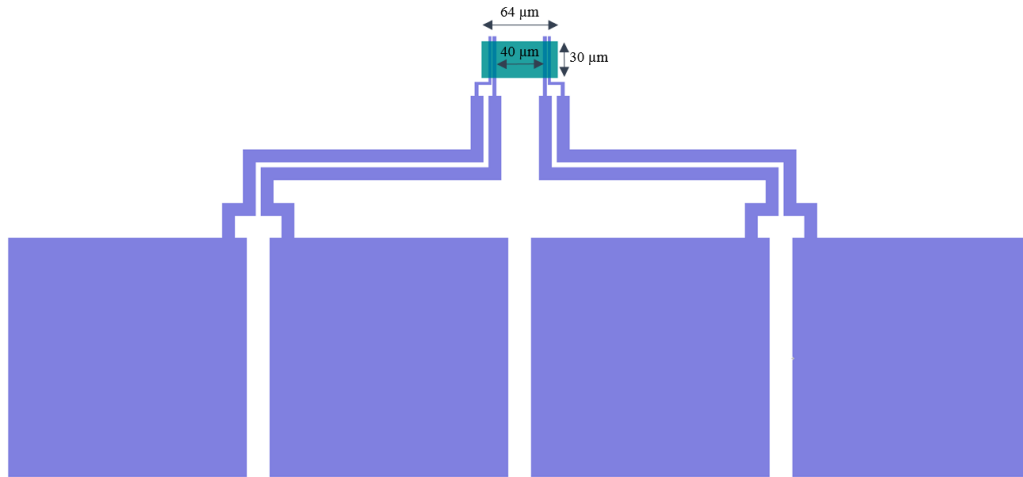
Figure 4.1: Mask design for structuring SnO_2 thin film (in green) and electrodes in four-point configuration (in blue).

For gas detection with metal oxides, elevated temperatures are necessary. Therefore, two discrete platinum heaters (10 x 2 Pt 6.8, Delta R [127]) were used for heating the silicon based SnO_2 gas sensors up to a maximum temperature of 500 °C. A thermocouple (3 x 0.8 Pt 100 B, Delta R) was employed to measure and control the temperature of the resistance heater. To ensure a uniform heat distribution over the entire silicon substrate, a high temperature dielectric ceramic adhesive (Ceramabond 865; Aremco) with high thermal conductivity was used for assembling the silicon based SnO_2 thin film structures together with two discrete heaters and a thermocouple on a bare silicon substrate acting as support material. In the last step of the gas sensor fabrication, the silicon based SnO_2 thin film gas sensor was mounted on a chip carrier. The connecting wires of the two heaters and the thermocouple were soldered to the carrier pads and for the electrical characterization of the SnO_2 thin film the four-point electrode configuration was wire-bonded to the pads on the carrier using Au wires with a thickness of 25 µm (type 5550, F & K DELVOTEC Bondtechnik GmbH).

Figure 4.2 shows the assembled and mounted silicon based SnO_2 thin film gas sensor and a light microscope image of the processed and wire bonded SnO_2 structure is depicted in Figure 4.3.
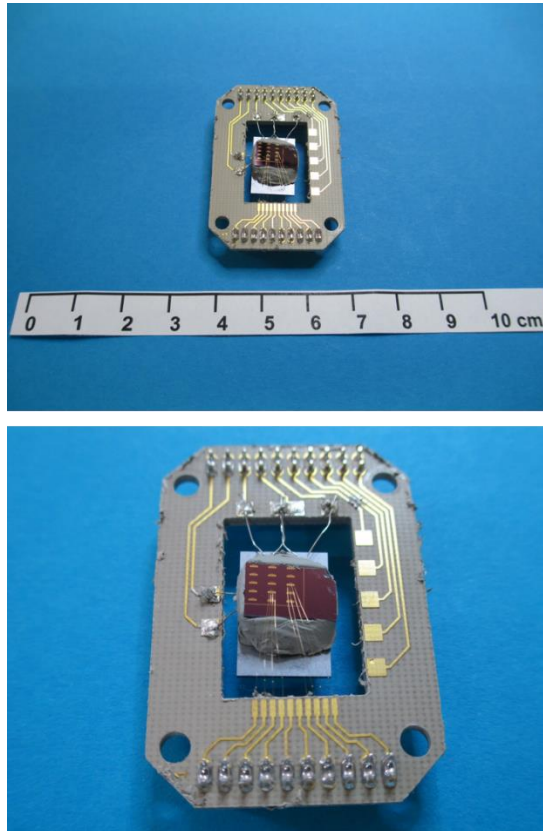
Figure 4.2: Silicon based SnO$_2$ thin film gas sensor mounted on chip carrier.
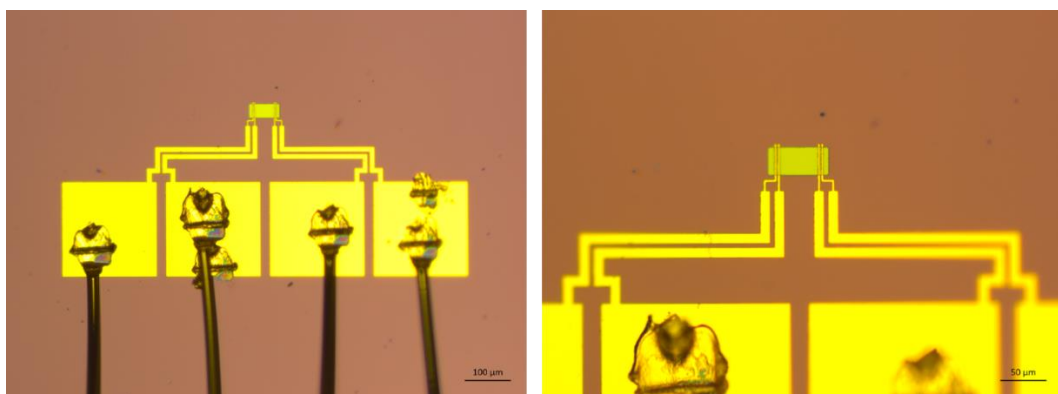
Figure 4.3: Light microscope image of wire bonded silicon based SnO$_2$ thin film gas sensor.

4.2 CMOS based SnO$_2$ thin film gas sensors

In this work, SnO$_2$ thin films were integrated on microhotplates using spray pyrolysis as a compatible CMOS post-processing step. The ams AG [128] fabricated and provided the CMOS microhotplates. Within the EU-project "MSP - Multi Sensor Platform for Smart Building Management" two generations of CMOS microchips were developed and fabricated in a standard 0.35 µm CMOS technology by ams AG:

- First generation: MPW3
- Second generation: MPW4

4.2.1 MPW3

The abbreviation "MPW" stands for multi project wafer, and the idea behind ams' MPW service, which is also known as shuttle runs, is fast and efficient prototyping of CMOS microchips. Several designs from different customers are combined on a single wafer, which results in significant cost advantages by sharing the costs for wafers and masks among different shuttle participants.

The first generation of CMOS microchips within the MSP project, called MPW3, is illustrated in Figure 4.4. On the left, the design of the microchip is depicted and an image taken with a digital microscope (Shuttle Pix P400-R, Nikon) is shown on the right. The microchip, with dimensions of 2.05 mm x 2.05 mm, comprised two microhotplates (µhp), which were suspended in air and connected to the rest of the chip by four arms. The microhotplates were built up by a specific CMOS stack from ams AG. The dimensions of the suspended membrane were 72 µm x 72 µm with a thickness of 8 µm. The two microhotplates only differed in the length of the arms to evaluate the mechanically most stable configuration, with 150 µm for the "large" microhotplate and 50 µm for the "small" microhotplate and a width of 12 µm for both microhotplates. Two sensor layers could be fabricated on one membrane and each sensor layer was contacted by four metal contacts for a four-point measurement. The metal contacts were composed of tungsten and each contact was formed by eight subunits (tungsten plugs).
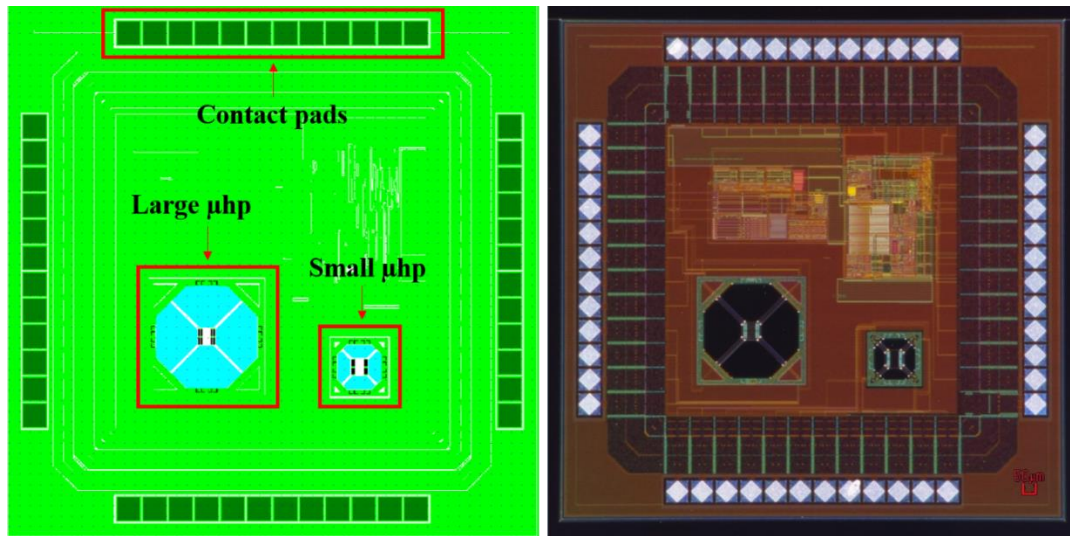
Figure 4.4: Design of MPW3 microchip on the left (blue area depicts under-etched region; ~ 80 µm depth) and digital microscope image of MPW3 microchip on the right.

For heating the microhotplate a polysilicon heater was used and a uniform heat distribution over the whole microhotplate surface was achieved by a metal heat spreader. Rapid heating to temperatures of up to 400 °C were achieved with rise/fall times of under 10 milliseconds [129]. The power consumed of the MPW3 microhotplate to reach temperatures between 150 °C and 400 °C is illustrated in Figure 4.5. For heating the MPW3 microhotplate to 400 °C, a power of 13.5 mW was required.

The fabrication process for CMOS based SnO_2 thin film gas sensors was similar to the fabrication process of silicon based SnO_2 thin film gas sensors. On a stepfield of 20 mm x 20 mm, which contained two MPW3 microchips for gas sensor fabrication, SnO_2 was deposited by spray pyrolysis (see Chapter 3.1). After annealing the thin film at 400 °C for 45 minutes, the SnO_2 thin film was patterned by photolithography (see Table 4.1) and SnO_2 was removed from the unprotected areas on the CMOS microchip by dry physical Ar ion etching (IonSys 500, Roth und Rau AG). In the next step, the patterned SnO_2 structures were protected in another photolithography step using the same photoresist and process parameters as for patterning. The MPW3 microchips were cut from the 20 mm x 20 mm stepfield by ams AG. The microhotplates were released in a dry and isotropic etching process using XeF_2 by an external partner (memsstar Limited).
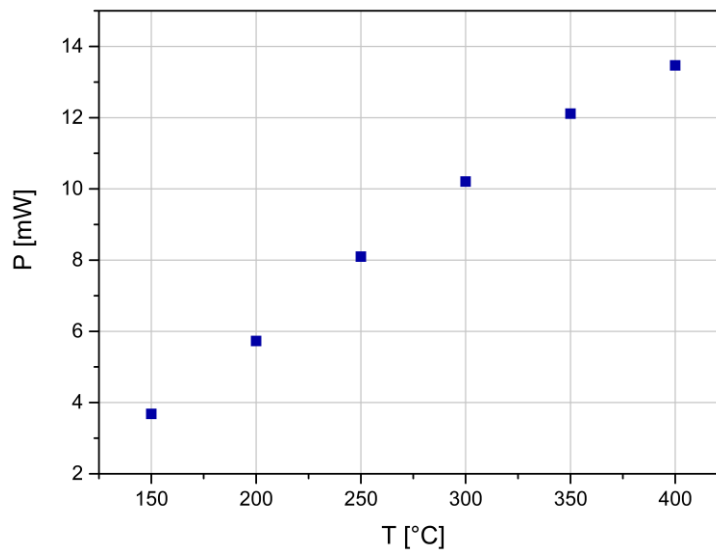
Figure 4.5: Required power for heating MPW3 microhotplate to temperatures between 150 °C and 400 °C.

After releasing the microhotplates, the photoresist protection layer on the SnO_2 structures was removed by oxygen plasma. The patterned SnO_2 thin film on top of the underetched microhotplate was characterized by scanning electron microscopy (Auriga 40, Zeiss SMT) and the characterizations are shown in Figure 4.6.

In Figure 4.6, the top image shows the two patterned SnO_2 sensing layers, each with dimensions of 64 µm x 30 µm, on the MPW3 microhotplate and a side view of the under-etched MPW3 microhotplate is shown in the bottom image. The last step of the fabrication process was performed at ams AG. The MPW3 microchip was glued (Ablebond 8290, Ablestik) on a chip carrier (designed by mb Technologies GmbH) and contacting pads on the microchip were bonded to the carrier pads using aluminum wires (25 µm thickness) by wedge bonding (Bondjet 810, Hesse). Figure 4.7 shows a mounted and wire-bonded CMOS based SnO_2 thin film gas sensor.
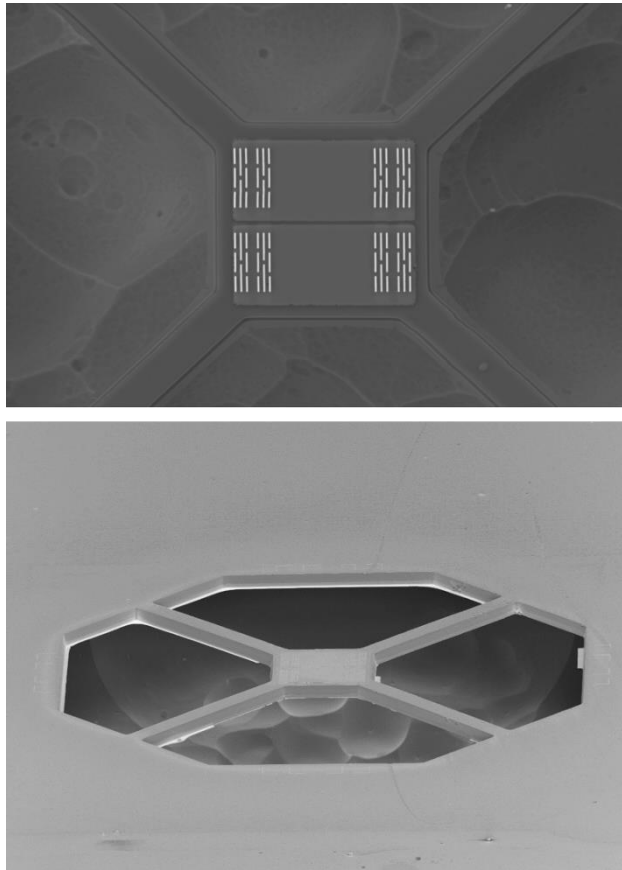
Figure 4.6: SEM image of SnO_2 sensing layers on MPW3 microhotplate (top) and side view of released MPW3 microhotplate (bottom).
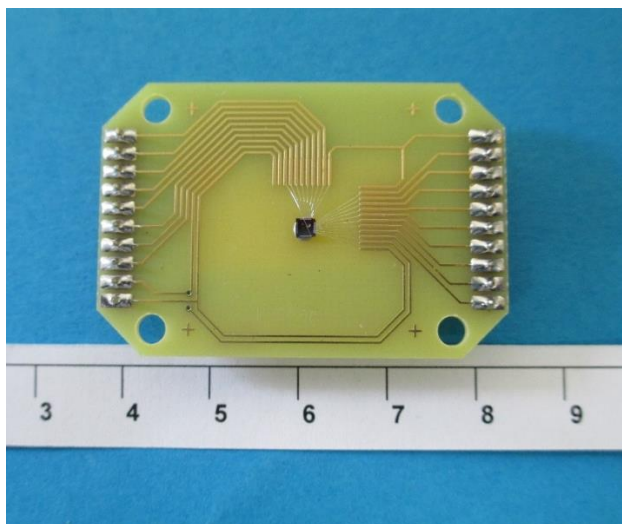
Figure 4.7: CMOS based SnO_2 thin film gas sensor integrated on MPW3 mounted and wire-bonded onto chip carrier.

4.2.2 MPW4

The second generation of CMOS microchips, called MPW4, was developed and fabricated within the MSP-project by ams AG for realizing the 3D-integration of gas sensors along with other sensors (e.g. particle sensor, IR sensor, UV-A/B sensor, etc.) on one smart multi-sensor platform, which was the project's central objective. Through-silicon-via (TSV) technology was employed for achieving the 3D-integration of the gas sensors on a platform chip. The second generation differed from the first generation in the number of microhotplates incorporated on the microchip, the material used for the contacting electrodes, and the application of TSVs for 3D-integration. The worldwide unique MPW4 microchip was comprised of eight microhotplates, which could be heated and characterized individually. The dimensions of the microchip were 5.1 mm x 4.65 mm. On each microhotplate, two sensing layers were processed.

For the MPW4, gold electrodes (Ti / Au = 10 nm / 200 nm) in a four-point configuration – fabricated in a CMOS post-processing step – were used for contacting the sensing layer because of better long-term thermal stability compared to tungsten plugs, which were used in the first generation. The MPW4 microchip is shown in Figure 4.8. On the left, the design of the microchip is illustrated and a digital microscope image is shown on the right. Figure 4.9 depicts the power consumed of the MPW4 microhotplate to reach temperatures between 150 °C and 400 °C. For heating the microhotplate to 400 °C, a power of 14.1 mW was required.

SnO_2 thin film gas sensors were fabricated on MPW4 microchips as well. The top layer on the MPW4 microhotplate differed from the top layer on the MPW3 microhotplate. To ensure that the same process parameters of the spray pyrolysis deposition (see Chapter 3.1) can be used and result in the same layer thickness and morphology, the SnO_2 thin film deposited on a MPW4 microchip was characterized by TEM. The high resolution image and the FFT image are shown in Figure 4.10.
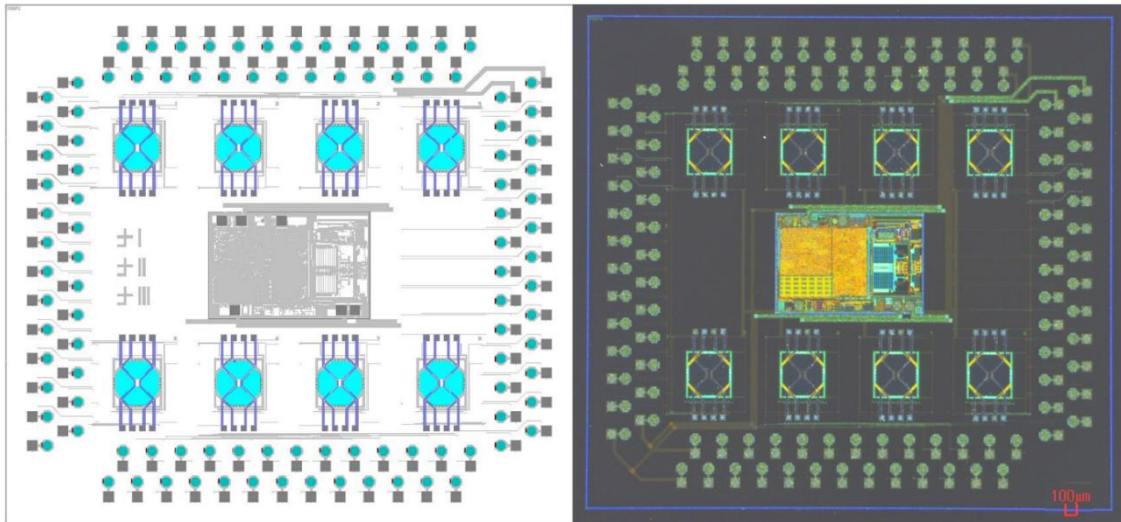
Figure 4.8: Design of MPW4 microchip on the left (blue area depicts under-etched region; ~ 80 µm depth) and digital microscope image of MPW4 microchip on the right.
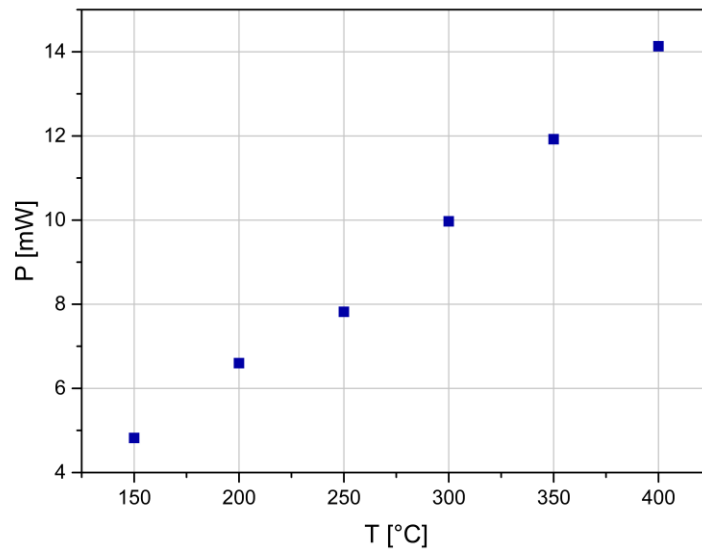

Figure 4.9: Required power for heating MPW4 microhotplate to temperatures between 150 °C and 400 °C.
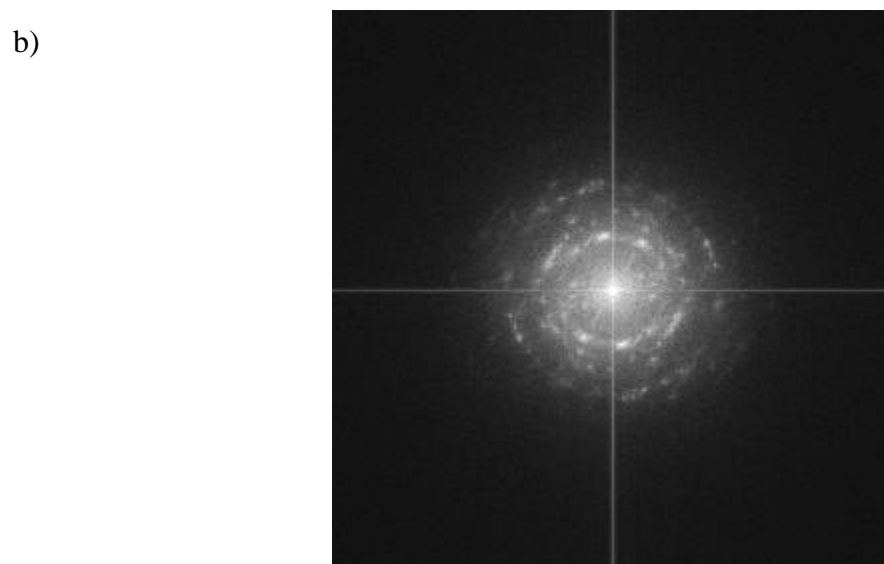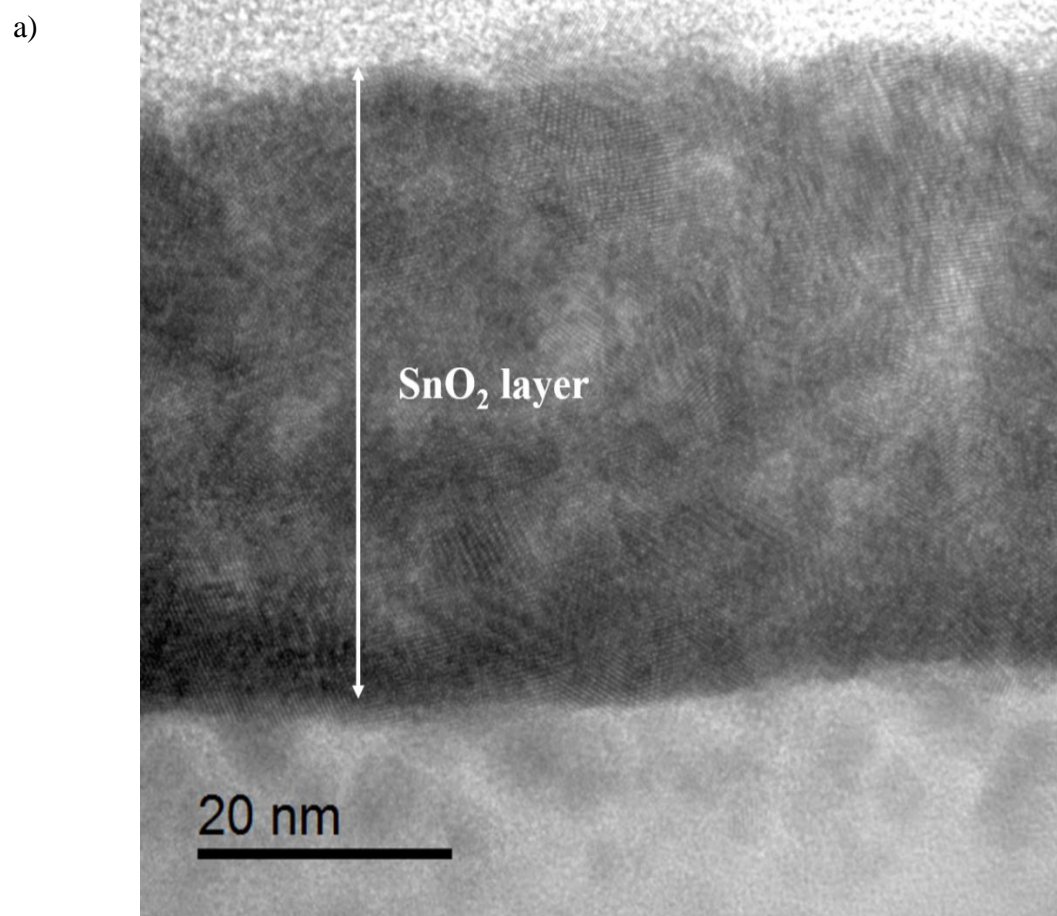
a)

b)

Figure 4.10: Morphology characterization of the SnO$_2$ thin film deposited on a MPW4 microhotplate by spray pyrolysis at 400 °C; a) high resolution image, b) Fast Fourier Transform (FFT) image.

A compact layer of SnO_2 is deposited by spray pyrolysis on the MPW4 microchip. The SnO_2 thin film is polycrystalline, formed by grains with different crystal orientations and an average grain size of 10 nm. The TEM images confirm that the same process parameters can be used for depositing SnO_2 thin films on MPW4 microhotplates by spray pyrolysis. The same process steps as for the MPW3 microchip were used for fabricating SnO_2 thin film gas sensors on MPW4 microchips. Figure 4.11 shows the fully processed CMOS based gas sensor integrated on MPW4 microchip characterized by SEM, depicting two sensor layers on one hotplate, each with a length (L) of 64 µm and a width (W) of 30 µm. A mounted and wire bonded MPW4 microchip on a chip carrier is depicted in Figure 4.12.
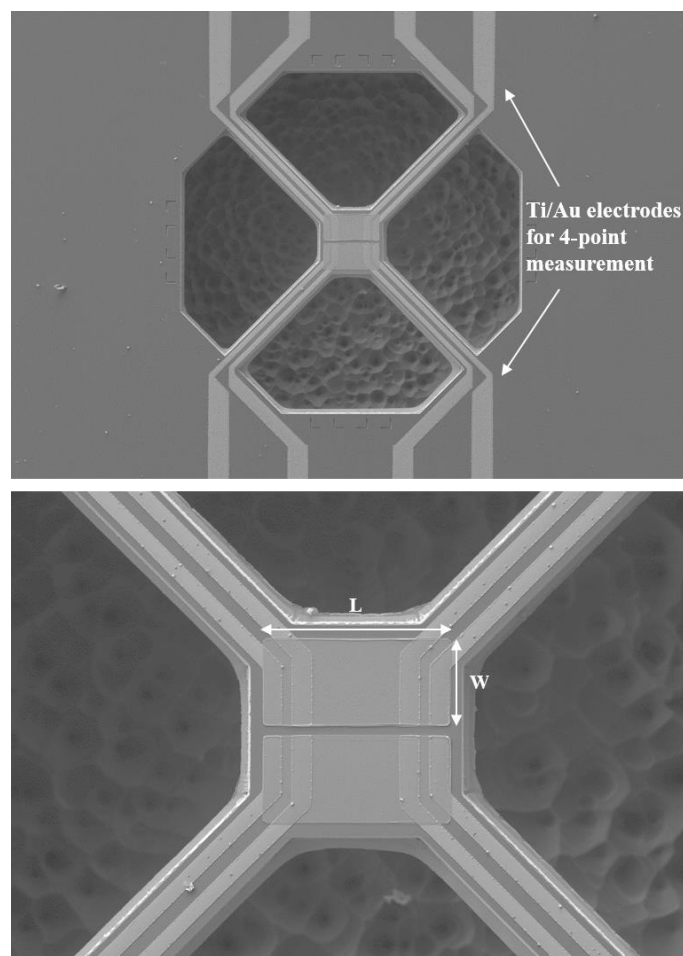
Figure 4.11: SEM image of SnO_2 thin film gas sensor on released MPW4 microhotplate.
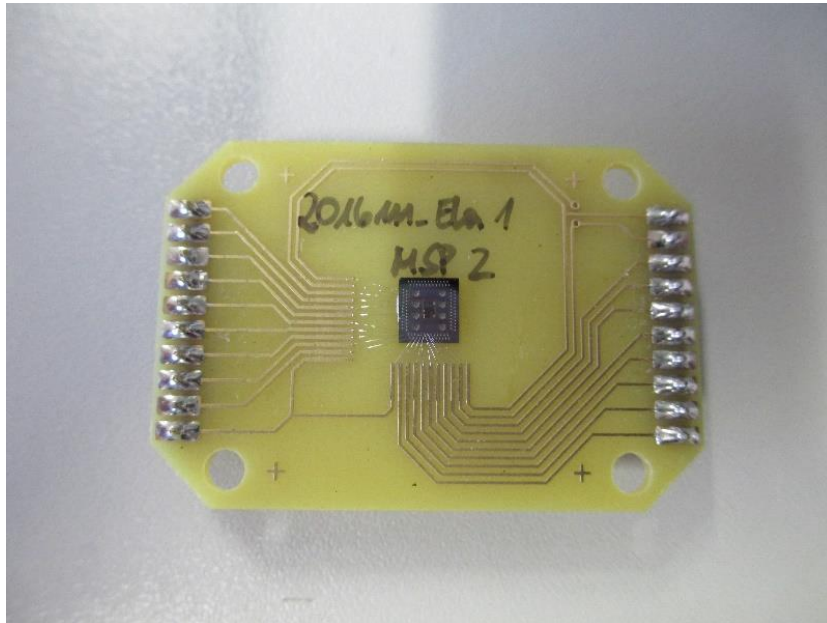
Figure 4.12: CMOS based SnO_2 thin film gas sensor integrated on MPW4 mounted and wire-bonded onto chip carrier.

5 Functionalization of SnO₂ thin film

Gas sensors based on metal oxides, including SnO_2, ZnO, and WO_3, respond to various compounds. The selectivity of these sensors is low and due to this cross-sensitivity, a differentiated detection of a particular gas in a gas mixture is not possible. One strategy to enhance the sensor's sensitivity and selectivity towards a specific gas is to use small amounts of catalysts or additives in the form of noble metals (e.g. Pt, Au, Pd, and Ag). Either the additives can be dispersed within the metal oxide layer or can be used to functionalize the surface of the sensing layer [130]–[133]. In this work, metallic and bimetallic nanoparticles were used for surface functionalization of the SnO_2 thin film and to fabricate thin film − nanoparticle heterostructures. Different methods for depositing nanoparticles on silicon based and CMOS based SnO_2 thin film gas sensors were investigated. In this chapter, the different nanoparticles and the deposition methods used for functionalizing SnO_2 thin film gas sensors are summarized and explained in detail.

5.1 Metallic and bimetallic nanoparticles

5.1.1 Au nanoparticles

Au nanoparticles in solution were provided by one of the project partners, CAN GmbH (Hamburg), within the RealNano-project. The nanoparticle solution, with a concentration of 213 µg/mL, was synthesized by a seeded growth approach. Sodium citrate was used for stabilizing the nanoparticle solution and water was used as solvent. Figure 5.1 shows high resolution TEM images of the Au nanoparticles. The Au nanoparticles are spherical with a diameter of 20 nm ± 5 nm.

5.1.2 NiPt nanoparticles

NiPt nanoparticles were also provided by CAN GmbH. The nanoparticles were synthesized in solution, with a concentration of 15 mg/mL, by a reduction method in batch using toluene as solvent and oleic acid (OA) as stabilizer. High resolution images of the NiPt nanoparticles are shown in Figure 5.2. The NiPt nanoparticles are spherical with a diameter of 2 nm ± 0.5 nm. The bimetallic nanoparticles are composed of approximately 85 % platinum and 15 % nickel.
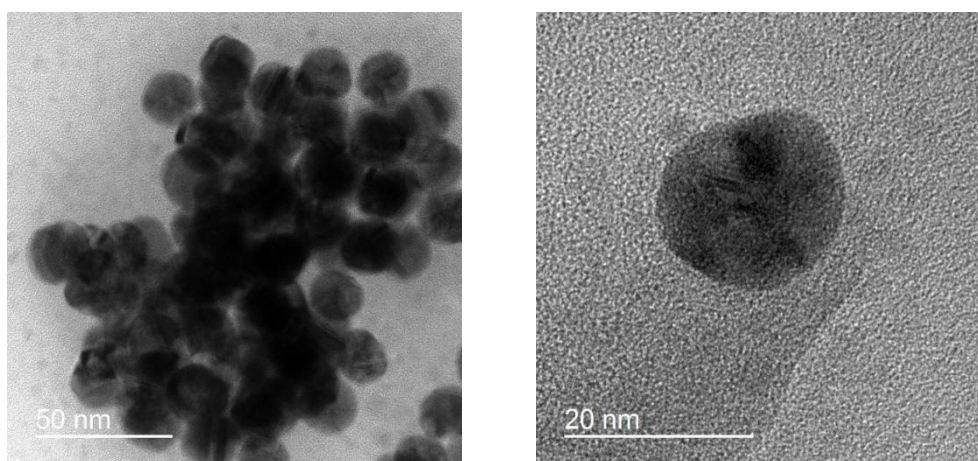
Figure 5.1: High resolution TEM images of citrate stabilized Au nanoparticles from CAN GmbH.
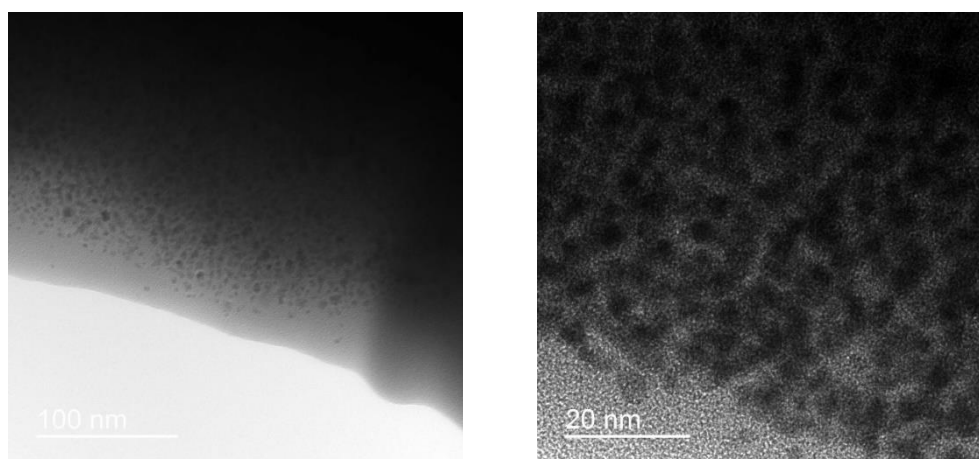
Figure 5.2: High resolution TEM images of OA / OLA stabilized NiPt nanoparticles synthesized by CAN GmbH.

5.1.3 AuPd nanoparticles

AuPd nanoparticles were provided by the University of Freiburg, a project partner within the MSP-Project. The bimetallic nanoparticle solution, with a concentration of 307 µg/mL, was synthesized by a water-in-oil microemulsion method with a molar ratio of Pd to Au of 3 to 7. The nanoparticles were stabilized in solution by using a non-ionic surfactant (Brij® L4) and n-heptane as solvent for the oil-phase. Figure 5.3 shows the TEM characterization of the AuPd nanoparticles; the nanoparticles are spherical and well separated with a diameter of 5 nm ± 3 nm.
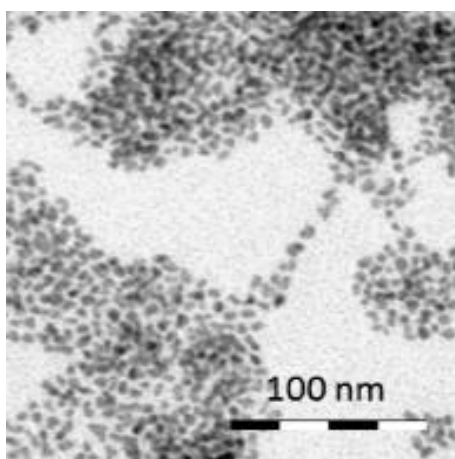
Figure 5.3: TEM image of Brij® L4 stabilized AuPd nanoparticles synthesized by University of Freiburg.

5.1.4 AuPt nanoparticles

AuPt nanoparticles were acquired commercially from the company Particular GmbH. The nanoparticles were synthesized in solution by a physical approach. The fabrication method was based on laser ablation and did not require any chemical precursors. The nanoparticles were electrostatically stabilized in the solution and therefore no chemical stabilizers or surfactants were required. The concentration of the nanoparticle solution was 250 µg/mL. High resolution TEM images of the AuPt nanoparticles are shown in

Figure 5.4. By the laser ablation method, spherical nanoparticles with a diameter of 12 nm ± 4 nm are synthesized.
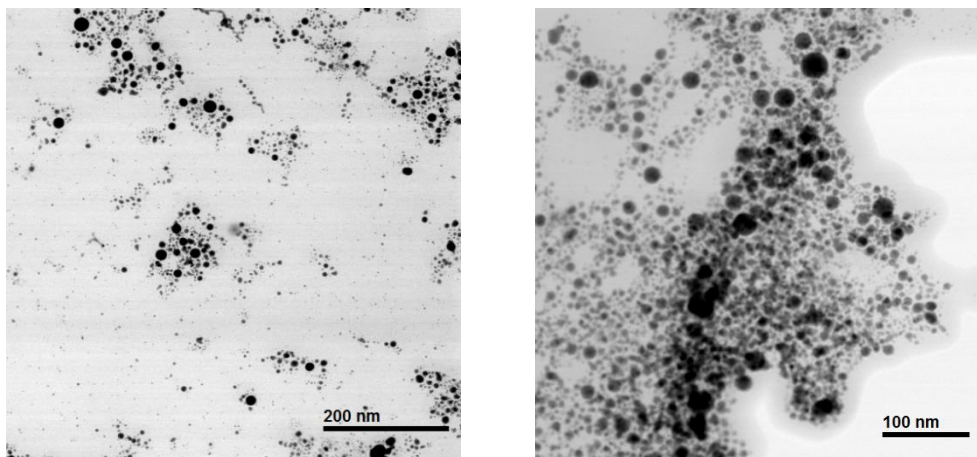

Figure 5.4: High resolution TEM images of electrostatically stabilized AuPt nanoparticles from Particular GmbH.

5.2   Functionalization by inkjet printing

Silicon based and CMOS based SnO_2 thin film gas sensors were functionalized with Au, NiPt and AuPd nanoparticles by inkjet printing. The nanoparticle solutions were used as provided by CAN GmbH and University of Freiburg for the printing process, without adding any additives for adjusting viscosity and surface tension of the nanoparticle solutions.

A Dimatix Material Printer from Fujifilm (DMP-2831) was used for inkjet printing. The DMP printer used piezo-driven, disposable, and user-fillable cartridges with a volume capacity of up to 1.5 mL. The cartridge comprised 16 nozzles, which had an orifice diameter of 21 µm, with a spacing of 254 µm in between the nozzles. The nozzles could be operated simultaneously as well as individually. A vacuum plate, which could be heated up to 60 °C, was used for securing the substrate. Substrate alignement and substrate inspection was achieved with a fiducial camera [134], [135]. These experiments were performed in the laboratories of the project partner EVGroup.

For printing the nanoparticle solutions, cartridges with a drop volume of 10 pL were used. The nozzle parameters, firing frequency and firing voltage, were adjusted to the respective nanoparticle solution to achieve stable drop formation with a drop velocity of $7 - 9$ m/s. The deposition of the nanoparticle solutions on the SnO_2 thin film was performed at room temperature. As already mentioned in Chapter 5.1.3, AuPd nanoparticles were synthesized by a microemulsion method, which required a high concentration of the non-ionic surfactant. To reduce the amount of surfactant in the emulsion, the AuPd nanoparticle emulsion was extracted with a polar solvent before printing and the viscosity was optimized for inkjet printing by diluting the surfactant-depleted emulsion with toluene. Au and NiPt nanoparticle solutions were printed without any pre-treatment. AuPt nanoparticles could not be deposited by inkjet printing because no stable drop formation was achieved due to the high evaporation rate of acetone which resulted in the drying of the jetting fluid system at the nozzle / air interface. Figure 5.5 and Figure 5.6 show a light microscope image of a CMOS based SnO_2 thin film gas sensor before and after deposition of NiPt nanoparticles by inkjet printing.
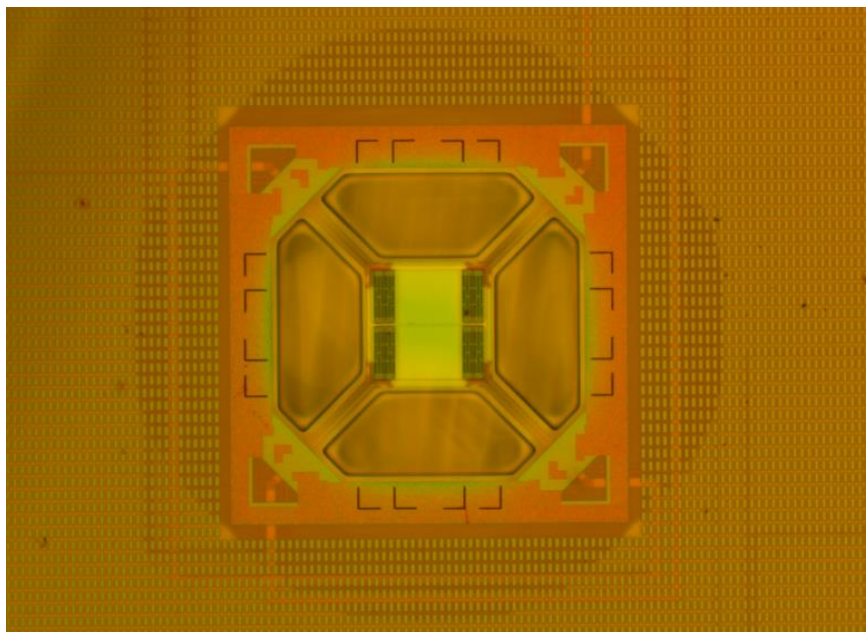
Figure 5.5: Light microscope image of small MPW3 microhotplate before nanoparticle deposition by inkjet printing.
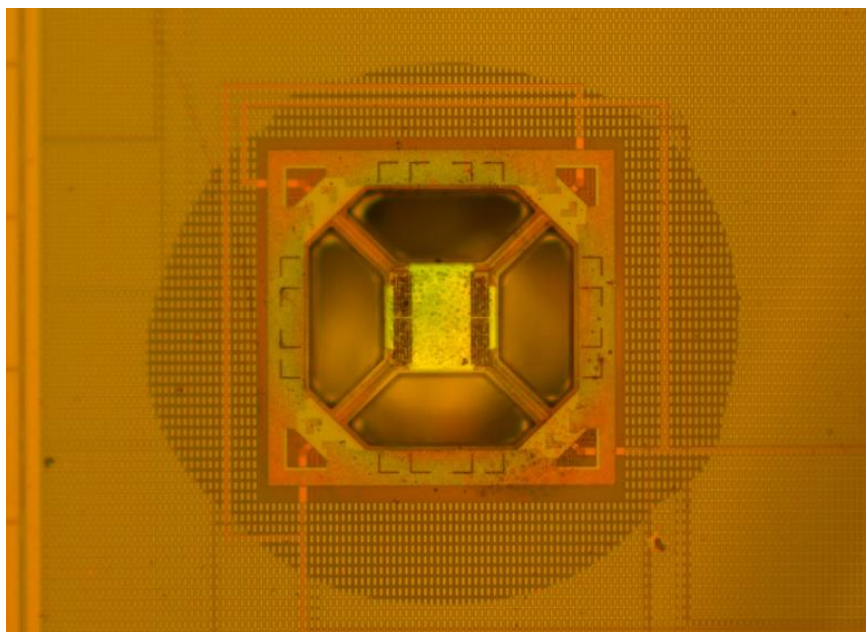
Figure 5.6: Light microscope image of small MPW3 microhotplate after NiPt nanoparticle deposition by inkjet printing.

5.3 Functionalization by spotting

AuPt nanoparticles were deposited on CMOS based SnO_2 thin film gas sensors using a non-contact, drop-on-demand spotter tool from Scienion AG (sciFLEXARRAYER SX, Scienion AG). These experiments we performed by courtesy of Scienion AG. A sciDROP PICO dispensing unit with an uncoated piezo dispensing inert glass capillary (PDC 60) was used for the deposition of the nanoparticle solution [136], [137]. A stable drop formation with a drop volume of 60 pL was achieved by applying a voltage of 61 V to the ceramic piezo element. The deposition was performed at 20 °C and a 10 x 10 test pattern array with a dot pitch of 150 µm was deposited on glass substrates before depositing the nanoparticle solution on CMOS based SnO_2 thin film gas sensors. Due to the fast evaporation of acetone, the 10 x 10 array was not visible anymore after spotting, but the spotting process of the nanoparticle solution was captured with a CCD camera. Figure 5.7 depicts the drop formation and the spotting process of the AuPt nanoparticle solution on a glass substrate.
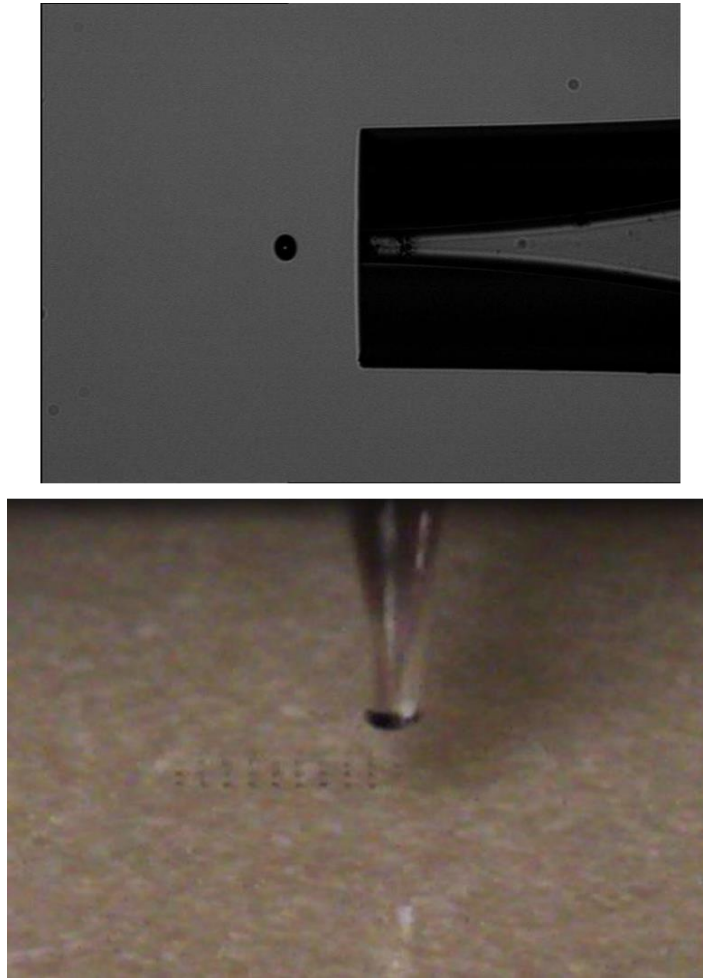
Figure 5.7: Drop formation (top) and spotting process (bottom) of AuPt nanoparticle solution captured with CCD camera.

5.4 Functionalization by sputtering

In addition to the previously described deposition of nanoparticles in solution by inkjet printing and spotting, sputtering technology was utilized to simultaneously synthesize and deposit nanoparticles. The functionalization of CMOS based SnO_2 thin film gas sensors was performed at the Okinawa Institute of Science and Technology Graduate University (OIST) in Japan. The nanoparticle deposition and characterization was performed by Stephan Steinhauer and Vidyadhar Singh. A magnetron sputtering inert-gas condensation deposition system operated in high-vacuum (Mantis Deposition Ltd UK) was used for functionalizing the sensing layer with Pt nanoparticles with sizes of 1.5 nm and 3 nm. A

detailed description of this approach and the latest achievements in this field can be found in the review article by Grammatikopoulos *et al.* [138]. The in-line quadrupole mass filter (QMF) was used for the size selection of nanoparticles. For characterizing the size, shape and surface coverage, the nanoparticles were additionally deposited on TEM grids and silicon substrates alongside the CMOS based SnO_2 thin film gas sensors. Table 5.1 summarizes the deposition parameters for the differently sized nanoparticles.

The deposited nanoparticles were characterized with an FEI Titan G2 Environmental TEM, operated at 300 kV. Automated image analysis (Image J software) was used to obtain size distributions from TEM micrographs. CMOS based SnO_2 gas sensors were functionalized with Pt nanoparticles with mean nanoparticle diameters of 1.5 nm and 3 nm, respectively. Furthermore, the nanoparticle areal densities were determined using the image analysis software. For the Pt nanoparticles with a size of 1.5 nm, an areal density

Table 5.1: Process parameters for nanoparticle deposition by magnetron sputtering inert-gas condensation.

Pressure settings	
Base pressure, before deposition [mbar]	10^{-8}
Main chamber pressure, during deposition [mbar]	10^{-4}
Aggregation zone pressure, during deposition [mbar]	10^{-1}
Rotation substrate holder [rpm]	2
Deposition parameters for 1.5 nm Pt nanoparticles	
Magnetron power [W]	3
Ar flow [sccm]	70
He flow [sccm]	5
Aggregation length [mm]	80
Deposition time [min]	20
Deposition parameters for 3 nm Pt nanoparticles	
Magnetron power [W]	7
Ar flow [sccm]	70
Aggregation length [mm]	100
Deposition time [min]	10

of ~ 4630 µm^{-2} was calculated, and for 3 nm Pt nanoparticles, the areal density was calculated to be ~ 8670 µm^{-2}. The TEM characterizations of both 1.5 nm and 3 nm Pt nanoparticles are shown in Figure 5.8 a and b, respectively. A MultiMode 8 from Bruker, operated in tapping mode, was used for AFM measurements of the Pt nanoparticles on silicon substrates. The surface coverage of 1.5 nm and 3 nm Pt nanoparticles, which depends on the size distribution and the areal density of the nanoparticles, are shown in Figure 5.8 c.
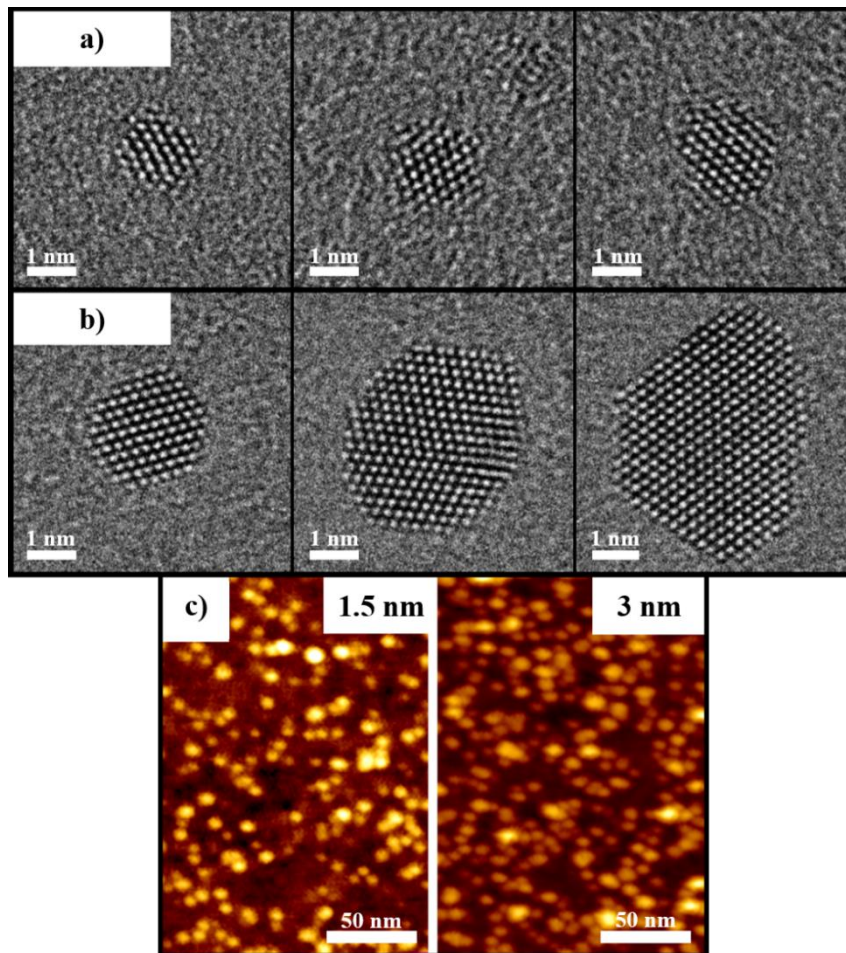
Figure 5.8: a) TEM micrographs of three representative 1.5 nm Pt nanoparticles. b) TEM micrographs of three representative 3 nm Pt nanoparticles. c) AFM characterization for determining surface coverage with 1.5 nm and 3 nm Pt nanoparticles.

5.5 Thin film – Nanoparticle Heterostructures

Metal nanoparticles deposited on SnO_2 thin films act as heterogeneous catalysts, which enhance and accelerate the reaction of target gases with the sensing layer. Due to their small size, nanoparticles have high-surface area, which correlates with an excess surface energy and makes smaller particles energetically less stable than larger particles. Thermal activation of nanoparticles leads to sintering of smaller particles into larger particles, reducing the surface area and thereby possibly reducing the catalytic activity of nanoparticles [139]–[141]. In literature, two generic mechanisms for the sintering process of nanoparticles can be found [142]–[144]:

1. Entire particles diffuse over the support material followed by coalescence with other particles. This mechanism is known as particle migration and coalescence (PMC).

2. Atomic species (metal atoms or oxidized metal atoms) detach from a particle, migrate over the support material, and attach to another particle. This mechanism is commonly known as Oswald ripening (OR).

Operation of functionalized SnO_2 thin film gas sensors at high temperatures (150 °C – 400 °C) could lead to an increase of the mean diameter of the nanoparticles and could alter the sensor performance over time due to deactivation of the heterogeneous catalysts. Incorporation of nanoparticles into the sensing layer could be a way to reduce or slow down the sintering process of nanoparticles and ensure the consistency of the nanoparticle surface area.

Heterostructures with nanoparticles embedded between two layers of a SnO_2 thin film were fabricated on bare silicon substrates and silicon substrates with Au electrodes (5 nm Ti / 200 nm Au) patterned on top. Au nanoparticles (CAN GmbH) and AuPt nanoparticles (Particular GmbH) were used for fabricating the heterostructures. First, 50 nm of SnO_2 were deposited on the 20 mm x 20 mm silicon substrates by spray pyrolysis (see Chapter 3.1). After annealing the SnO_2 thin film at 400 °C for 45 minutes, 100 µL of a nanoparticle solution were deposited homogeneously onto the silicon substrate by

drop coating. The samples coated with Au nanoparticles were placed on a heating plate at 75 °C for faster evaporation of the solvent (water), followed by an annealing step at 400 °C for 45 minutes to remove the surfactant sodium citrate. The samples coated with AuPt nanoparticles were dried at room temperature. Next, the deposited nanoparticles were covered with another layer of 50 nm SnO_2 by spray pyrolysis and the samples were annealed at 400 °C for 45 minutes. On the silicon substrates with Au electrodes, the SnO_2 layers were patterned by photolithography (see Chapter 4.1). Light microscope images were taken after embedding the nanoparticles between two layers of SnO_2 thin films and SEM characterizations of the heterostructures with both nanoparticles were performed. Figure 5.9 and Figure 5.10 show the heterostructures, fabricated on silicon substrates with Au electrodes on top, with Au nanoparticles (image on the left) and AuPt nanoparticles (image on the right). Although the samples with Au nanoparticles were annealed at 400 °C for 45 minutes, it seems that residue of the surfactant (sodium citrate) still remains on the substrate after the thermal treatment. The residue was characterized by EDX which confirmed that the residue contained carbon and sodium (see Appendix A). The high amount of surfactant residue is visible in the SEM images, shown in Figure 5.11. It was not possible to embed Au nanoparticles between two SnO_2 layers due to the non-residue-free decomposition of the surfactant used as stabilizer in the Au nanoparticle solution.
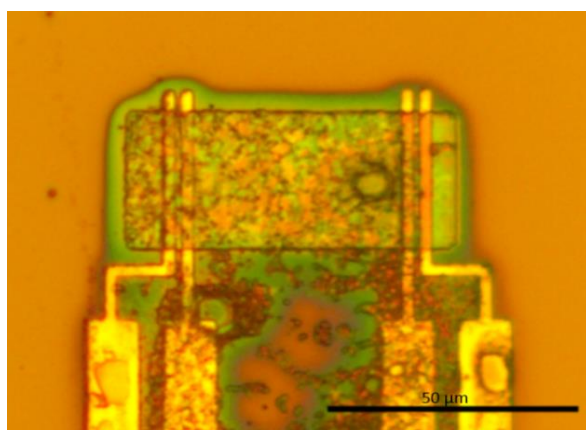
Figure 5.9: Light microscope image of heterostructures with Au nanoparticles, fabricated on silicon substrates with patterned Au electrodes.
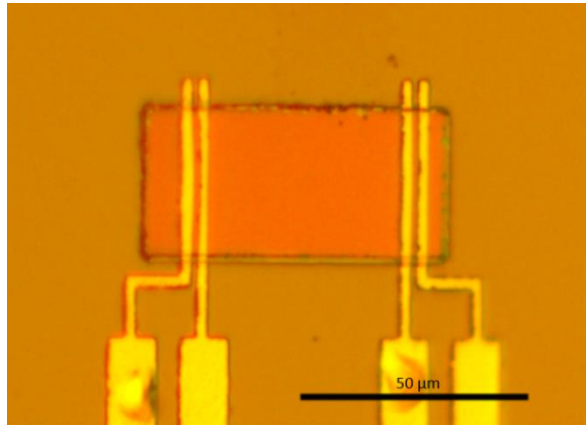
Figure 5.10: Light microscope image of heterostructures with AuPt nanoparticles, fabricated on silicon substrates with patterned Au electrodes.

AuPt nanoparticles were electrostatically stabilized in the solution without any chemical stabilizer. Therefore, no residue of a surfactant is visible in the light microscope image (see Figure 5.10). Figure 5.12 shows the FIB-cut cross-section of the $SnO_2 - AuPt$ heterostructure at different magnifications, characterized by SEM. The AuPt nanoparticles are nicely distributed over the SnO_2 surface and covered homogeneously with another SnO_2 thin film. By using the surfactant-free solution, AuPt nanoparticles were embedded successfully between two SnO_2 thin films.
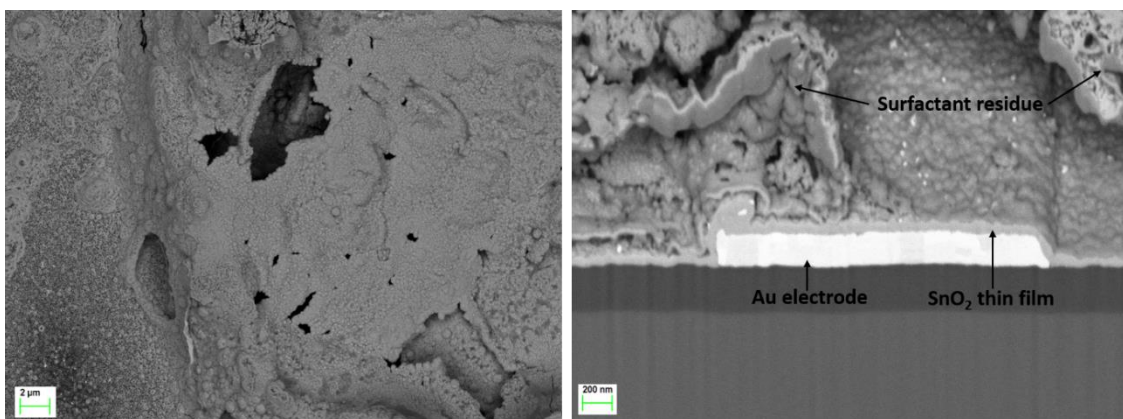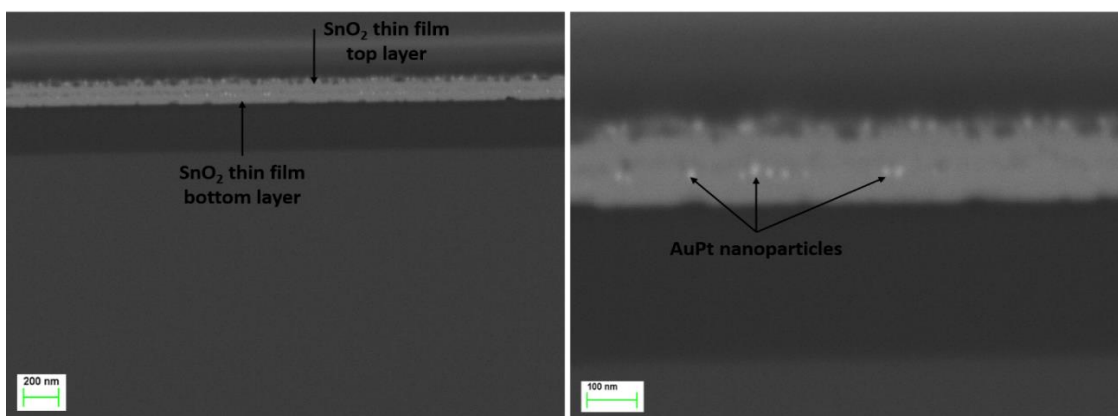

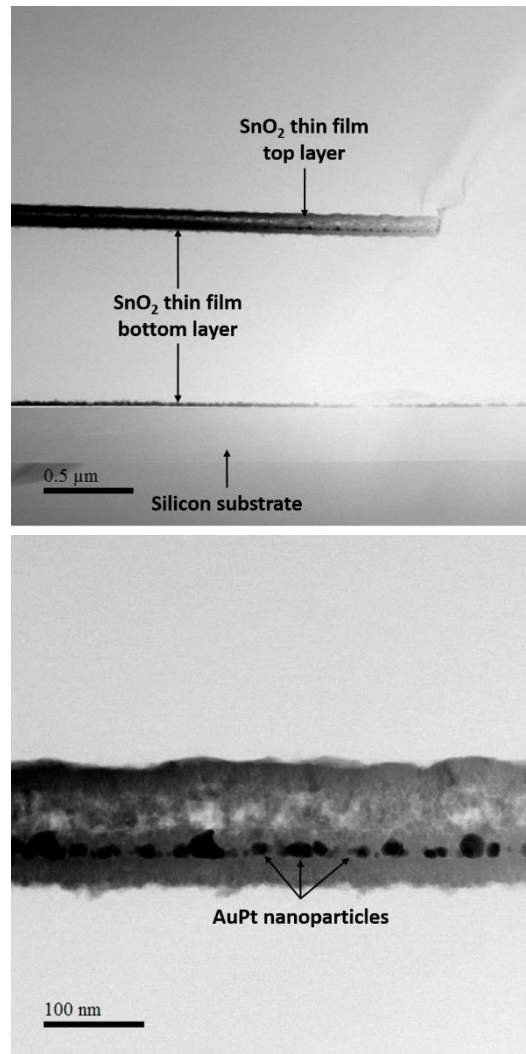Figure 5.11: SEM characterization of thin film – nanoparticle heterostructure with Au nanoparticles fabricated on silicon substrates with patterned Au electrodes. Left: topography image of heterostructure. Right: FIB-cut cross-section of heterostructure.

The samples fabricated on silicon substrates were used for characterizing the $SnO_2 - AuPt$ heterostructures by TEM. A TEM lamella was mechanically prepared. The TEM micrographs are shown in Figure 5.13. Due to the mechanical sample preparation, the heterostructure detached from the silicon substrate with a small portion of the bottom SnO_2 thin film still sticking to the silicon substrate, as can be seen in the top image of Figure 5.13. The bottom image in Figure 5.13 shows that the AuPt nanoparticles are nicely distributed and embedded between the two SnO_2 layers.

The goal of this study was to compare sensors with "embedded" nanoparticles with sensors functionalized with nanoparticles on the surface. For characterizing the sensor performance of the heterostructures, silicon based gas sensors were fabricated using the $SnO_2 - AuPt$ heterostructure samples on silicon substrates with Au electrodes. For the gas sensor assembly, the same process steps were carried out as described in Chapter 4.1. Unfortunately, for unknown reasons, the wire bonds did not adhere to the electrode pads on the silicon substrate and it was not possible to connect the silicon based gas sensors to the carrier. Therefore, the sensor performance of thin film – nanoparticle heterostructure gas sensors could not be evaluated in the gas measurement setup.

Figure 5.12: SEM characterization of thin film – nanoparticle heterostructure with AuPt nanoparticles fabricated on silicon substrates with patterned Au electrodes.

Figure 5.13: TEM characterization of thin film – nanoparticle heterostructure with AuPt nanoparticles fabricated on silicon substrates.

6 Gas sensing characterization of bare and functionalized SnO₂ thin film gas sensors

The sensor response of bare and functionalized SnO_2 thin film gas sensors to industrially and environmentally important target gases was evaluated. In this chapter, the gas measurement setup used for evaluating the sensor performance is explained in detail. Properties of target gases and their reactions with the sensing material are summarized. The sensor performances of bare and functionalized SnO_2 thin film gas sensors are presented and discussed.

6.1 Gas measurement setup

The performance of the SnO_2 thin film gas sensors was evaluated in an automated gas measurement setup, which is shown in Figure 6.1 and Figure 6.2. Mass flow controllers (Bronkhorst High-Tech B.V.) were used for regulating the flow rate of the test gas and background gas, which enabled precise tuning of the gaseous environment. The test gas compositions are described in detail in Appendix B. Synthetic air (80 % nitrogen, 20 % oxygen) was employed as background gas and the total flow rate was kept at 1000 sccm. For humid air, a certain percentage of the background gas was passed through a gas-washing bottle filled with deionized water. A commercial sensor (AFK-E, KOBOLD Messring GmbH) was used for measuring humidity and temperature in the test chamber. The electrical measurements were performed in a four point configuration, using Source Measure Units (SMU 2400; Keithley), which can simultaneously source and measure current (from 1 pA to 10 A) and voltage (from 100 nV to 200 V). For the sensor characterization, a constant current of 100 nA was applied to the outer electrodes and the voltage drop was measured at the inner electrodes. The sensor performance was evaluated at temperatures ranging from 150 °C up to 400 °C. Relative humidity (rh, at 20 °C) levels of 25 %, 50 %, and 75 % were chosen. The SnO_2 thin film gas sensors were exposed to different target gases with concentrations of

10 ppm, 30 ppm, 60 ppm, 100 ppm, 150 ppm, and 200 ppm. A duration of the target gas pulse of 5 minutes with 15 minutes breaks of synthetic air in between were chosen.

Figure 6.1: Automated gas measurement setup (on the left) with Source Measure Units (SMU) for electrical characterization and power supply for mass flow controllers (on the right).
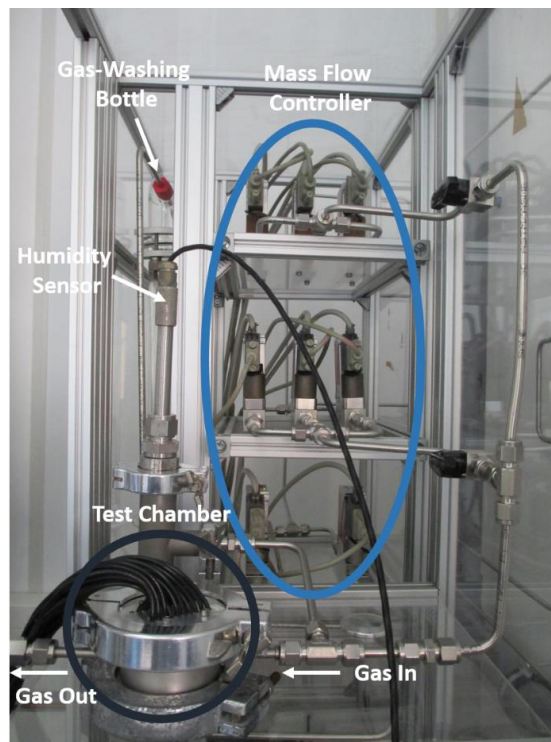

Figure 6.2: Zoom of automated gas measurement setup.

6.2 Parameters for sensor performance evaluation

The electrical resistance of SnO_2 thin film gas sensors and its change when exposed to target gases was measured at different temperatures and gas concentrations. To compare the results of the bare and functionalized gas sensors, the sensitivity, response time, and recovery time of the sensors were calculated and determined. Figure 6.3 depicts a schematic of a typical response curve of an n-type metal oxide gas sensor to a reducing gas. The base resistance of the sensor has a certain value in ambient air (R_{air}) and by exposing the sensor to reducing gases the sensor conductivity increases and the sensor resistance drops to a saturation value (R_{gas}). When exposed to ambient air again, the sensor recovers and the resistance goes back to its base resistance in ambient air.

An important parameter for comparing the sensor performance of different sensing materials to a certain gas is the sensitivity (S). In literature, different definitions of the gas sensor sensitivity can be found [14], [145], [146]. IUPAC defines sensitivity as the slope
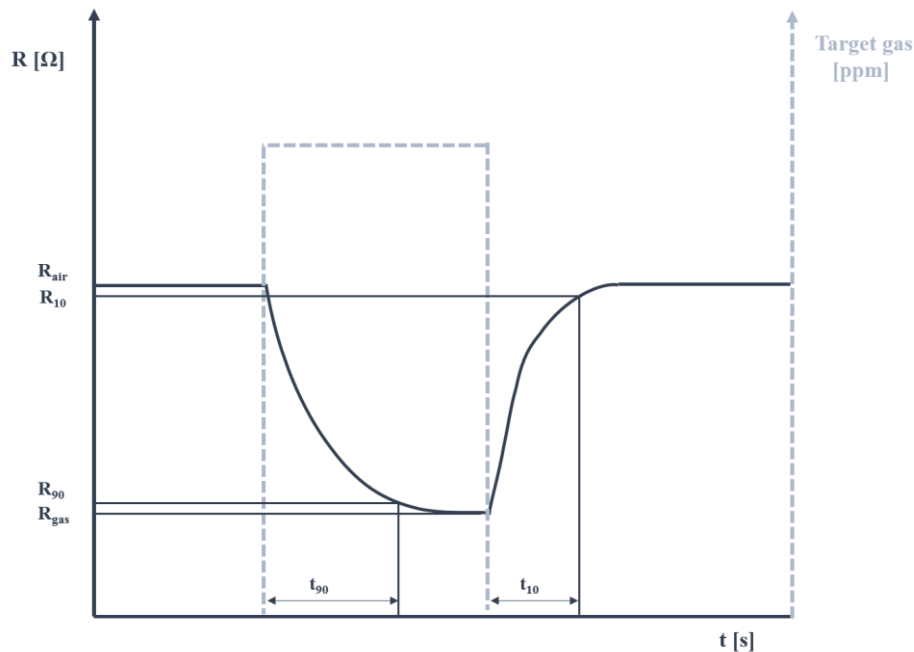
Figure 6.3: Schematic of response curve of an n-type metal oxide gas sensor to a reducing gas.

of the calibration curve (gas response versus gas concentration) [147]. In this work, sensitivity was defined as the relative resistance change of the gas sensor due to interaction with the target gas [148], [149]:

$$S = \frac{|R_{gas} - R_{air}|}{R_{air}} \cdot 100 \ \% \qquad (14)$$

In this work, sensitivity and gas response both describe the term defined in equation 14. Apart from the sensitivity of the bare and functionalized SnO_2 thin film gas sensors, the response and recovery time of the sensors were determined as well. Response time (t_{90}) is the time the sensor needs to reach 90 % of its saturation value (R_{gas}) during a gas pulse (see Figure 6.3). Recovery time (t_{10}) is the time a sensor needs to reach a resistance within 10 % of the original resistance in ambient air (base resistance, R_{air}, see Figure 6.3) [146].

6.3 Target gases

In this work, the sensor performance of bare and functionalized SnO_2 thin film gas sensors was evaluated to target gases carbon monoxide (CO) and hydrogen (H_2), and the influence humidity has on the sensor response was investigated. In this chapter, the properties and the reactions of the target gases with the sensing layer are summarized and discussed.

6.3.1 Carbon monoxide (CO)

Carbon monoxide (CO) is a color- and odorless gas, which is highly flammable and toxic. Table 6.1 summarizes some of the physical and chemical properties. CO is formed by the incomplete combustion of carbon due to limited supply of oxygen. Burning of hydrocarbon fuels (e.g. petrol, diesel, natural gas) also leads to the formation of CO as a pollutant. CO promotes combustion and it burns with a blue flame. CO is used in the steel industry as reducing agent (extraction of iron from its ore) and in the chemical industry for producing bulk chemicals. CO is a very toxic gas due to its ability to bind to transition metals, such as iron, which is found in hemoglobin in red blood cells. CO shows an over

200 times stronger affinity to hemoglobin than oxygen, which forces the red blood cells to transport CO instead of oxygen and inhibits the delivery of oxygen within the body. Symptoms of CO poisoning include headache, dizziness, nausea, vomiting, and fatigue. Prolonged exposure to CO can eventually be fatal. Incomplete combustion of natural gas in gas appliances, like boilers, gas fires, or gas cookers can lead to people being exposed to CO in their homes [150]. The MAK (maximale Arbeitsplatzkonzentration) value, which is the German maximum permitted concentration in the workplace, for CO is 30 ppm [151]. For safety applications, gas sensors which can detect CO concentrations below 100 ppm are required.

CO is a reducing gas and interaction with the SnO_2 layer leads to an increased conductivity of the sensing material. Operating SnO_2 sensors in ambient air, CO primarily reacts with pre-adsorbed oxygen species on the sensor surface, which releases electrons back into the sensor layer [152]. Between 200 °C – 370 °C, CO_2 was experimentally determined to be the main reaction product in ambient air [153]. Investigation of oxygen-free and low-oxygen atmospheres show that CO reacts directly with the SnO_2 surface if no or little oxygen is available. In this case, CO acts as donor and increases the sensor conductivity [154], [155]. The interactions of CO with SnO_2, depending on the oxygen concentration and in absence of water, are shown in Figure 6.4.

Table 6.1: Physical and chemical properties of CO [156].

Properties	
Molar mass [g/mol]	28.01
Melting point [°C]	-205.1
Boiling point [°C]	-191.5
Vapor Density (0 °C, 1013 mbar) [kg/m^3]	1.251
Solubility (20 °C) [mg/mL]	30
Explosion limits	10.9 – 76 vol.%

The following reactions are possible depending on the type and density of already adsorbed species, oxygen concentration in the air, and temperature [152], [154], [157], [158]:
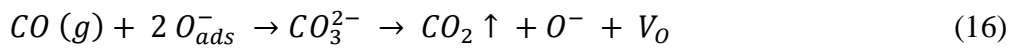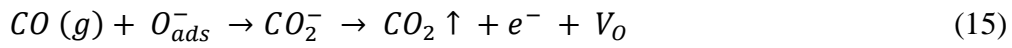
$$CO \ (g) + O_{ads}^- \rightarrow CO_2^- \rightarrow CO_2 \uparrow + e^- + V_O \tag{15}$$

$$CO \ (g) + 2 \ O_{ads}^- \rightarrow CO_3^{2-} \rightarrow CO_2 \uparrow + O^- + V_O \tag{16}$$

$$CO \ (g) + OH_{ads}^- \rightarrow HCOO^- \rightarrow CO_2 \uparrow + H_2 \uparrow + V_O + e^- \tag{17}$$

$$CO \ (g) + O_{lat} \rightarrow CO_2 + V_O \tag{18}$$

$$CO_{ads} \rightarrow CO_{ads}^+ + e^- \tag{19}$$
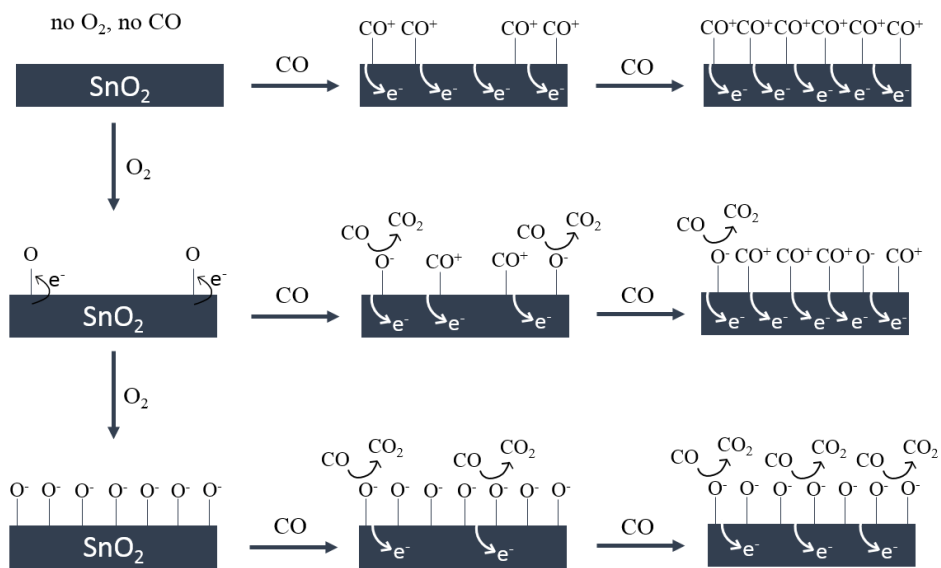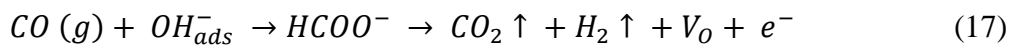
Figure 6.4: Interaction of CO with SnO₂ depending on oxygen concentration and in absence of water; adapted from [154].

How CO reacts with SnO_2 in the presence of humidity is not fully understood. Generally accepted is the formation of hydroxyl groups (Sn-OH and HO_{lat}) and H_{ads} when water is present, which can function as additional reactants for the interaction with CO [154]:

$$CO + HO_{ads} \leftrightarrow HCOO_{ads} \tag{20}$$
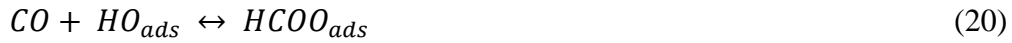
Above 230 °C, the formate decomposes to CO_2 and hydrogen and an electron is released into the sensing layer:

$$HCOO_{ads} \leftrightarrow CO_2 + H_{ads} + e^- \tag{21}$$

The formate can also react with another hydroxyl group, which decreases the sensor conductivity by providing two adsorbed oxygen species:

$$HCOO_{ads} + OH_{ads} \leftrightarrow H_2CO + 2\,O_{ads} \tag{22}$$
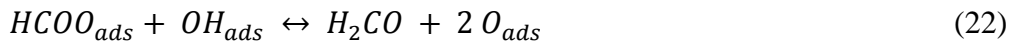
6.4 Hydrogen (H_2)

Hydrogen (H_2) is an odor- and colorless gas, which is highly flammable and can form explosive mixtures with aerial oxygen. Some physical and chemical properties are summarized in Table 6.2.

Hydrogen is used diversely in the chemical industry. In the Haber-Bosch process, ammonia is produced by the reaction of hydrogen and nitrogen. Methanol is synthesized from syngas, which is a mixture of hydrogen and carbon monoxide. Another important application of hydrogen in industry is the production of liquid hydrocarbons (e.g. oil, petrol, and diesel) by the Fischer-Tropsch process. Hydrogen also finds use in the food industry, steel industry, and semiconductor industry [146]. Beside well-established applications in the chemical industry, new markets for hydrogen are emerging. Using hydrogen as an energy carrier in various applications is becoming more and more important. Hydrogen is a sustainable energy source by generating power from fuel cells for stationary and automotive applications. To ensure safe handling of these applications, hydrogen sensors are essential for leak detection and alert if hydrogen concentrations approach hazardous levels [159], [160].

Hydrogen is a reducing gas and the interaction of the gas with SnO_2 leads to an increase of the sensing layer conductivity. At temperatures above 350 °C – 400 °C, the reaction mechanism of H_2 with the SnO_2 surface is divided into two stages [161]. At the first stage,

Table 6.2: Physical and chemical properties of H_2 [156].

Properties	
Molar mass [g/mol]	2.02
Melting point [°C]	-259.19
Boiling point [°C]	-252.76
Vapor Density (0 °C, 1013 mbar) [kg/m^3]	0.0899
Solubility (20 °C) [mg/mL]	1.6
Explosion limits	4.0 – 77 vol.%

hydrogen molecules are dissociated into atoms on the SnO$_2$ surface. At the second stage, negatively charged hydroxyl groups are formed by the reaction of hydrogen atoms with double charged oxygen ions (O^{2-}), followed by a recombination of the hydroxyl groups, which leads to the formation of water molecules and oxygen vacancies:

$$H_2 \leftrightarrow 2\,H \tag{23}$$

$$2\,H + 2\,O^{2-} \leftrightarrow 2\,OH^- + 2\,e^- \tag{24}$$

$$2\,H + 2\,OH^- \leftrightarrow 2\,H_2O \uparrow + 2\,V_o + 2\,e^- \tag{25}$$
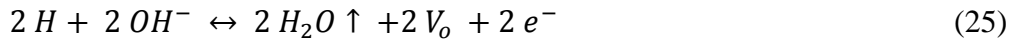
By the interaction of hydrogen atoms with oxygen ions or hydroxyl groups, a maximum of two electrons are released back into the conduction band of the sensing material per hydrogen molecule, increasing the SnO$_2$ conductivity. At temperatures between 100 °C – 300 °C, no dissociation of H$_2$ occurs. Hydrogen molecules react directly with the pre-adsorbed oxygen species [51]:

$$2\,H_2 + O_2^- \leftrightarrow 2\,H_2O + e^- \tag{26}$$

$$H_2 + O^- \leftrightarrow H_2O + e^- \tag{27}$$

$$H_2 + O^{2-} \leftrightarrow H_2O + 2\,e^- \tag{28}$$

6.5 Gas sensing characterization of bare SnO$_2$ thin film gas sensors

SnO$_2$ thin film gas sensors were fabricated on silicon substrates, MPW3 microhotplates, and MPW4 microhotplates. The sensor performance of the SnO$_2$ thin film was evaluated on all three substrates. The sensors were exposed to CO concentrations ranging from 10 ppm to 200 ppm at operating temperatures between 250 °C and 400 °C and relative humidity levels of 25 %, 50 %, and 75 % (at 20 °C).

Figure 6.5 shows the gas response (S) of the SnO$_2$ thin film on the different substrates to 200 ppm CO at 50 % relative humidity depending on the operating temperature. By integrating SnO$_2$ thin films on CMOS microhotplates, the gas response to CO was increased. The improved sensor response of the CMOS integrated SnO$_2$ thin film to CO can be explained by the fast rise time (< 10 ms) and the uniform heat distribution of the microhotplate. Thermocouples, which were placed directly on the microhotplate, enabled a precise temperature regulation. The macroscopic assembly of the silicon based gas sensors using discrete heaters and thermocouples can lead to heat dissipation, heat loss, and non-uniform heat distribution over the whole silicon substrate.
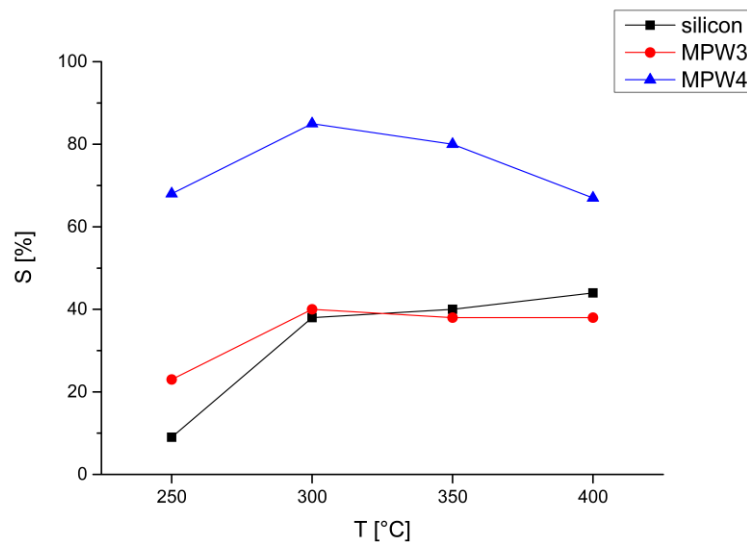
Figure 6.5: Gas response versus temperature of SnO$_2$ thin film gas sensor on silicon, MPW3, and MPW4 substrates (200 ppm CO, 50 % relative humidity).

The decreased sensor response of the SnO_2 thin film on the MPW3 microhotplate can be explained by the low thermal stability of the contacting electrodes used in the first generation of the microhotplate (see Chapter 4.2.1). The tungsten plugs were oxidized at elevated temperatures, which lead to an increased volume of the plugs and a deformation of the electrodes. The adhesion of the sensing layer on the electrodes was decreased, which probably resulted in reduced sensitivity due to signal drift. The highest gas response of the bare SnO_2 thin film on CMOS microhotplates to CO was achieved at 300 °C (see Figure 6.5). The sensor performance of the SnO_2 thin film gas sensor integrated on MPW3 at 300 °C and relative humidity levels of 25 %, 50 %, and 75 % is shown in Figure 6.6. The gas response of bare SnO_2 was influenced by humidity. With increasing humidity level, the sensor response to CO decreased. The negative influence of humidity on the sensor performance of bare SnO_2 thin film gas sensors is shown in Figure 6.7 by comparing the gas response to CO concentrations from 10 ppm to 200 ppm
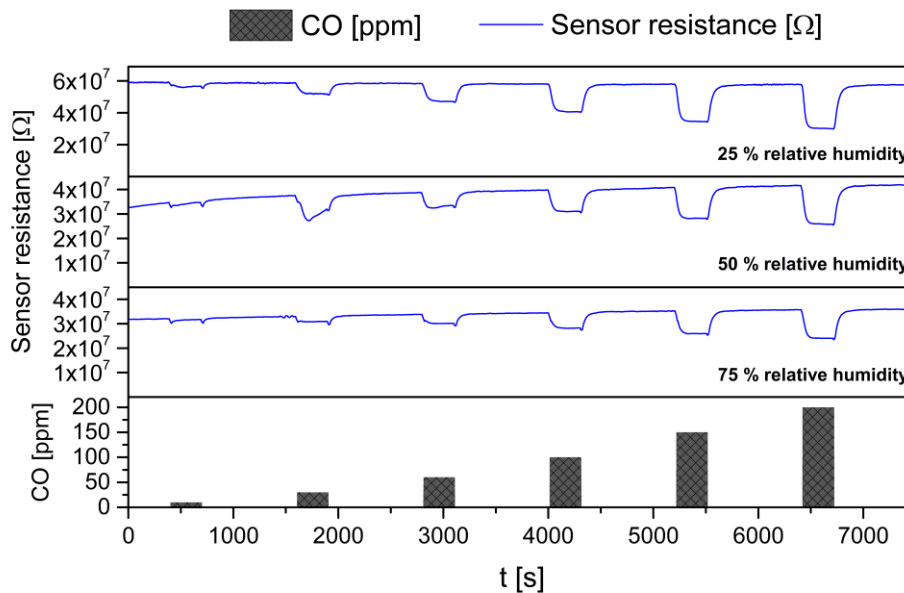
Figure 6.6: Sensor performance of SnO_2 thin film gas sensor on MPW3 microhotplate at an operating temperature of 300 °C exposed to concentrations of CO ranging from 10 ppm up to 200 ppm at 25 %, 50 %, and 75 % relative humidity.
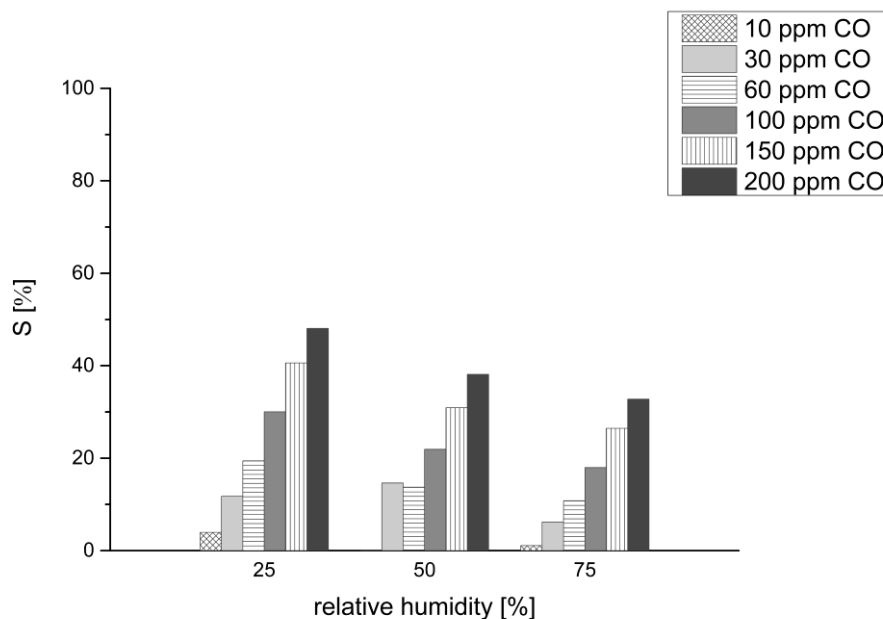
Figure 6.7: Gas response versus humidity of SnO$_2$ thin film on MPW3 microhotplate to CO at 300 °C.

at 25 %, 50 %, and 75 % relative humidity. Response times (t$_{90}$) and recovery times (t$_{10}$) of the SnO$_2$ thin film for CO on all three substrates were determined. Table 6.3 summarizes the response times of all three sensor types for 200 ppm CO at an operating temperature of 400 °C. With decreasing operation temperature the response time increased. The recovery times were in the range of 3 − 7 minutes at an operating temperature of 250 °C depending on relative humidity; with increasing humidity level the recovery time decreased. Also with increasing operating temperature, the recovery time decreased significantly. At an operating temperature of 400 °C, the recovery time was in the range of 60 seconds.

Table 6.3: Response times (t$_{90}$) of SnO$_2$ thin film gas sensors on different substrates for humidity levels of 25 %, 50 %, and 75 % exposed to 200 ppm CO at 400 °C.

200 ppm CO / 400 °C	SnO$_2$ on silicon	SnO$_2$ on MPW3	SnO$_2$ on MPW4
25 % rh	8 s	7 s	8 s
50 % rh	8 s	8 s	9 s
75 % rh	9 s	7 s	8 s

6.6   Gas sensing characterization of SnO$_2$ thin film gas sensors functionalized with Au nanoparticles

SnO$_2$ thin film gas sensors, integrated on MPW3 microhotplates, were functionalized with Au nanoparticles (see Chapter 5.1.1) by inkjet printing. After depositing the nanoparticles, the gas sensors were annealed at 400 °C for one hour to remove the surfactant from the surface of the sensing layer. The sensors were exposed to CO at operating temperatures from 250 °C up to 400 °C. The sensor resistance was not stable and the Au functionalized SnO$_2$ thin film showed no sensitivity to CO (see Figure 6.8). As described in Chapter 5.5, the decomposition of sodium acetate, which was used as surfactant for stabilizing the Au nanoparticles in solution, seemed to be not residue-free and sodium and carbon residues were covering the sensing material after the annealing process, which resulted in the unstable sensor resistance and insensitivity to CO.
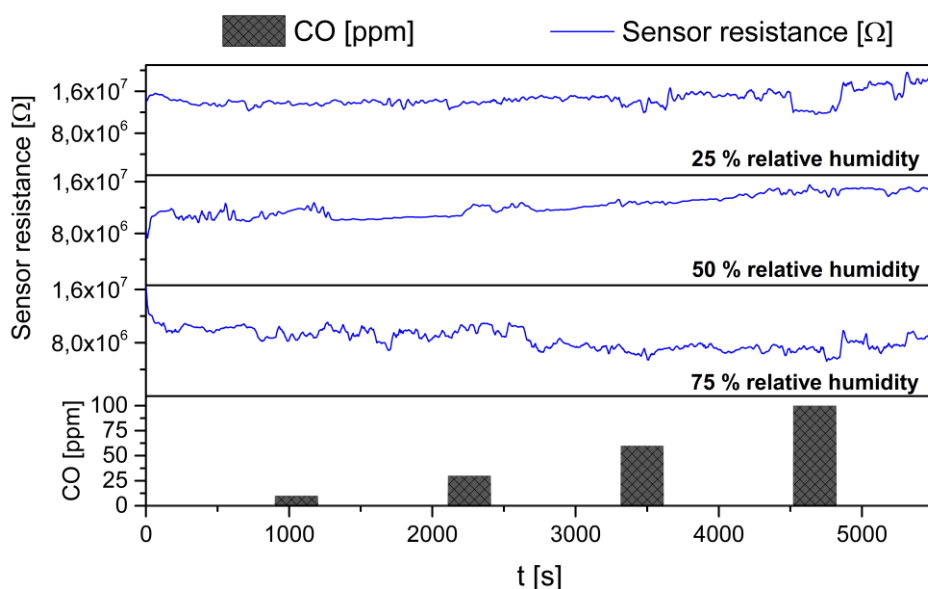
Figure 6.8: Sensor performance of Au functionalized SnO$_2$ thin film gas sensor at an operating temperature of 350 °C exposed to CO concentrations from 10 ppm to 100 ppm.

6.7 Gas sensing characterization of SnO₂ thin film gas sensors functionalized with Pt nanoparticles

Differently sized Pt nanoparticles were deposited on CMOS integrated SnO_2 thin film gas sensors by a magnetron sputtering inert-gas condensation deposition system (see Chapter 5.4). The gas sensors were functionalized with 1.5 nm and 3 nm Pt nanoparticles, respectively. The size-selective nanoparticle deposition was achieved by using an in-line quadrupole mass filter (QMF).

The gas sensors were annealed at 400 °C for stabilizing the sensor resistance. The influence of the differently sized Pt nanoparticles on the sensor performance to CO was evaluated at 350 °C, 375 °C, and 400 °C and relative humidity levels of 25 %, 50 % and, 75 %. At lower operating temperatures, the sensor resistance was unstable with a low signal-to-noise ratio. The most stable sensor performance was achieved at 375 °C. Figure 6.9 summarizes the gas response of bare and Pt functionalized gas sensors at an operating temperature of 375 °C to CO concentrations of 10 ppm to 200 ppm at 75 % relative humidity.
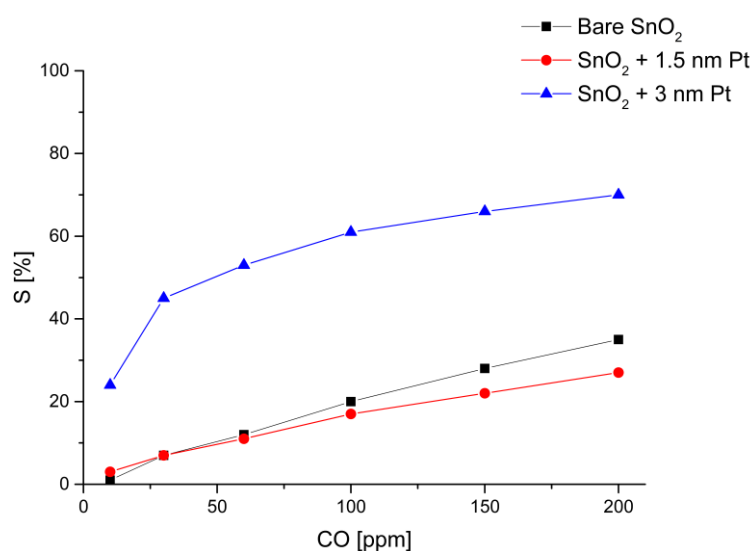
Figure 6.9: Comparison of gas response of bare and Pt functionalized CMOS integrated SnO_2 thin film gas sensors to CO at 375 °C and a relative humidity level of 75 %.

In the case of 1.5 nm Pt nanoparticles, the gas response to CO was not improved compared to bare SnO_2 thin films. But the functionalization of the gas sensor with 3 nm Pt nanoparticles increased the gas response to CO significantly. Especially at CO concentrations in the low ppm-level range, the gas response was several times higher than for bare SnO_2 thin films. The sensor performance of the 3 nm Pt functionalized gas sensor at 375 °C is shown in Figure 6.10. In contrast to bare SnO_2 thin films, humidity had no influence on the gas sensing performance of Pt functionalized SnO_2 thin films. The gas response to CO of both – 1.5 nm and 3 nm Pt – functionalized sensors at 375 °C is summarized in Figure 6.11, which shows that the cross-sensitivity to humidity is eliminated by Pt nanoparticles.

In literature, many studies were performed to understand how humidity influences the sensor performance but the reaction mechanism of humidity interference on the detection of target gases is still not fully clarified [162]–[164]. The detection of CO in dry and humid atmosphere was studied extensively with pristine SnO_2-based gas sensors [28], [39], [154] and the beneficial impact doping of SnO_2-based gas sensors with Sb [165], NiO [166], or Pd[167] has on the gas response in humid atmospheres. The type of adsorbed oxygen species on the SnO_2 surface greatly influences the gas response:

$$O_2 + 2e^- \leftrightarrow 2O^- \tag{29}$$

$$O_2 + 4e^- \leftrightarrow 2O^{2-} \tag{30}$$

A high concentration of O^{2-}-adsorption sites leads to a high sensor response. It was proposed that in dry atmosphere mainly O^{2-} is adsorbed on the SnO_2 surface. In wet atmosphere, the adsorption of O^{2-} is suppressed by water vapor, leaving only O^- on the surface. The interference of humidity on the surface oxygen species results in a reduced sensor response [168], [169]. Recently, it was found that functionalization of SnO_2 with Pd or Sb eliminates the effect humidity has on the surface oxygen species. In the presence of Pd or Sb, the concentration of O^{2-} on the surface is maintained with increasing humidity
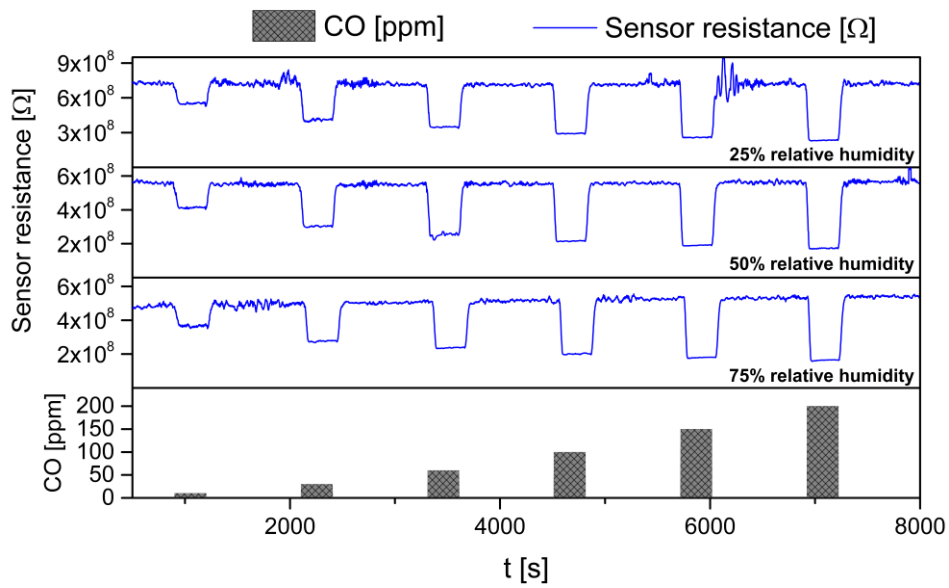
Figure 6.10: Sensor performance of CMOS integrated SnO_2 thin film gas sensor functionalized with 3 nm Pt nanoparticles at 375 °C.
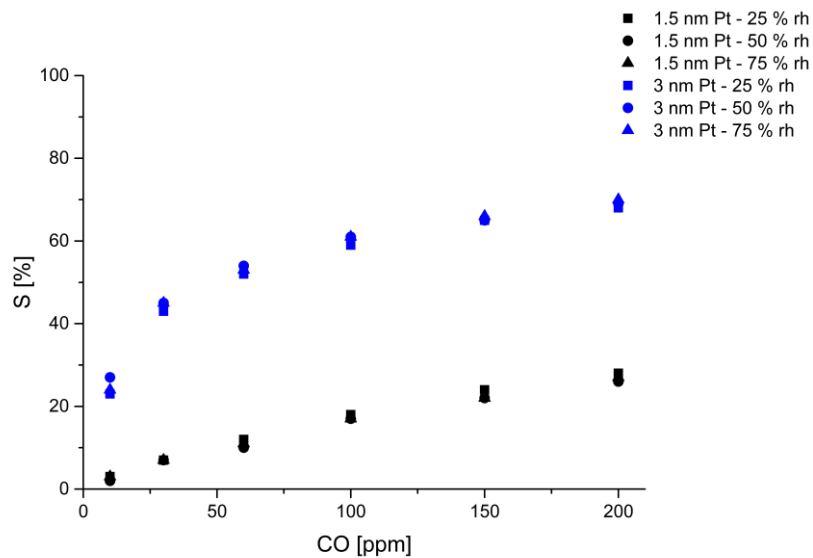
Figure 6.11: Gas response of SnO_2 thin film gas sensors functionalized with 1.5 nm and 3 nm Pt nanoparticles to CO concentrations of 10 ppm to 200 ppm at 375 °C and relative humidity levels of 25 %, 50 %, and 75 %.

concentration, which results in the suppression of the negative influence of humidity on the sensor performance [165], [170]. The humidity-independent gas response to CO of Pt functionalized CMOS integrated SnO_2 thin film sensors could be explained in a similar way. Both 1.5 nm and 3 nm Pt nanoparticles promoted the dissociative adsorption of O^{2-} oxygen species on the SnO_2 surface.

A reason for the comparatively low sensor response of SnO_2 thin film sensors functionalized with 1.5 nm Pt nanoparticles could be that the CO oxidation took place on additional reaction sites on the Pt nanoparticles, which were electronically decoupled from the SnO_2 thin film and therefore had no impact on the sensor signal [171]. Response and recovery times for bare and Pt functionalized sensors were evaluated. The response time to CO was not influenced by the functionalization; the response time of SnO_2 thin film functionalized with Pt nanoparticles was 10 s at an operating temperature of 400 °C and relative humidity of 25 %. However, the recovery time was improved by functionalizing SnO_2 with 3 nm Pt nanoparticles. The recovery time of SnO_2 decorated with 1.5 nm Pt nanoparticles was in the range of bare SnO_2. Table 6.4 summarizes the recovery times of the different sensors for operating temperatures of 350 °C to 400 °C exposed to 200 ppm CO at 25 % relative humidity.

Table 6.4: Recovery times (t_{10}) of bare and Pt functionalized SnO_2 thin film gas sensors for different operating temperatures exposed to 200 ppm H_2 at 25 % relative humidity.

200 ppm H_2 / 25 % rh	Bare SnO_2	SnO_2 + 1.5 nm Pt	SnO_2 + 3 nm Pt
350 °C	102 s	112 s	39 s
375 °C	60 s	52 s	30 s
400 °C	48 s	55 s	32 s

6.8 Gas sensing characterization of SnO$_2$ thin film gas sensors functionalized with NiPt nanoparticles

NiPt nanoparticles (see Chapter 5.1.2) were used to functionalize SnO$_2$ thin film gas sensors on MPW3 microhotplates by inkjet printing. The sensors were exposed to CO at operating temperatures from 150 °C up to 400 °C and relative humidity levels of 25 %, 50 %, and 75 %.

The sensor showed excellent performance to CO at 150 °C and at a CO concentration of 200 ppm and 75 % relative humidity, a gas response of 90 % was achieved. The gas response at 150 °C for all three humidity levels are summarized in Table 6.5. Unfortunately, the sensor performance greatly deteriorated at higher operating temperatures and at operating temperatures of 300 °C and higher, the gas sensor showed no sensitivity to CO anymore. The gas measurements were repeated again and the sensor performance at 150 °C was significantly degraded. The two gas measurements at 150 °C are shown in Figure 6.12. After heating the gas sensor to temperatures of up to 400 °C, the gas response to 200 ppm CO at 75 % relative humidity was decreased to 7 %.

Table 6.5: Gas response of NiPt functionalized SnO$_2$ thin film gas sensor to CO at 150 °C and 25 %, 50 % and 75 % relative humidity.

| CO / 150 °C	25 % rh	50 % rh	75 % rh
10 ppm	16	6	12
30 ppm	26	22	31
60 ppm	51	62	61
100 ppm	75	85	78
150 ppm	84	92	86
200 ppm	88	94	90
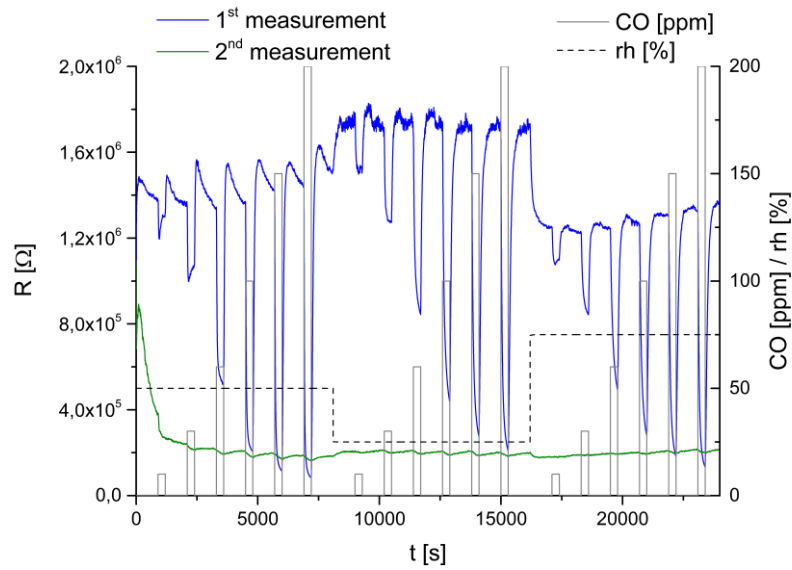
Figure 6.12: Sensor performance of NiPt functionalized SnO_2 thin film gas sensor to CO concentrations from 10 ppm to 200 ppm at 150 °C and 25 %, 50 %, and 75% relative humidity.

The characterization of the gas sensor by SEM showed that a non-continuous layer was covering the SnO_2 thin film (see Figure 6.13). A possible explanation for the formation of this layer could be found in the high concentration of NiPt nanoparticles in the solution. The assumption is that the NiPt nanoparticles melt on the surface of the sensing material at elevated temperatures and, due to the high nanoparticle concentration, form a film which covers the sensing material almost completely. Although the melting point of bulk nickel and bulk platinum is 1455 °C [172] and 1768 °C [173], respectively, the melting point of a material decreases significantly with decreasing particle size [174]–[176]. The layer covering the SnO_2 thin film offered additional reaction sites for the target gas but those reaction sites were not electronically coupled to the metal oxide [81], [177]. Therefore, the layer had no influence on the electrical signal, which lead to the strong decrease in the gas response of the sensor. To reduce the nanoparticle concentration, the solution was diluted 1:10 with toluene. Unfortunately, a reduced nanoparticle concentration could not be deposited on CMOS integrated SnO_2 thin films gas sensors by inkjet printing because it was not possible to achieve a stable drop formation with the diluted solution.
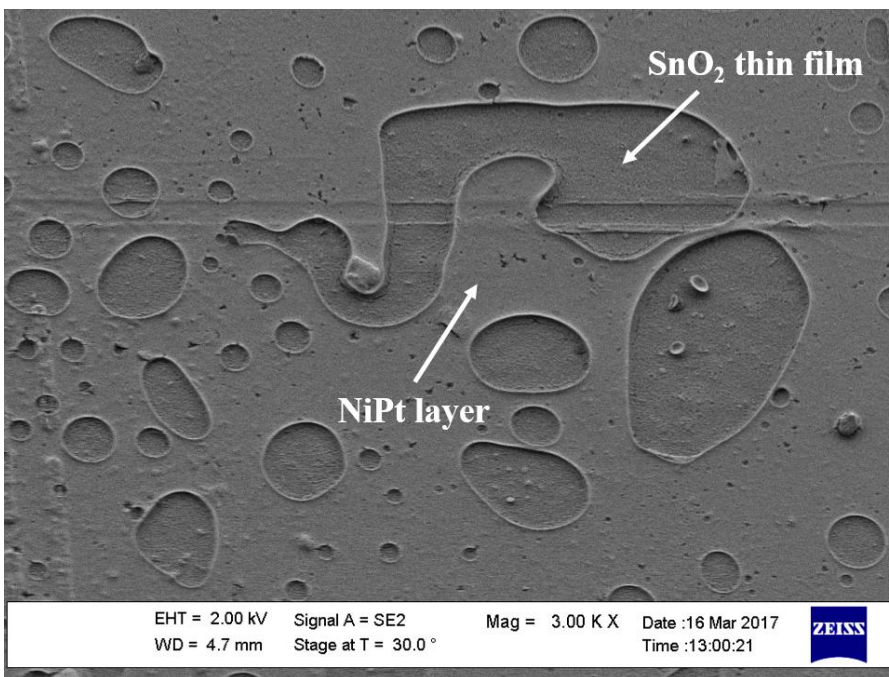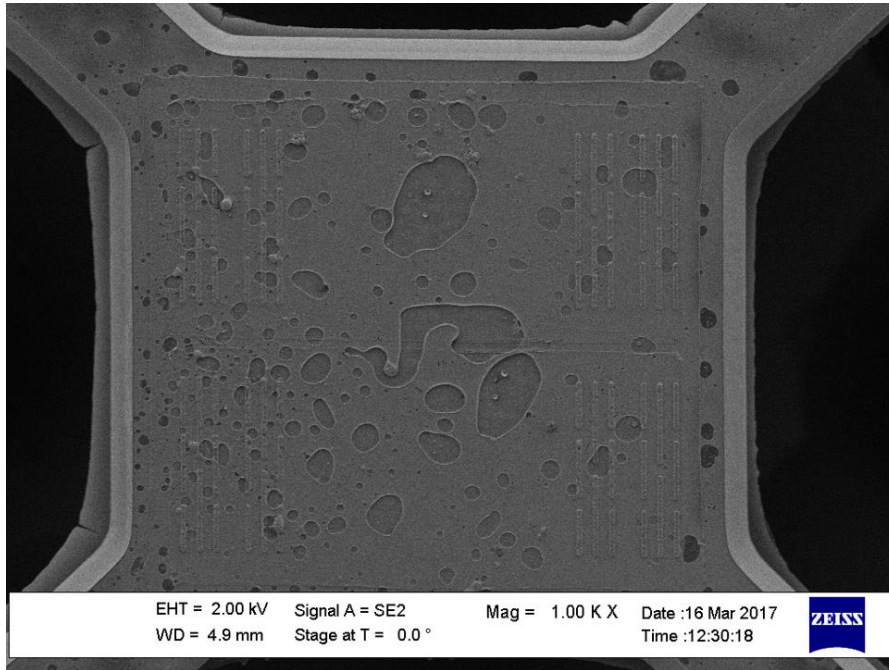
Figure 6.13: SEM characterization of NiPt functionalized SnO$_2$ thin film gas sensor after sensor operation at temperatures of up to 400 °C.

6.9 Gas sensing characterization of SnO_2 thin film gas sensors functionalized with AuPd nanoparticles

AuPd nanoparticles (see Chapter 5.1.3) were deposited on SnO_2 thin film gas sensors, integrated on MPW3 microhotplates, by inkjet printing. The sensor performance to CO and H_2 was evaluated at operating temperatures from 250 °C to 400 °C and relative humidity levels of 25 %, 50 %, and 75 %.

The gas response of bare SnO_2 thin film gas sensors and SnO_2 thin film gas sensors functionalized with AuPd nanoparticles to 200 ppm CO and H_2 at 25 % relative humidity and different temperatures is shown in Figure 6.14. The sensitivity to CO at operating temperatures of 250 °C and 300 °C was strongly reduced by the functionalization with AuPd nanoparticles. At 350 °C, the gas response increased significantly and at 400 °C the gas response was improved compared to bare SnO_2 thin films. The AuPd functionalized sensor showed good sensitivity to H_2 with a gas response of 76 % to 200 ppm H_2 at 250 °C and 25 % relative humidity. The gas response to H_2 was only slightly improved at 250 °C by the AuPd functionalization but showed no improvement at higher temperatures compared to bare SnO_2 thin films.
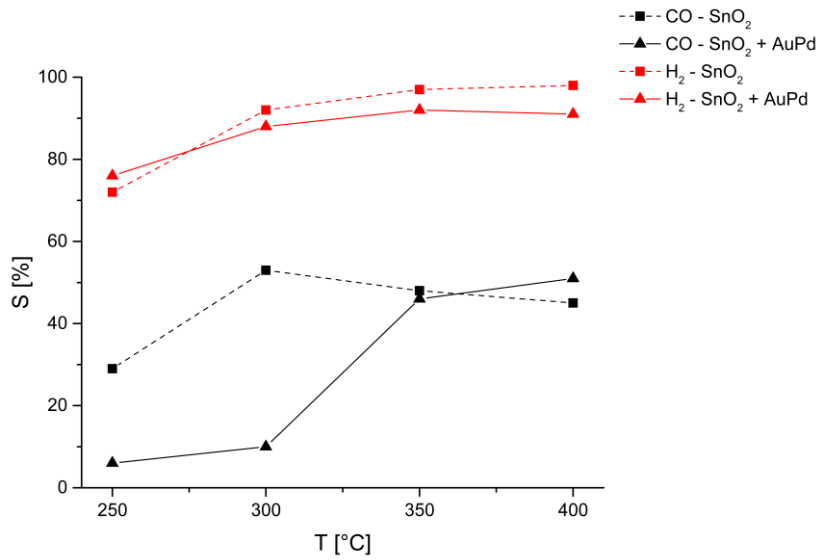
Figure 6.14: Comparison of gas response to 200 ppm CO and H_2 at different temperatures of bare and AuPd functionalized SnO_2 thin film gas sensors (gas concentration 200 ppm; 25 % relative humidity).
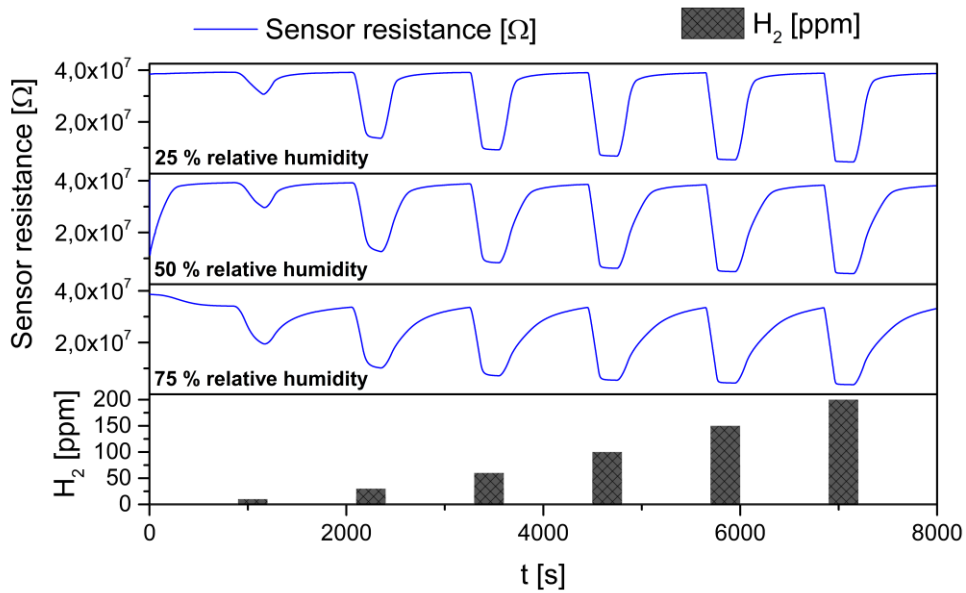
Figure 6.15: Sensor performance of AuPd functionalized SnO_2 thin film gas sensor to H_2 concentrations of 10 ppm to 200 ppm at 300 °C.

By functionalizing the SnO_2 thin film gas sensor with AuPd nanoparticles, the selectivity to H_2 was improved at operating temperatures of 250 °C and 300 °C. The sensor performance of the AuPd functionalized SnO_2 thin film gas sensor to H_2 at 300 °C is shown in Figure 6.15. Furthermore, a significant improvement of cross-sensitivity to humidity was achieved by the functionalization with AuPd nanoparticles for both H_2 and CO detection. The influence humidity has on the gas response of bare SnO_2 thin film sensors to H_2 concentrations of 10 ppm up to 200 ppm is shown in Figure 6.16. Especially at low gas concentrations, the gas response was significantly reduced with increasing humidity levels, which poses a problem to the application of the sensors in real life conditions. In comparison, the gas response of AuPd functionalized sensors was not influenced by humidity, which is depicted in Figure 6.17.
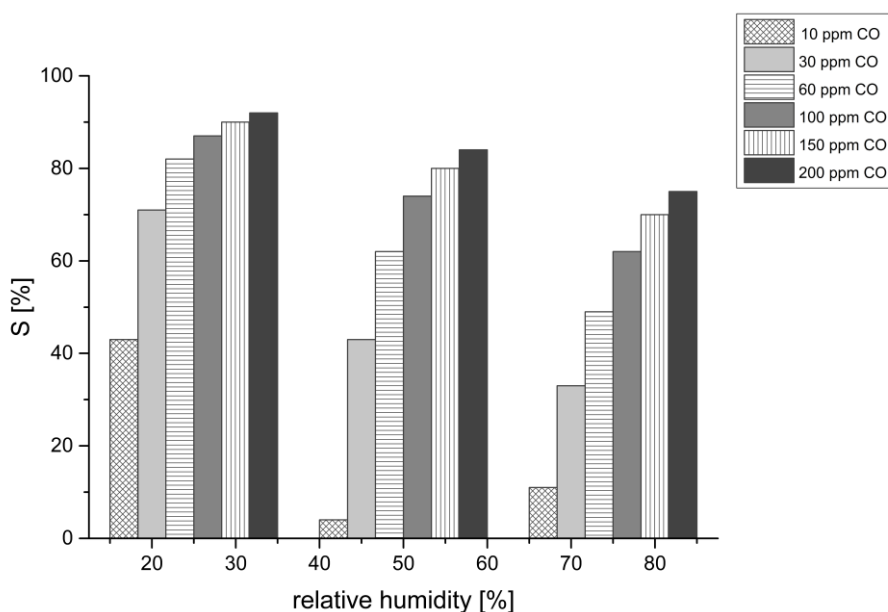
Figure 6.16: Gas response of bare SnO_2 thin film gas sensor to H_2 at 300 °C.
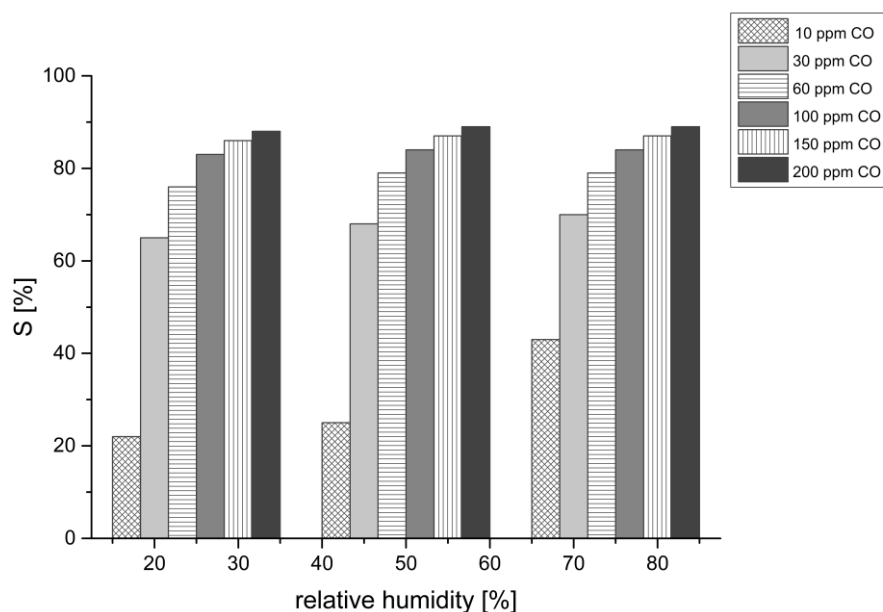
Figure 6.17: Gas response of AuPd functionalized SnO_2 thin film gas sensor to H_2 at 300 °C.

Response times and recovery times were evaluated for bare and AuPd functionalized sensors. The response time was not influenced by the functionalization, but the recovery time was reduced significantly by the AuPd nanoparticles. The response time of AuPd functionalized SnO_2 at 400 °C and 25 % relative humidity was 9 s. The recovery times of bare and functionalized sensors exposed to 200 ppm H_2 at 25 % relative humidity for operating temperatures from 250 °C to 400 °C are summarized in Table 6.6.

Table 6.6: Recovery times (t_{10}) of bare and AuPd functionalized SnO_2 thin film gas sensors for different operating temperatures exposed to 200 ppm H_2 at 25 % relative humidity.

200 ppm H_2 / 25 % rh	Bare SnO_2	SnO_2 + AuPd
250 °C	458	225
300 °C	396	118
350 °C	422	142
400 °C	471	120

6.10 Gas sensing characterization of SnO_2 thin film gas sensors functionalized with AuPt nanoparticles

AuPt nanoparticles (see Chapter 5.1.4) were used for functionalizing SnO_2 thin films integrated on MPW4 microhotplates. The nanoparticles were deposited by spotting. The sensor performance to the exposure of CO and H_2 was evaluated at operating temperatures from 150 °C to 400 °C and relative humidity levels of 25 %, 50 %, and 75 %.

Figure 6.18 and Figure 6.19 summarize the gas response of bare and AuPt functionalized SnO_2 thin film gas sensors, integrated on MPW4 microhotplates, at 75 % relative humidity to 10 ppm CO and H_2, respectively. The sensor performance of AuPt functionalized SnO_2 thin film gas sensors at 250 °C is shown in Figure 6.20. By functionalizing SnO_2 with AuPt nanoparticles, the highest sensitivity to CO was achieved at 250 °C, compared to 300 °C for bare SnO_2. For operating temperature between 150 °C and 300 °C, the gas response to CO was improved significantly by AuPt nanoparticles. For the detection of H_2, the highest sensor performance was achieved at 250 °C for both bare and AuPt functionalized SnO_2 thin film gas sensors.
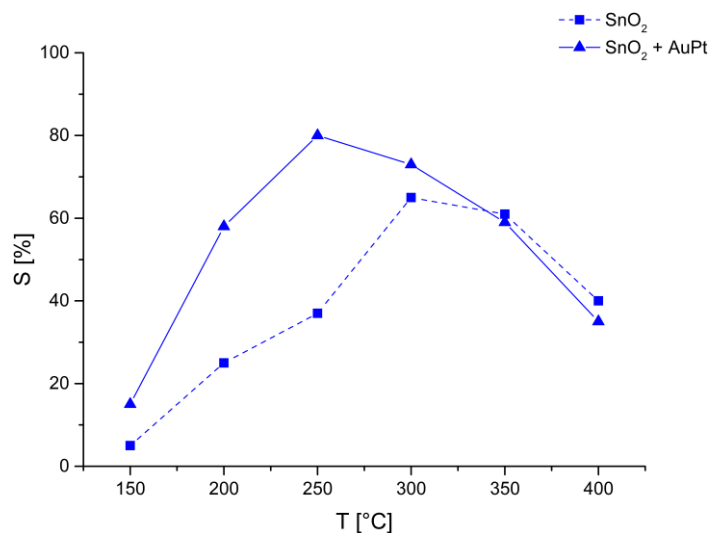
Figure 6.18: Gas response versus operating temperature of bare and AuPt functionalized SnO_2 thin film gas sensors on MPW4 microhotplate to 10 ppm CO at 75 % relative humidity.
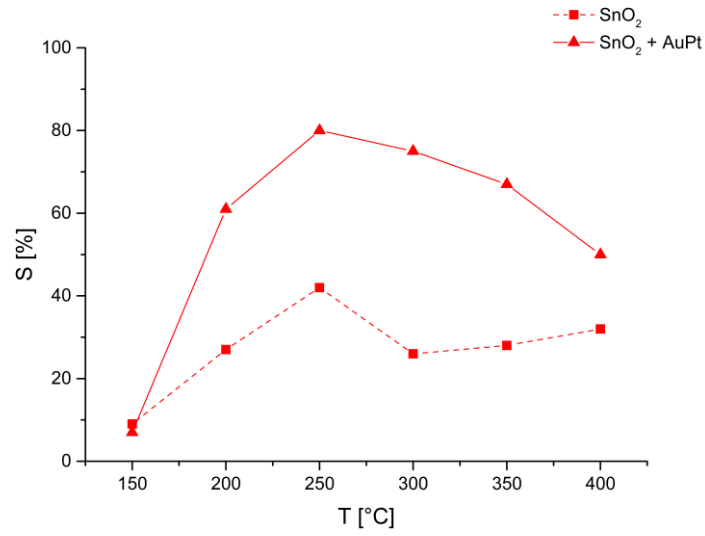
Figure 6.19: Gas response versus operating temperature of bare and AuPt functionalized SnO_2 thin film gas sensors on MPW4 microhotplate to 10 ppm H_2 at 75 % relative humidity.
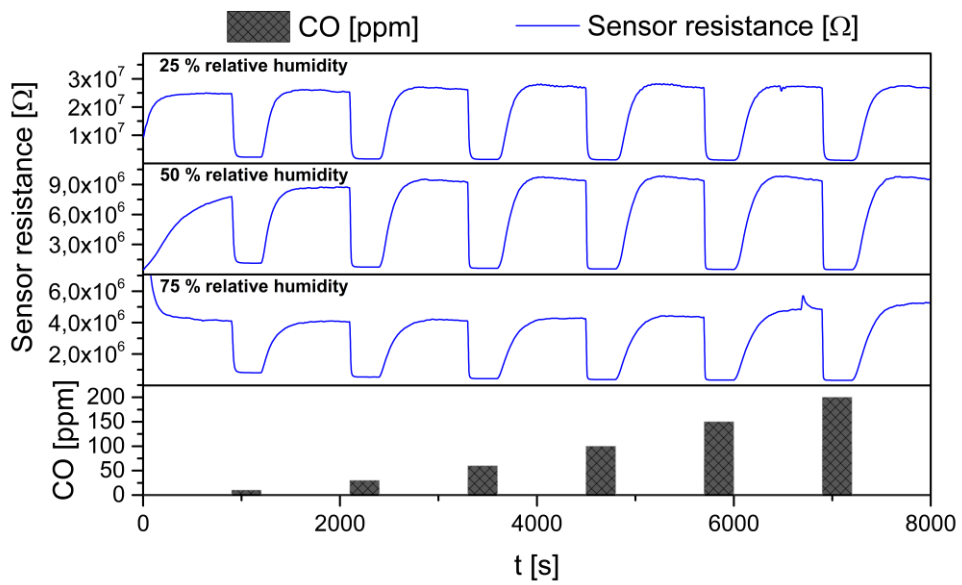
Figure 6.20: Sensor performance of AuPt functionalized SnO_2 thin film gas sensors to CO concentrations of 10 – 200 ppm at 250 °C and relative humidity levels of 25 %, 50 %, and 75 %.

A higher gas response to H_2 was achieved at operating temperatures from 200 °C to 400 °C by the functionalization with AuPt nanoparticles. The impact of humidity on the sensor performance was slightly reduced but not eliminated by the functionalization with AuPt nanoparticles. The evaluation of response and recovery times of bare and AuPt functionalized sensors showed that the recovery time was reduced by the functionalization with AuPt nanoparticles. Table 6.7 summarizes the recovery times to the exposure of 200 ppm CO at an operating temperature of 300 °C for humidity levels of 25 %, 50 %, and 75 %. The response time of AuPt functionalized SnO_2 at 400 °C and 25 % relative humidity was 11 s.

Table 6.7: Recovery times (t_{10}) of bare and AuPt functionalized SnO_2 thin film gas sensors for different humidity levels exposed to 200 ppm CO at 300 °C.

200 ppm CO / 300 °C	Bare SnO_2	SnO_2 + AuPt
25 % rh	173 s	103 s
50 % rh	136 s	110 s
75 % rh	133 s	122 s

IV. Summary and Outlook

Summary

In 1968, the first gas sensor based on SnO_2 was commercialized by Taguchi. Since then, a vast number of different gas sensing materials based on metal oxides have been investigated and developed. Nevertheless, SnO_2 is still the most investigated and used metal oxide for gas sensing. Today, a variety of metal oxide gas sensors are commercially available. However, the sensors on the market are quite bulky and expensive devices, and the applications of these sensors are limited to laboratories or industrial processing. Gas sensors based on metal oxides are operated at elevated temperature, therefore, a heating element has to be provided, which is usually the component with the highest power consumption. The high power consumption is one of the factors preventing the application of these sensors in mobile applications. For fabricating smart and cheap gas sensors with low power consumption, the combination with CMOS technology is inevitable. Integration of metal oxide gas sensors on CMOS microchips accesses a new market in portable electronics. Miniaturized gas sensors with reduced power consumption can be used as personal safety devices in smart phones or smart watches. The aim of this work was the fabrication and characterization of CMOS-integrable SnO_2 thin film gas sensors functionalized with metallic and bimetallic nanoparticles for enhanced sensor performance.

Spray pyrolysis was the method of choice for the integration of SnO_2 thin films on CMOS microchips. A self-made spray pyrolysis setup with an air atomizing nozzle was used for the CMOS compatible deposition of 50 nm thin SnO_2 layers at 400 °C. An annealing step of 45 minutes at 400 °C was performed to obtain a polycrystalline and stable film. The SnO_2 thin film was characterized by TEM and AFM to determine the morphology and roughness of the deposited thin film. The TEM characterization revealed that a compact crystalline layer was formed by the spray pyrolysis process. The polycrystalline layer is composed of differently oriented grains with crystallite sizes of about 10 nm. AFM measurements of the SnO_2 thin film determined that a smooth and continuous granular layer with a root mean square (RMS) roughness in the range of 1 nm was deposited by spray pyrolysis.

SnO$_2$ thin film gas sensors were fabricated on CMOS microhotplates, which were designed and fabricated by the project partner ams AG within the project "MSP – Multi Sensor Platform for Smart Building Management" (Framework Programm 7). The microhotplates were built up by a specific CMOS stack, fabricated in a standard 0.35 µm CMOS technology. For thermal insulation and reduction of power consumption, the microhotplates were released in a CMOS post-processing step by dry and isotropic ion etching, resulting in a suspended membrane with dimensions of 72 µm x 72 µm connected to the rest of the microchip by four arms. Rapid heating to temperatures of up to 400 °C were achieved with rise/fall times of under 10 milliseconds. A power of 13.5 mW was required to heat the microhotplates to 400 °C. The patterning of the SnO$_2$ thin film was achieved by photolithography followed by dry Ar ion etching. Additionally, SnO$_2$ gas sensors were fabricated on silicon substrates using discrete heaters and a thermocouple for assembling the sensor. The silicon based SnO$_2$ thin film gas sensors were used for a fast and low-cost investigation of different deposition techniques for nanoparticles.

This thesis was also partly performed within the project "RealNano – Industrielle Realisierung innovativer CMOS basierter Nanosensoren" funded by the Austrian Research Promotion Agency. Different deposition techniques for functionalizing the CMOS integrated SnO$_2$ thin film gas sensors with metallic and bimetallic nanoparticles were investigated. The deposition techniques were required to be compatible with CMOS microchips with a maximum deposition temperature of 400 °C and to allow scale up of nanoparticle deposition to wafer level. Inkjet printing, spotting, and sputtering were the techniques used to functionalize CMOS integrated SnO$_2$ thin film gas sensors with metallic and bimetallic nanoparticles. For inkjet printing, a Dimatix Material Printer from Fujifilm was employed. The deposition experiments were performed in the laboratories of the project partner EVGroup. The deposition of nanoparticle solutions by spotting was performed by courtesy of Scienion AG, using a non-contact, drop-on-demand spotter tool (sciFLEXARRAYER SX). Both deposition techniques allowed a precise deposition of metallic and bimetallic nanoparticle solutions on the microhotplates with dimensions of 72 µm x 72 µm. Size-selected deposition of noble metal nanoparticles on CMOS integrated SnO$_2$ thin film gas sensors was achieved by using a magnetron sputtering

inert-gas condensation deposition system. The experiments were performed at the Okinawa Institute of Science and Technology Graduate University (OIST).

The sensor performance of bare and functionalized CMOS integrated SnO_2 thin film gas sensors to CO and H_2 was evaluated in dry and wet atmosphere at different operating temperatures. For the functionalization of SnO_2 thin films, Au, Pt, NiPt, AuPd, and AuPt nanoparticles were used, which were provided by project partners or commercially acquired. Au and NiPt nanoparticles did not improve the sensor performance of SnO_2 thin film gas sensors. Non-residue-free decomposition of the stabilizing surfactant in the Au nanoparticle solution was the reason for the deterioration of the sensor performance, showing no gas sensitivity. The highly concentrated NiPt nanoparticle solution lead to the formation of a layer on top of the SnO_2 thin film at elevated operating temperatures, reducing the gas response to CO significantly. The functionalization of CMOS based SnO_2 thin film gas sensors with Pt, AuPd, and AuPt nanoparticles resulted in an improved sensor performance. Pt nanoparticles increased the gas response to CO significantly, especially to CO concentrations in the low ppm range, and cross-sensitivity to humidity was also eliminated by the Pt functionalization. SnO_2 thin films functionalized with AuPd nanoparticles showed enhanced selectivity to H_2 at operating temperatures of 250 °C and 300 °C. The functionalization with AuPt nanoparticles lead to a significantly improved gas response to CO concentrations down to 10 ppm, reducing the operating temperature for CO detection from 300 °C to 150 °C. SnO_2 thin film gas sensors showed a response time (t_{90}) of < 10 s, which correlates well with values reported in literature for SnO_2 based gas sensors [51], [178], [179]. The response time was not influenced by the nanoparticles. The recovery time (t_{10}) of SnO_2 thin films was in the range of 1-7 minutes, which is in good agreement with literature values [180], [181]. The recovery time for CO and H_2 was decreased significantly by functionalizing SnO_2 thin films with nanoparticles.

In summary, SnO_2 thin film gas sensors were integrated on CMOS microhotplates and functionalized successfully with various metallic and bimetallic nanoparticles using different deposition techniques. The nanoparticle functionalization improved the gas response to CO and H_2, reduced the cross-sensitivity to humidity, and decreased the recovery time of SnO_2 thin film gas sensors significantly.

Outlook

In this thesis, spray pyrolysis was used for the deposition of SnO_2 thin films. Low cost, easy handling, fast deposition, and no need for expensive vacuum equipment are some of the many advantages compared to other deposition techniques like CVD and PVD. Within the framework of the project "MSP", a new spray pyrolysis tool was developed by the Materials Center Leoben Forschung GmbH. This new tool allows the deposition of SnO_2 thin films to be scaled-up to wafer level. A precise pressure control unit, a high temperature hotplate with a fast and accurate temperature regulation, and a finely adjustable exhaust system enable reproducible deposition of SnO_2 thin films on full-wafer-scale. Additionally, deposition of new gas sensitive metal oxide materials, like CuO or ZnO, by spray pyrolysis is currently being investigated.

Within the "MSP – Multi Sensor Platform for Smart Building Management"-project, a new microchip, the MPW4, was designed and fabricated by the project partner ams AG. It incorporates eight microhotplates, which can be operated simultaneously, and on each microhotplate two metal oxide gas sensors can be implemented. By employing TSV technology, flexible 3D- integration of MPW4 microchips on CMOS electronic platform chips is possible. A worldwide unique multi gas sensor device could be realized by integrating different metal oxide nanomaterials on MPW4 microchips. The combination of bare and functionalized metal oxide thin film and nanowire gas sensors on one microchip would allow the fabrication of a CMOS integrated nanosensor array with enhanced sensitivity and selectivity to various target gases. For the characterization of such devices, a new gas measurement setup was designed together with

mb-Technologies GmbH and is currently being implemented into the well-established gas measurement setup used so far. With this new setup, all of the sixteen gas sensors can be operated and characterized simultaneously, generating huge amounts of valuable data. In the future, work in the field of data mining, pattern recognition, and algorithm development are planned within the microelectronics group of Materials Center Leoben for further enhancing sensitivity and selectivity of this CMOS integrated sensor array.

The development of a screening platform for optimizing metal oxide gas sensors with combinations of different functional nanoparticles is the goal of a new project called "FunkyNano – Optimierte Funktionalisierung von Nanosensoren zur Gasdetektion durch Screening von Hybrid-Nanopartikeln", which started on May 1st, 2017, and is funded by the Austrian Research Promotion Agency. The follow-up project of "RealNano – Industrielle Realisierung innovativer CMOS basierter Nanosensoren" focuses on the fabrication of nanosensor arrays using different gas sensitive metal oxide thin films. The sensor arrays are functionalized with various nanoparticles, concentration and combination of nanoparticles are systematically modified, and simultaneous characterization of nanosensor arrays in a gas measurement setup allows fast and efficient screening of different material combinations. Through this screening process, the optimum functionalization of metal oxide based gas sensors can be identified for a variety of target gases. The final goal of the project is the realization of a CMOS-based laboratory prototype comprising 16 gas sensors, each functionalized specifically for a certain test gas.

Bibliography

[1]   S. Sharma and M. Madou, "A new approach to gas sensing with nanotechnology.," *Philos. Trans. A. Math. Phys. Eng. Sci.*, vol. 370, pp. 2448–2473, 2012.

[2]   A. Ponzoni, E. Comini, I. Concina, M. Ferroni, M. Falasconi, E. Gobbi, V. Sberveglieri, and G. Sberveglieri, "Nanostructured Metal Oxide Gas Sensors, a Survey of Applications Carried out at SENSOR Lab, Brescia (Italy) in the Security and Food Quality Fields," *Sensors*, vol. 12, pp. 17023–17045, 2012.

[3]   T. Seiyama, A. Kato, K. Fujiishi, and M. Nagatani, "A New Detector for Gaseous Components Using Semiconductive Thin Films," *Anal. Chem.*, vol. 34, pp. 1502–1503, 1962.

[4]   P. Feng, F. Shao, Y. Shi, and Q. Wan, "Gas sensors based on semiconducting nanowire field-effect transistors," *Sensors (Basel).*, vol. 14, no. 9, pp. 17406–17429, 2014.

[5]   G. Eranna, B. C. Joshi, D. P. Runthala, R. P. Gupta, G. Eranna, B. C. Joshi, D. P. Runthala, and R. P. Gupta, "Oxide Materials for Development of Integrated Gas Sensors — A Comprehensive Review," *Crit. Rev. Solid State Mater. Sci.*, vol. 29, pp. 111–188, 2004.

[6]   N. Barsan, D. Koziej, and U. Weimar, "Metal oxide-based gas sensor research: How to?," *Sensors Actuators B Chem.*, vol. 121, pp. 18–35, 2007.

[7]   J. M. Smulko, M. Trawka, C. G. Granqvist, R. Ionescu, F. Annanouch, E. Llobet, and L. B. Kish, "New approaches for improving selectivity and sensitivity of resistive gas sensors: a review," *Sens. Rev.*, vol. 35, pp. 340–347, 2015.

[8]   T. Hübert, L. Boon-Brett, G. Black, and U. Banach, "Hydrogen sensors - A review," *Sensors Actuators, B Chem.*, vol. 157, pp. 329–352, 2011.

[9]   B. Bahrami, A. Khodadadi, M. Kazemeini, and Y. Mortazavi, "Enhanced CO sensitivity and selectivity of gold nanoparticles-doped SnO2 sensor in presence of propane and methane," *Sensors Actuators B Chem.*, vol. 133, pp. 352–356, 2008.

[10]   A. Caron, N. Redon, F. Thevenet, B. Hanoune, and P. Coddeville, "Performances and limitations of electronic gas sensors to investigate an indoor air quality event," *Build. Environ.*, vol. 107, pp. 19–28, 2016.

[11]   P. Kumar, A. N. Skouloudis, M. Bell, M. Viana, M. C. Carotta, G. Biskos, and L. Morawska, "Real-time sensors for indoor air monitoring and challenges ahead in deploying them to urban buildings," *Sci. Total Environ.*, vol. 560–561, pp. 150–159, 2016.

[12]   J. Gardner, P. Guha, F. Udrea, and J. A. Covington, "CMOS interfacing for integrated gas sensors: A review," *IEEE Sens. J.*, vol. 10, pp. 1833–1848, 2010.

[13]   "IHS Markit." [Online]. Available: https://ihsmarkit.com/. [Accessed: 05-Jun-2017].

[14]   R. Jaaniso and O. K. Tan, Eds., *Semiconductor gas sensors*. Woodhead Publishing Limited, 2013.

[15]   S. Capone, A. Forleo, L. Francioso, R. Rella, P. Siciliano, J. Spadavecchia, D. S. Presicce, and A. M. Taurino, "Solid State Gas Sensors: State of the Art and Future Activities," *J. Optoelectron. Adv. Mater.*, vol. 5, pp. 1335–1348, 2003.

[16]   J. Zhang and K. Hoshino, *Molecular Sensors and Nanodevices*. Elsevier, 2014.

[17]   K. Arshak, E. Moore, G. M. Lyons, J. Harris, and S. Clifford, "A review of gas sensors employed in electronic nose applications," *Sens. Rev.*, vol. 24, pp. 181–198, 2004.

[18]   J. Hodgkinson and R. P. Tatam, "Optical gas sensing: a review," *Meas. Sci. Technol.*, vol. 24, pp. 1–59, 2013.

[19]   X. Liu, S. Cheng, H. Liu, S. Hu, D. Zhang, and H. Ning, "A Survey on Gas Sensing Technology," *Sensors*, vol. 12, pp. 9635–9665, 2012.

[20] J. R. Stetter, W. R. Penrose, and S. Yao, "Sensors, Chemical Sensors, Electrochemical Sensors, and ECS," *J. Electrochem. Soc.*, vol. 150, pp. 11–16, 2003.

[21] C. Wang, L. Yin, L. Zhang, D. Xiang, and R. Gao, "Metal oxide gas sensors: sensitivity and influencing factors," *Sensors*, pp. 2088–2106, 2010.

[22] Y.-F. Sun, S.-B. Liu, F.-L. Meng, J.-Y. Liu, Z. Jin, L.-T. Kong, and J.-H. Liu, "Metal Oxide Nanostructures and Their Gas Sensing Properties: A Review," *Sensors*, vol. 12, pp. 2610–2631, 2012.

[23] G. F. Fine, L. M. Cavanagh, A. Afonja, and R. Binions, "Metal oxide semi-conductor gas sensors in environmental monitoring.," *Sensors (Basel).*, vol. 10, pp. 5469–502, Jan. 2010.

[24] H. Kim and J. Lee, "Highly sensitive and selective gas sensors using p-type oxide semiconductors: Overview," *Sensors Actuators B. Chem.*, vol. 192, pp. 607–627, 2014.

[25] G. Korotcenkov, "Metal oxides for solid-state gas sensors: What determines our choice?," *Mater. Sci. Eng. B*, vol. 139, pp. 1–23, 2007.

[26] M. Batzill and U. Diebold, "The surface and materials science of tin oxide," *Prog. Surf. Sci.*, vol. 79, pp. 47–154, 2005.

[27] G. B. González, "Investigating the Defect Structures in Transparent Conducting Oxides Using X-ray and Neutron Scattering Techniques," *Materials (Basel).*, vol. 5, pp. 818–850, 2012.

[28] N. Barsan and U. Weimar, "Understanding the fundamental principles of metal oxide based gas sensors; the example of CO sensing with SnO2 sensors in the presence of humidity," *J. Phys. Condens. Matter*, vol. 15, pp. 813–839, 2003.

[29] M. E. Franke, T. J. Koplin, and U. Simon, "Metal and metal oxide nanoparticles in chemiresistors: does the nanoscale matter ?," *Small*, vol. 2, pp. 36–50, 2006.

[30]   M. A. Carpenter, S. Mathur, and A. Kolmakov, Eds., *Metal Oxide Nanomaterials for Chemical Sensors*. Springer, 2013.

[31]   K. Geckeler and E. Rosenberg, Eds., *Functional Nanomaterials*. American Scientific Publishers, 2006.

[32]   D. E. Williams, "Semiconducting oxides as gas-sensitive resistors," *Sensors Actuators B. Chem.*, vol. 57, pp. 1–16, 1999.

[33]   F.-G. Banica, Ed., "Resistive Gas Sensors (Chemiresistors)," in *Chemical Sensors and Biosensors: Fundamentals and Applications*, First Edit., John Wiley & Sons, Ltd., 2012.

[34]   D. G. Rickerby and A. M. Serventi, "Nanostructured Metal Oxide gas sensors for air-quality monitoring," in *Environanotechnology*, I. Wright, R. Slimane, Z. L. Wang, A. Bland, C. P. Huang, and M. Fan, Eds. Elsevier, 2010, pp. 99–136.

[35]   S. Seal and S. Shukla, "Nanocrystalline SnO Gas Sensors in View of Surface Reactions and Modifications," *J. Miner. Met. Mater. Soc.*, vol. 54, pp. 35–39, 2002.

[36]   C. Xu, J. Tamaki, N. Miura, and N. Yamazoe, "Correlation between gas sensitivity and crystallite size in porous SnO2-based sensors," *Chem. Lett.*, pp. 441–444, 1990.

[37]   C. Xu, J. Tamaki, N. Miura, and N. Yamazoe, "Grain size effects on gas sensitivity of porous Sn02-based elements," *Sensors Actuators B. Chem.*, vol. 3, pp. 147–155, 1991.

[38]   J. F. McAleer, P. T. Moseley, J. W. Norris, D. E. Williams, and O. O. X. Ora, "Tin dioxide gas sensors Part 1: apects of the surface chemistry revealed by electrical conductance variations," *J. Chem. Soc. Faraday Trans. 1*, vol. 83, pp. 1323–1346, 1987.

[39]   A. Harkoma-Mattila, P. Romppainen, H. Torvela, and S. Lepp, "Sensitivity of SnO2 Semiconductor Gas Sensors to CO in the Presence of High Concentrations of Water Vapour," *J. Eur. Ceram. Soc.*, vol. 6, pp. 361–367, 1990.

[40] W. Thornton and P. G. Harrison, "Tin Oxide Surfaces Part 1: Surface Hydroxyl Groups and the Chemisorption of Carbon Dioxide and Carbon Monoxide on Tin(IV) Oxide," *J. Chem. Soc. Faraday Trans. 1*, vol. 71, pp. 461–472, 1975.

[41] S. Lenaerts, J. Roggen, and G. Maes, "FT-IR characterization of tin dioxide gas sensor materials under working conditions," *Spectrochim. Acta*, vol. 51, pp. 883–894, 1995.

[42] N. Yamazoe, J. Fuchigami, M. Kishikawa, and T. Seiyama, "Interactions of tin oxide surface with O2, H2O and H2," *Surf. Sci.*, vol. 86, pp. 335–344, 1979.

[43] M. Egashira, M. Nakashima, and S. Kawasumi, "Change of Thermal Desorption Behaviour of Adsorbed Oxygen with Water Coadsorption on Ag+-doped Tin(IV) Oxide," *J. Chem. Soc. Chem. Commun.*, vol. 20, pp. 1047–1049, 1981.

[44] G. Heiland and D. Kohl, *Chemical Sensor Technology, Volume 1*. Tokyo: Kodansha Ltd.

[45] S. Morrison, *The Chemical Physics of Surfaces*. New York: Springer US, 1977.

[46] V. E. Henrich and P. A. Cox, *The Surface Science of Metal Oxides*. Cambridge: Cambridge University Press, 1994.

[47] M. Graf, A. Gurlo, N. Bârsan, U. Weimar, and A. Hierlemann, "Microfabricated gas sensor systems with sensitive nanocrystalline metal-oxide films," *J. Nanoparticle Res.*, vol. 8, pp. 823–839, 2006.

[48] L. F. Francis, "Sol-Gel Methods for Oxide Coatings," *Mater. Manuf. Process.*, vol. 12, pp. 963–1015, 1997.

[49] C. J. Brinker, A. J. Hurd, P. R. Schunk, G. C. Frye, and C. S. Ashley, "Review of sol-gel thin film formation," *J. Non. Cryst. Solids*, vol. 147–148, pp. 424–436, 1992.

[50] D. Chen, "Anti-reflection (AR) coatings made by sol-gel processes : A review," *Sol. energy Mater. Sol. cells*, vol. 68, pp. 313–336, 2001.

[51] J. Gong, Q. Chen, W. Fei, and S. Seal, "Micromachined nanocrystalline SnO2 chemical gas sensors for electronic nose," *Sensors Actuators B. Chem.*, vol. 102, pp. 117–125, 2004.

[52] W. Chung, J. Lim, D. Lee, N. Miura, and N. Yamazoe, "Thermal and gas-sensing properties of planar-type micro gas sensor," *Sensors Actuators B Chem.*, vol. 64, pp. 118–123, 2000.

[53] J. Cerdà, A. Cirera, A. Vila, A. Cornet, and J. R. Morante, "Deposition on micromachined silicon substrates of gas sensitive layers obtained by a wet chemical route : a CO/CH 4 high performance sensor," *Thin Solid Films*, vol. 391, pp. 265–269, 2001.

[54] P. Fau, M. Sauvan, S. Trautweiler, C. Nayral, L. Erades, A. Maisonnat, and B. Chaudret, "Nanosized tin oxide sensitive layer on a silicon platform for domestic gas applications," *Sensors Actuators B. Chem.*, vol. 78, pp. 83–88, 2001.

[55] I. Jiménez, A. Cirera, J. Folch, A. Cornet, and J. R. Morante, "Innovative method of pulverisation coating of prestabilized nanopowders for mass production of gas sensors," *Sensors Actuators B. Chem.*, vol. 78, pp. 78–82, 2001.

[56] K. Sahner and H. L. Tuller, "Novel deposition techniques for metal oxide: Prospects for gas sensing," *J. Electroceramics*, vol. 24, pp. 177–199, 2010.

[57] D. Vincenzi, M. A. Butturi, V. Guidi, M. C. Carotta, and G. Martinelli, "Development of a low-power thick-film gas sensor deposited by screen-printing technique onto a micromachined hotplate," *Sensors Actuators B. Chem.*, vol. 77, pp. 95–99, 2001.

[58] L. Gonzalez-Macia, A. Morrin, M. R. Smyth, and A. J. Killard, "Advanced printing and deposition methodologies for the fabrication of biosensors and biodevices," *Analyst*, vol. 135, pp. 845–867, 2010.

[59] B. Riviere, J. Viricelle, and C. Pijolat, "Development of tin oxide material by screen-printing technology for micro-machined gas sensors," *Sensors Actuators B. Chem.*, vol. 93, pp. 531–537, 2003.

[60] D. M. Mattox, *Handbook of Physical Vapor Deposition (PVD) Processing*. Elsevier Inc., 2010.

[61] G. Müller, A. Friedberger, P. Kreisl, S. Ahlers, O. Schulz, and T. Becker, "A MEMS toolkit for metal-oxide-based gas sensing systems," *Thin Solid Films*, vol. 436, pp. 34–45, 2003.

[62] A. Friedberger, P. Kreisl, E. Rose, G. Müller, G. Kühner, J. Wöllenstein, and H. Böttner, "Micromechanical fabrication of robust low-power metal oxide gas sensors," *Sensors Actuators B. Chem.*, vol. 93, pp. 345–349, 2003.

[63] K. Sarakinos, J. Alami, and S. Konstantinidis, "High power pulsed magnetron sputtering: A review on scientific and engineering state of the art," *Surf. Coat. Technol.*, vol. 204, pp. 1661–1684, 2010.

[64] P. J. Kelly and R. D. Arnell, "Magnetron sputtering: a review of recent developments and applications," *Vacuum*, vol. 56, pp. 159–172, 2000.

[65] E. Comini, G. Faglia, and G. Sberveglieri, Eds., "Electrical-based gas sensing," in *Solid State Gas Sensing*, Springer US, 2009.

[66] V. Demarne and A. Grisel, "A new SnO2 low temperature deposition technique for integrated gas sensors," *Sensors Actuators B. Chem.*, vol. 15–16, pp. 63–67, 1993.

[67] H. O. Pierson, *Handbook of Chemical Vapor Deposition (CVD) Principles, Technology, and Application*, Second Edi. Park Ridge: Noyes Publications, 1999.

[68] A. K. Pattanaik and V. K. Sarin, "Basic Principles of CVD Thermodynamics and Kinetics," in *Chemical Vapor Deposition*, J.-H. Park and T. S. Sudarshan, Eds. ASM International, 2001.

[69] J. Vetrone and Y.-W. Chung, "Organometallic chemical vapor deposition of SnO2 single crystal and polycrystalline films," *J. Vac. Sci. Technol. A Vacuum, Surfaces, Film.*, vol. 9, pp. 3041–3047, 1991.

[70] P. Montmeat, C. Pijolat, G. Tournier, and J. Viricelle, "The influence of a platinum membrane on the sensing properties of a tin dioxide thin film," *Sensors Actuators B. Chem.*, vol. 84, pp. 148–159, 2002.

[71] R. R. Chamberlin and J. S. Skarman, "Chemical spray deposition process for inorganic films," *J. Electrochem. Soc.*, vol. 113, no. 1, pp. 86–89, 1966.

[72] C. Guild, S. Biswas, Y. Meng, T. Jafari, A. M. Gaffney, and S. L. Suib, "Perspectives of spray pyrolysis for facile synthesis of catalysts and thin films: An introduction and summary of recent directions," *Catal. Today*, vol. 238, pp. 87–94, Dec. 2014.

[73] P. Patil, "Versatility of chemical spray pyrolysis technique," *Mater. Chem. Phys.*, vol. 59, pp. 185–198, 1999.

[74] D. Perednis and L. J. Gauckler, "Thin Film Deposition Using Spray Pyrolysis," *J. Electroceramics*, vol. 14, pp. 103–111, 2005.

[75] G. Korotcenkov and B. K. Cho, "Spray pyrolysis deposition of undoped SnO2 and In2O3 films and their structural properties," *Prog. Cryst. Growth Charact. Mater.*, vol. 63, pp. 1–47, 2017.

[76] G. Korotcenkov, V. Brinzari, J. Schwank, M. Dibattista, and A. Vasiliev, "Peculiarities of SnO2 thin film deposition by spray pyrolysis for gas sensor application," *Sensors Actuators B. Chem.*, vol. 77, pp. 244–252, 2001.

[77] L. C. Nehru, M. Umadevi, and C. Sanjeeviraja, "Studies on Structural, Optical and Electrical Properties of ZnO Thin Films Prepared by the Spray Pyrolysis Method," *Int. J. Mater. Eng.*, vol. 2, pp. 12–17, 2012.

[78] A. K. Nayak, R. Ghosh, S. Santra, P. K. Guha, and D. Pradhan, "Hierarchical Nanostructured WO3-SnO2 for Selective Sensing of Volatile Organic Compounds," *Nanoscale*, vol. 7, pp. 12460–12473, 2015.

[79] E. Dilonardo, M. Penza, M. Alvisi, C. Di Franco, F. Palmisano, L. Torsi, and N. Cioffi, "Evaluation of gas-sensing properties of ZnO nanostructures electrochemically doped with Au nanophases," *Beilstein J. Nanotechnol.*, vol. 7, pp. 22–31, 2016.

[80] S. Morrison, "Selectivity in semiconductor gas sensors," *Sensors and Actuators*, vol. 12, pp. 425–440, 1987.

[81] G. Korotcenkov, "Gas response control through structural and chemical modification of metal oxide films: state of the art and approaches," *Sensors Actuators B Chem.*, vol. 107, pp. 209–232, May 2005.

[82] V. E. Bochenkov and G. B. Sergeev, "Preparation and chemiresistive properties of nanostructured materials," *Adv. Colloid Interface Sci.*, vol. 116, pp. 245–254, 2005.

[83] G. Velmathi, S. Mohan, and R. Henry, "Analysis of Factors for Improving Functionality of Tin Oxide Gas Sensor," *IETE Tech. Rev.*, vol. 33, pp. 122–129, 2016.

[84] G. Korotcenkov and B. K. Cho, "Engineering approaches for the improvement of conductometric gas sensor parameters Part 1. Improvement of sensor sensitivity and selectivity (short survey)," *Sensors Actuators B. Chem.*, vol. 188, pp. 709–728, 2013.

[85] F. Ménil, C. Lucat, and H. Debcda, "The thick-film route to selective gas sensors," *Sensors Actuators B. Chem.*, vol. 24–25, pp. 415–420, 1995.

[86] G. G. Mandayo, E. Castaño, F. J. Gracia, A. Cirera, A. Cornet, and J. R. Morante, "Built-in active filter for an improved response to carbon monoxide combining thin- and thick-film technologies," *Sensors Actuators B. Chem.*, vol. 87, pp. 88–94, 2002.

[87] M. Frietsch, F. Zudock, J. Goschnick, and M. Bruns, "CuO catalytic membrane as selectivity trimmer for metal oxide gas sensors," *Sensors*, vol. 65, pp. 379–381, 2000.

[88] L. De Angelis and R. Riva, "Selectivity and stability of a tin dioxide sensor for methane," *Sensors*, vol. 28, pp. 25–29, 1995.

[89] S. Yamaguchi, "Gold colloid as applied to the H2S gas sensor," *Mater. Chem.*, vol. 6, pp. 505–508, 1981.

[90] P. McGeehin, "Self-diagnostic gas sensors which differentiate carbon monoxide from interference gases for residential applications," *Sens. Rev.*, vol. 16, pp. 37–39, 1996.

[91] M. Schweizer-Berberich, S. Strathmann, W. Göpel, R. Sharma, and A. Peyre-Lavigne, "Filters for tin dioxide CO gas sensors to pass the UL2034 standard," *Sensors Actuators B. Chem.*, vol. 66, pp. 34–36, 2000.

[92] A. P. Lee and B. J. Reedy, "Temperature modulation in semiconductor gas sensing," *Sensors Actuators B. Chem.*, vol. 60, pp. 35–42, 1999.

[93] A. Heilig, N. Barsan, U. Weimar, M. Schweizer-Berberich, J. Gardner, and W. Göpel, "Gas identification by modulating temperatures of SnO2 -based thick film sensors," *Sensors Actuators B. Chem.*, vol. 43, pp. 45–51, 1997.

[94] X. Huang, F. Meng, Z. Pi, W. Xu, and J. Liu, "Gas sensing behavior of a single tin dioxide sensor under dynamic temperature modulation," *Sensors Actuators B. Chem.*, vol. 99, pp. 444–450, 2004.

[95] R. E. Cavicchi, J. S. Suehle, K. G. Kreider, M. Gaitan, and P. Chaparala, "Fast temperature programmed sensing for micro-hotplate gas sensors," *IEEE Electron Device Lett.*, vol. 16, pp. 286–288, 1995.

[96] W. Göpel, "Chemical imaging: I . Concepts and visions for electronic and bioelectronic noses," *Sensors Actuators B. Chem.*, vol. 52, pp. 125–142, 1998.

[97] K. Persaud and G. Dodd, "Analysis of discrimination mechanisms in the mammalian olfactory system using a model nose," *Nature*, vol. 299, pp. 352–355, 1982.

[98] J. W. Gardner and P. N. Bartlett, "A brief history of electronic noses," *Sensors Actuators B. Chem.*, vol. 18–19, pp. 211–220, 1994.

[99] M. S. Cosio, M. Scampicchio, and S. Benedetti, "Electronic Noses and Tongues," in *Chemical Analysis of Food: Techniques and Applications*, Elsevier Inc., 2012.

[100] W. Ping and X. Jun, "A novel recognition method for electronic nose using artificial neural network and fuzzy recognition," *Sensors Actuators B. Chem.*, vol. 37, pp. 169–174, 1996.

[101] J. Brezmes, B. Ferreras, E. Llobet, X. Vilanova, and X. Correig, "Neural network based electronic nose for the classification of aromatic species," *Anal. Chim. Acta*, vol. 348, pp. 503–509, 1997.

[102] J.-E. Haugen and K. Kvaal, "Electronic Nose and Artificial Neural Network," *Meat Sci.*, vol. 49, pp. 273–286, 1998.

[103] J. Fu, G. Li, Y. Qin, and W. J. Freeman, "A pattern recognition method for electronic noses based on an olfactory neural network," *Sensors Actuators B. Chem.*, vol. 125, pp. 489–497, 2007.

[104] A. Ortega, S. Marco, T. Sundic, and J. Samitier, "New pattern recognition systems designed for electronic noses," *Sensors Actuators B. Chem.*, vol. 69, pp. 302–307, 2000.

[105] M. Falasconi, M. Pardo, M. Vezzoli, and G. Sberveglieri, "Cluster validation for electronic nose data," *Sensors Actuators B. Chem.*, vol. 125, pp. 596–606, 2007.

[106] "Paragon Sensoren." [Online]. Available: http://www.paragon.ag/geschaeftsbereiche/sensoren.html. [Accessed: 04-Jun-2017].

[107] "MICS Microchemical Systems." [Online]. Available: http://www.microchemical.com/. [Accessed: 04-Jun-2017].

[108] "City Technology - Engineering Safety." [Online]. Available: https://www.citytech.com/. [Accessed: 04-Jun-2017].

[109] "FIGARO." [Online]. Available: http://www.figarosensor.com/. [Accessed: 04-Jun-2017].

[110] C. Gamauf, M. Siegele, A. Nemecek, G. C. Mutinati, S. Steinhauer, E. Brunet, A. Kock, J. Kraft, J. Siegert, and F. Schrank, "Fully Integrated System-On Chip Gas Sensor in CMOS Technology," in *IEEE Sensors*, 2013, pp. 1–4.

[111] M. S. Haque, K. B. K. Teo, N. L. Rupensinghe, S. Z. Ali, I. Haneef, S. Maeng, J. Park, F. Udrea, and W. I. Milne, "On-chip deposition of carbon nanotubes using CMOS microhotplates.," *Nanotechnology*, vol. 19:025607, Jan. 2008.

[112] M. Graf, D. Barrettino, S. Taschini, C. Hagleitner, A. Hierlemann, and H. Baltes, "Metal oxide-based monolithic complementary metal oxide semiconductor gas sensor microsystem," *Anal. Chem.*, vol. 76, pp. 4437–4445, 2004.

[113] S. Joo and R. B. Brown, "Chemical sensors with integrated electronics," *Chem. Rev.*, vol. 108, pp. 638–651, 2008.

[114] M. Afridi, J. Suehle, M. E. Zaghloul, D. W. Berning, A. R. Hefner, R. E. Cavicchi, S. Semancik, C. B. Montgomery, and C. J. Taylor, "A monolithic CMOS microhotplate-based gas sensor system," *IEEE Sens. J.*, vol. 2, pp. 644–655, 2002.

[115] L. Sheng, Z. Tang, J. Wu, P. Chan, and J. Sin, "A low-power CMOS compatible integrated gas sensor using maskless tin oxide sputtering," *Sensors Actuators B Chem.*, vol. 49, pp. 81–87, 1998.

[116] E. Barborini, "Microhotplates and Integration with Metal-Oxide Nanomaterials," in *Integrated Analytical Systems*, M. A. Carpenter, A. Kolmakov, and S. Mathur, Eds. New York: Springer, 2013.

[117] A. Hierlemann, "Integrated chemical microsensor systems in CMOS-technology," in *The 13th International Conference on Solid-State Sensors, Actuators and Microsystems, 2005*, 2005, pp. 1134–1137.

[118] A. Lombardi, M. Grassi, P. Malcovati, S. Capone, L. Francioso, P. Siciliano, and A. Baschirotto, "A CMOS integrated interface circuit for metal-oxide gas sensors," *Sensors Actuators B Chem.*, vol. 142, pp. 82–89, 2009.

[119] B. K. Dable, K. S. Booksh, R. Cavicchi, and S. Semancik, "Calibration of microhotplate conductometric gas sensors by non-linear multivariate regression methods," *Sensors Actuators, B Chem.*, vol. 101, pp. 284–294, 2004.

[120] A. Götz, I. Gracia, J. Plaza, C. Cané, P. Roetsch, H. Böttner, and K. Seibert, "A novel methodology for the manufacturability of robust CMOS semiconductor gas sensor arrays," *Sensors Actuators B Chem.*, vol. 77, pp. 395–400, 2001.

[121] G. C. Mutinati, "3D-CMOS integrable gas sensor device based on nanocrystalline tin dioxide films," 2013.

[122] "Spraying Systems Co." [Online]. Available: http://www.spray.de/. [Accessed: 04-Jun-2017].

[123] "Harry Gestigkeit GmbH Fabrik für Labor-Apparate." [Online]. Available: http://www.gestigkeit.de/. [Accessed: 04-Jun-2017].

[124] T. Arai, "The study of the optical properties of conducting tin oxide films and their interpretation in terms of a tentative band scheme," *J. Phys. Soc. Japan*, vol. 15, pp. 916–927, 1961.

[125] J. C. Manifacier, "Thin metallic oxides as transparent conductors," *Thin Solid Films*, vol. 90, pp. 297–308, 1982.

[126] "Austrian Centre for Electron Microscopy and Nanoanalysis." [Online]. Available: https://www.felmi-zfe.at/. [Accessed: 04-Jun-2017].

[127] "Delta R - Die Temperatur-Experten." [Online]. Available: http://delta-r.de/de/. [Accessed: 04-Jun-2017].

[128] "ams sensor solutions." [Online]. Available: http://ams.com/eng. [Accessed: 04-Jun-2017].

[129] M. Siegele, C. Gamauf, A. Nemecek, G. C. Mutinati, S. Steinhauer, A. Köck, J. Kraft, J. Siezert, and F. Schrank, "Optimized integrated micro-hotplates in CMOS technology," in *2013 IEEE 11th International New Circuits and Systems Conference, NEWCAS 2013*, 2013, pp. 1–4.

[130] G. Sberveglieri, "Recent developments in semiconducting thin-film gas sensors," *Sensors Actuators B. Chem.*, vol. 23, pp. 103–109, 1995.

[131] H. Cheong, J. Choi, H. P. Kim, J. Kim, J. Kim, and G.-S. Churn, "The role of additives in tin dioxide-based gas sensors," *Sensors Actuators B. Chem.*, vol. 9, pp. 227–231, 1992.

[132] M. S. Wagh, G. H. Jain, D. R. Patil, S. A. Patil, and L. A. Patil, "Modified zinc oxide thick film resistors as NH3 gas sensor," *Sensors Actuators B. Chem.*, vol. 115, pp. 128–133, 2006.

[133] M. Stankova, X. Vilanova, J. Calderer, E. Llobet, J. Brezmes, I. Gràcia, C. Cané, and X. Correig, "Sensitivity and selectivity improvement of rf sputtered WO3 microhotplate gas sensors," *Sensors Actuators B. Chem.*, vol. 113, pp. 241–248, 2006.

[134] Fujifilm Diamtix Inc., "Dimatix Materials Printer DMP-2850, Data Sheet No. PDS00085."

[135] Fujifilm Diamtix Inc., "Jettable Fluid Formulation Guidelines."

[136] Scienion AG, "sciFLEXARRAYER Ultra-Low Volume Dispensers, Data Sheet."

[137] Scienion AG, "sciDROP PICO, Data Sheet."

[138] P. Grammatikopoulos, S. Steinhauer, J. Vernieres, V. Singh, and M. Sowwan, "Nanoparticle design by gas-phase synthesis," *Adv. Phys. X*, vol. 1, pp. 81–100, 2016.

[139] S. R. Challa, A. T. Delariva, T. W. Hansen, S. Helveg, J. Sehested, P. L. Hansen, F. Garzon, and A. K. Datye, "Relating Rates of Catalyst Sintering to the Disappearance of Individual Nanoparticles during Ostwald Ripening," *J. Am. Chem. Soc.*, vol. 133, pp. 20672–20675, 2011.

[140] A. K. Datye, Q. Xu, K. C. Kharas, and J. M. McCarty, "Particle size distributions in heterogeneous catalysts: What do they tell us about the sintering mechanism?," *Catal. Today*, vol. 111, pp. 59–67, 2006.

[141] J. Yang, V. Tschamber, D. Habermacher, F. Garin, and P. Gilot, "Effect of sintering on the catalytic activity of a Pt based catalyst for CO oxidation: Experiments and modeling," *Appl. Catal. B Environ.*, vol. 83, pp. 229–239, 2008.

[142] V. P. Zhdanov, E. M. Larsson, and C. Langhammer, "Novel aspects of Ostwald ripening of supported metal nanoparticles," *Chem. Phys. Lett.*, vol. 533, pp. 65–69, 2012.

[143] S. Bredmose Simonsen, I. Chorkendorff, S. Dahl, M. Skoglundh, J. Sehested, and S. Helveg, "Ostwald ripening in a Pt/SiO2 model catalyst studied by in situ TEM," *J. Catal.*, vol. 281, pp. 147–155, 2011.

[144] T. W. Hansen, A. T. Delariva, S. R. Challa, and A. K. Datye, "Sintering of Catalytic Nanoparticles : Particle Migration or Ostwald Ripening?," *Acc. Chem. Res.*, vol. 46, pp. 1720–1730, 2013.

[145] W. Jin, S. Yan, L. An, W. Chen, S. Yang, C. Zhao, and Y. Dai, "Enhancement of ethanol gas sensing response based on ordered V2O5 nanowire microyarns," *Sensors Actuators, B Chem.*, vol. 206, pp. 284–290, 2015.

[146] T. Hübert, L. Boon-Brett, and W. J. Buttner, *Sensors for safety and process control in hydrogen technologies*. Taylor & Francis Group, 2016.

[147] L. A. Currie, "Nomenclature in evaluation of analytical methods including detection and quantification capabilities," *Pure Appl. Chem.*, vol. 67, pp. 1699–1723, 1995.

[148] K. Hassan, A. S. M. Iftekhar Uddin, and G. S. Chung, "Fast-response hydrogen sensors based on discrete Pt/Pd bimetallic ultra-thin films," *Sensors Actuators, B Chem.*, vol. 234, pp. 435–445, 2016.

[149] C. Hsiao and L. Luo, "A Rapid Process for Fabricating Gas Sensors," *Sensors*, vol. 14, pp. 12219–12232, 2014.

[150] M. Thompson, "Carbon monoxide - molecule of the month." [Online]. Available: http://www.chm.bris.ac.uk/motm/co/coh.htm.

[151] Deutsche Forschungsgemeinschaft, *List of MAK and BAT Values 2016 Maximum Concentrations and Biological Tolerance Values at the Workplace*. Weinheim: Wiley-Vch, 2016.

[152] D. Kohl, "Surface processes in the detection of reducing gases with SnO2-based devices," *Sensors and Actuators*, vol. 18, pp. 71–113, 1989.

[153] S. Lenaerts, M. Honoré, G. Huyberechts, J. Roggen, and G. Maes, "In situ infrared and electrical characterization of tin dioxide gas sensors in nitrogen/oxygen mixtures at temperatures up to 720 K," *Sensors Actuators B. Chem.*, vol. 18–19, pp. 478–482, 1994.

[154] S. H. Hahn, N. Barsan, U. Weimar, S. G. Ejakov, J. H. Visser, and R. E. Soltis, "CO sensing with SnO2 thick film sensors: role of oxygen and water vapour," *Thin Solid Films*, vol. 436, pp. 17–24, 2003.

[155] W. Schmid, N. Barsan, and U. Weimar, "Sensing of hydrocarbons and CO in low oxygen conditions with tin dioxide sensors: possible conversion paths," *Sensors Actuators B. Chem.*, vol. 103, pp. 362–368, 2004.

[156] Institute for Occupational Safety and Health of the German Social Accident Insurance, "GESTIS Substance database." [Online]. Available: http://www.dguv.de/ifa/gestis/gestis-stoffdatenbank/index-2.jsp. [Accessed: 20-Jul-2005].

[157] D. S. Vlachos, C. A. Papadopoulos, and J. N. Avaritsiotis, "Characterisation of the catalyst-semiconductor interaction mechanism in metal-oxide gas sensors," *Sensors Actuators B. Chem.*, vol. 44, pp. 458–461, 1997.

[158] G. S. V Coles, G. Williams, and B. Smith, "The effect of oxygen partial pressure on the response of tin (IV) oxide based gas sensors," *J. Phys. D. Appl. Phys.*, vol. 24, pp. 633–641, 1991.

[159] L. Boon-brett, J. Bousek, G. Black, P. Moretto, P. Castello, T. Hu, and U. Banach, "Identifying performance gaps in hydrogen safety sensor technology for automotive and stationary applications," *Int. J. Hydrogen Energy*, vol. 35, pp. 373–384, 2010.

[160] W. J. Buttner, M. B. Post, R. Burgess, and C. Rivkin, "An overview of hydrogen safety sensors and requirements," *Int. J. Hydrogen Energy*, vol. 36, pp. 2462–2470, 2011.

[161] V. V Malyshev and A. V Pislyakov, "Investigation of gas-sensitivity of sensor structures to hydrogen in a wide range of temperature, concentration and humidity of gas medium," *Sensors Actuators B. Chem.*, vol. 134, pp. 913–921, 2008.

[162] N. Yamazoe, K. Suematsu, and K. Shimanoe, "Two types of moisture effects on the receptor function of neat tin oxide gas sensor to oxygen," *Sensors Actuators B. Chem.*, vol. 176, pp. 443–452, 2013.

[163] R. G. Pavelko, H. Daly, C. Hardacre, A. Vasiliev, and E. Llobet, "Interaction of water, hydrogen and their mixtures with SnO2 based materials: the role of surface hydroxyl groups in detection mechanisms," *Phys. Chem. Chem. Phys.*, vol. 12, pp. 2639–2647, 2010.

[164] S. Harbeck, A. Szatvanyi, N. Barsan, U. Weimar, and V. Hoffmann, "DRIFT studies of thick film un-doped and Pd-doped SnO2 sensors: temperature changes effect and CO detection mechanism in the presence of water vapour," *Thin Solid Films*, vol. 436, pp. 76–83, 2003.

[165] K. Suematsu, M. Sasaki, M. Yuasa, and K. Shimanoe, "Antimony-Doped Tin Dioxide Gas Sensors Exhibiting High Stability in the Sensitivity to Humidity Changes," *ACS Sensors*, vol. 1, pp. 913–920, 2016.

[166] H.-R. Kim, A. Haensch, I.-D. Kim, N. Barsan, U. Weimar, and J.-H. Lee, "The Role of NiO Doping in Reducing the Impact of Humidity on the Performance of SnO2-Based Gas Sensors: Synthesis Strategies, and Phenomenological and Spectroscopic Studies," *Adv. Funct. Mater.*, vol. 21, pp. 4456–4463, 2011.

[167] D. Koziej, N. Barsan, K. Shimanoe, N. Yamazoe, J. Szuber, and U. Weimar, "Spectroscopic insights into CO sensing of undoped and palladium doped tin dioxide sensors derived from hydrothermally treated tin oxide sol," *Sensors Actuators B. Chem.*, vol. 118, pp. 98–104, 2006.

[168] N. Yamazoe, K. Suematsu, and K. Shimanoe, "Gas reception and signal transduction of neat tin oxide semiconductor sensor for response to oxygen," *Thin Solid Films*, vol. 548, pp. 695–702, 2013.

[169] N. Yamazoe, K. Suematsu, and K. Shimanoe, "Extension of receptor function theory to include two types of adsorbed oxygen for oxide semiconductor gas sensors," *Sensors Actuators B. Chem.*, vol. 163, pp. 128–135, 2012.

[170] N. Ma, K. Suematsu, M. Yuasa, T. Kida, and K. Shimanoe, "Effect of Water Vapor on Pd-Loaded SnO2 Nanoparticles Gas Sensor," *ACS Appl. Mater. Interfaces*, vol. 7, pp. 5863–5869, 2015.

[171] D. Degler, H. W. Pereira devCarvalho, K. Kvashnina, J. Grunwaldt, U. Weimar, and N. Barsan, "Structure and chemistry of surface-doped Pt:SnO2 gas sensing materials," *RSC Adv.*, vol. 6, pp. 28149–28155, 2016.

[172] Royal Society of Chemistry, "Periodic Table - Nickel." [Online]. Available: http://www.rsc.org/periodic-table/element/28/nickel. [Accessed: 07-Jun-2017].

[173] Royal Society of Chemistry, "Periodic Table - Platinum." [Online]. Available: http://www.rsc.org/periodic-table/element/78/platinum. [Accessed: 07-Jun-2017].

[174] E. Roduner, "Size matters: why nanomaterials are different," *Chem. Soc. Rev.*, vol. 35, pp. 583–592, 2006.

[175] P. Buffat and J. Borel, "Size effect on the melting temperature of gold particles," *Phys. Rev. A*, vol. 13, pp. 2287–2298, 1976.

[176] C. R. M. Wronski, "The size dependence of the melting point of small particles of tin," *Br. J. Appl. Phys.*, vol. 18, pp. 1731–1737, 1967.

[177] G. Korotcenkov, V. Brinzari, L. B. Gulina, and B. K. Cho, "The influence of gold nanoparticles on the conductivity response of SnO2-based thin film gas sensors," *Appl. Surf. Sci.*, vol. 353, pp. 793–803, 2015.

[178] N. Pinna, G. Neri, M. Antonietti, and M. Niederberger, "Nonaqueous Synthesis of Nanocrystalline Semiconducting Metal Oxides for Gas Sensing," *Angew. Chemie Int. Ed.*, vol. 43, pp. 4345–4349, 2004.

[179] L. Xu, Z. Dai, G. Duan, L. Guo, Y. Wang, H. Zhou, Y. Liu, W. Cai, Y. Wang, and T. Li, "Micro/Nano Gas Sensors: A New Strategy Towards In-Situ Wafer-Level Fabrication of High-Performance Gas Sensing Chips," *Sci. Rep.*, vol. 5:10507, 2015.

[180] G. Korotcenkov, "The role of morphology and crystallographic structure of metal oxides in response of conductometric-type gas sensors," *Mater. Sci. Eng. R Reports*, vol. 61, pp. 1–39, 2008.

[181] J. Guo, J. Zhang, H. Gong, D. Ju, and B. Cao, "Au nanoparticle-functionalized 3D SnO2 microstructures for high performance gas sensor," *Sensors Actuators, B Chem.*, vol. 226, pp. 266–272, 2016.

List of figures

141

List of tables

Glossary

µhp   Microhotplate

AFM   Atomic Force Microscopy

CMOS   Complementary Metal-Oxide-Semiconductor

CVD   Chemical Vapor Deposition

EDX   Energy-dispersive X-ray

FFT   Fast Fourier Transform

FIB   Focused Ion Beam

HVAC   Heating, Ventilation, and Air Conditioning

IAG   Indoor Air Quality

IR   Infrared

IUPAC   International Union of Pure and Applied Chemistry

MISFETS   Metal-Insulator-Semiconductor Field-Effect Transistor

MOCVD   Metallo-Organic Chemical Vapor Deposition

OR   Oswald Ripening

PM   Particle Matter

PMC   Particle Migration and Coalescence

PVD   Physical Vapor Deposition

PVDF   Polyvinylidene Fluoride

QCM   Quartz Crystal Microbalance

QMF   Quadrupole Mass Filter

RMS   Root Mean Square

SAW   Surface Acoustic Wave

SMU   Source Measure Unit

TEM   Transmission Electron Microscopy

TPD   Temperature Programmed Desorption

TSV   Through-Silicon-Via

VOCs   Volatile Organic Compounds
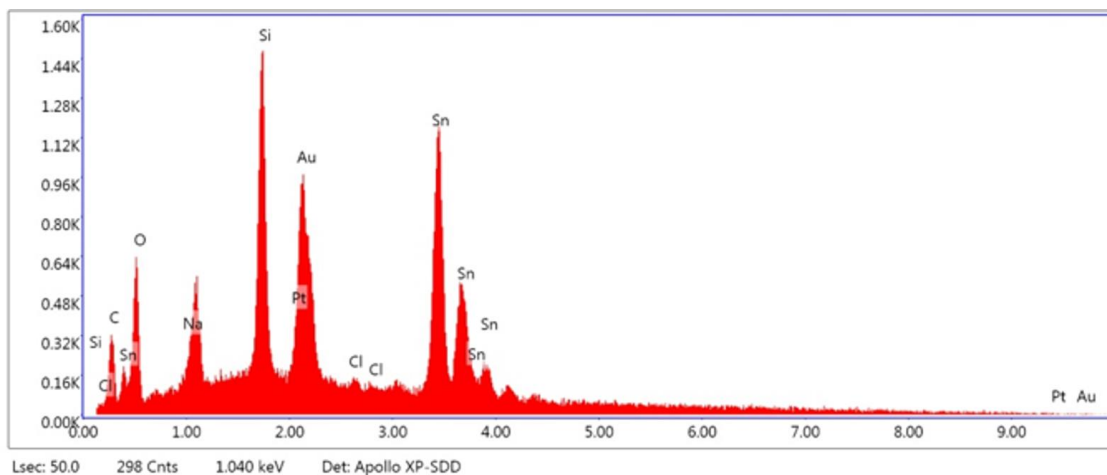
Appendices

A EDX spectra

Figure A. 1: EDX spectra of surfactant residue on thin-film heterostructure with Au nanoparticles.

B Test Gas Compositions

Table B. 1: Test gas compositions (Linde Gas).

Test gas	Diluted in	Concentration
Synthetic air	-	80 % N_2, 20 % O_2 <0.1 ppm hydrocarbons <0.1 ppm NO_x
CO	N_2	899 ppm
H_2	N_2	2465 ppm

List of Publications

E. Lackner, J. Krainer, R. Wimmer-Teubenbacher, F. Sosada, C. Gspan, K. Rohracher, E. Wachmann, A. Koeck, "CMOS nanocrystalline SnO_2 gas sensors for CO detection," Proceedings of 30th Eurosensors Conference, EUROSENSORS 2016, Procedia Engineering, vol. 168. pp. 297-300, 2016.

E. Lackner, J. Krainer, R. Wimmer-Teubenbacher, F. Sosada, M. Deluca, E. Laubender, O. Yurchenko, G. Urban, J. Bekacz, K. Rohracher, E. Wachmann, A. Koeck, "CMOS integrated tin dioxide gas sensors functionalized with bimetallic nanoparticles for improved carbon monoxide detection," Proceedings of IEEE SENSORS 2016. DOI:10.1109/ICSENS.2016.7808667

R. Wimmer-Teubenbacher, E. Lackner, J. Krainer, S. Steinhauer, A. Koeck, "Gas sensor devices based on CuO- and ZnO-nanowires directly synthesized on silicon substrate," *Proceedings of MRS Conference* 2015, *MRS Advances*, vol. 1, pp. 817-823, 2016.

J. Krainer, M. Deluca, E. Lackner, R. Wimmer-Teubenbacher, F. Sosada, C. Gspan, K. Rohracher, E. Wachmann, A. Koeck, "CMOS integrated tungsten oxide nanowire networks for ppb-level H_2S sensing," *Proceedings of 30th Eurosensors Conference*, *EUROSENSORS* 2016, *Procedia Engineering*, vol. 168, pp. 272-275, 2016.

J. Krainer, M. Deluca, E. Lackner, F. Sosada, R. Wimmer-Teubenbacher, C. Gspan, J. Bekacz, A. Poenninger, K. Rohracher, E. Wachmann, M. Schrems, A. Koeck, "CMOS integrated tungsten oxide nanowire networks for ppb-level hydrogen sulfide sensing," Proceedings of IEEE SENSORS 2016. DOI:10.1109/ICSENS.2016.7808634

Curriculum Vitae

Personal Data

Name	Eva Lackner
Date of birth	April 29th, 1988
Place of birth	Oberwart, Austria
Nationality	Austria

Education

May 2014 – Present   Doctorate Technical Sciences

Graz University of Technology, Austria

10/2011 – 03/2014   Master program Technical Chemistry

Graz University of Technology, Austria

10/2007 – 08/2011   Bachelor program Chemistry

Graz University of Technology, Austria

Career

05/2014 – Present   Materials Center Leoben Forschung GmbH, Austria

Department Materials for Microelectronics

PhD student

04/2013 – 02/2014   Graz University of Technology, Austria

Institute for Chemistry and Technology of Materials

Project Staff

09/2010 – 01-2012   Graz University of Technology, Austria

Institute of Inorganic Chemistry

Project Staff

09/2006 – 07/2007   River Island, United Kingdom

Staff Member in Retail